nature immunology

Article

https://doi.org/10.1038/s41590-023-01436-x

# Pyrimidine de novo synthesis inhibition selectively blocks effector but not memory T cell development

Received: 23 March 2022

Accepted: 13 January 2023

Published online: 16 February 2023

Check for updates

Stefanie Scherer[1,2,25], Susanne G. Oberle[2,20,25], Kristiyan Kanev[1,25], Ann-Katrin Gerullis[1], Ming Wu[1], Gustavo P. de Almeida[1], Daniel J. Puleston[3], Francesc Baixauli[3], Lilian Aly[4,5], Alessandro Greco[6], Tamar Nizharadze[6], Nils B. Becker[6], Madlaina v. Hoesslin[1], Lara V. Donhauser[1], Jacqueline Berner[1], Talyn Chu[1], Hayley A. McNamara[1], Zeynep Esencan[1,21], Patrick Roelli[1,22], Christine Wurmser[1], Ingo Kleiter[7,8], Maria J. G. T. Vehreschild[9], Christoph A. Mayer[10], Percy Knolle[11,12,13], Martin Klingenspor[14], Valeria Fumagalli[15,16], Matteo Iannacone[15,16], Martin Prlic[17,18], Thomas Korn[4,5,19], Erika L. Pearce[3,23,24], Thomas Höfer[6], Anna M. Schulz[1,26] ✉ & Dietmar Zehn[1,2,26] ✉

Blocking pyrimidine de novo synthesis by inhibiting dihydroorotate dehydrogenase is used to treat autoimmunity and prevent expansion of rapidly dividing cell populations including activated T cells. Here we show memory T cell precursors are resistant to pyrimidine starvation. Although the treatment effectively blocked effector T cells, the number, function and transcriptional profile of memory T cells and their precursors were unaffected. This effect occurred in a narrow time window in the early T cell expansion phase when developing effector, but not memory precursor, T cells are vulnerable to pyrimidine starvation. This vulnerability stems from a higher proliferative rate of early effector T cells as well as lower pyrimidine synthesis capacity when compared with memory precursors. This differential sensitivity is a drug-targetable checkpoint that efficiently diminishes effector T cells without affecting the memory compartment. This cell fate checkpoint might therefore lead to new methods to safely manipulate effector T cell responses.

Following an infection, pathogen-specific naïve or memory $CD8^+$ T cells transition through a proliferative phase[1]; acquire major gene expression, epigenetic and metabolic changes[2–5]; and form a clonally expanded but phenotypically and functionally heterogeneous cell population[6–11]. This population is dominated by effector cells, with limited expansion capacity, while a fraction of the population matures into memory T cells that can undergo massive secondary expansion following pathogen reexposure[12–16]. Over the past two decades, our knowledge of transcriptional networks and signaling pathways that control the differentiation of T cells has grown steadily. We know that memory T cell formation requires Tcf-1, Eomes, Foxo1 or Id3 (refs. [17–22]), whereas T-bet, Id2, Irf4 and FoxM1 (refs. [23–27]) are needed for the generation and proper expansion of effector T cells. Despite this progress, we are still in need of approaches and new targets to effectively manipulate T cell responses, for instance, to install larger numbers of memory T cells after prophylactic vaccination or to increase effector T cell numbers after therapeutic antitumor vaccination. Moreover, several medically relevant infections are characterized by excessive effector

A full list of affiliations appears at the end of the paper. ✉e-mail: anna.schulz@tum.de; dietmar.zehn@tum.de

T cell responses that drive immunopathology. For example, severe cases of fulminant hepatitis A and hepatitis B and influenza virus infections and probably also severe forms of acute respiratory syndrome coronavirus 2 (SARS-CoV-2) infections. Currently, such infections are often treated symptomatically, for example, with corticosteroids, despite broad suppression of anti-pathogen immunity using these drugs. Therefore, the identification of specific drug-targetable checkpoints to reduce effector T cells numbers or fine-tune their function is also of high medical importance.

There is a long history of targeting nucleotide synthesis or metabolism to alter T cell function. For example, immunosuppressive drugs including 5-fluorouracil, methotrexate and azathioprine block the survival and expansion of rapidly proliferating cells[28], but can result in nonspecific blockade of both effector and memory cell formation. The pyrimidine synthesis inhibitor leflunomide and its active compound teriflunomide[29,30], which are often used to treat rheumatoid arthritis and multiple sclerosis[31], are also potent inhibitors of T cell responses. These drugs inhibit dihydroorotate dehydrogenase (DHODH), an essential enzyme in the de novo pyrimidine synthesis pathway, thereby causing dose-dependent pyrimidine nucleotide starvation and substantial levels of cell death of in vitro activated T cells[32]. However, little is known about the effect of leflunomide on T cell responses in vivo.

Here we report that restricting pyrimidine biosynthesis is a powerful strategy to specifically reduce effector T cells numbers and functionality while maintaining memory T cells. We show that pyrimidine levels constitute a previously unknown checkpoint that controls effector T cell formation. We foresee potential in this mechanism, as pyrimidine synthesis inhibitors are already clinically validated for individuals with autoimmune diseases.

## Results

### Leflunomide limits T cell expansion but not memory formation

Prior studies and our own observations indicate that leflunomide-treated T cells fail to expand and undergo massive death upon ex vivo activation[33]. We therefore reasoned that individuals under DHODH inhibitor therapy (subsequently referred to as pyrimidine synthesis inhibition) may have diminished pathogen-specific T cell responses. To test this, we first explored Epstein–Barr virus (EBV)-specific and cytomegalovirus (CMV)-specific T cells in individuals suffering from multiple sclerosis who were treated with or without teriflunomide. In stark contrast to our expectations, we found similar frequencies of EBV-specific and insignificant differences for CMV-specific T cells in treated and not teriflunomide-treated individuals (Extended Data Fig. 1a,b). Thus, the drug-induced pyrimidine synthesis inhibition does not blunt the pool of frequently activated antigen-specific T cells. Nonetheless, it induced a significant bias toward a central memory phenotype among CMV-specific T cells (Extended Data Fig. 1c,d).

We also took advantage of the unique opportunity to study the impact of leflunomide or teriflunomide in human T cell responses in the context of SARS-CoV-2 vaccination. Here, we obtained peripheral blood mononuclear cells (PBMCs) from fully vaccinated leflunomide-treated individuals with multiple sclerosis and from healthy donors 2–3 weeks after their second vaccination. The PBMCs were stimulated with two overlapping peptide pools covering the SARS-CoV-2 spike protein. We saw a detectable response of vaccine-induced $CD4^+$ T cells in both healthy controls and in treated individuals. Phenotypically, we noticed a bias of T cells specific to spike pool 2 toward development of a central memory phenotype in the treated cohort (Extended Data Fig. 1e,f). That memory T cells are still detectable in leflunomide-treated or teriflunomide-treated individuals raised our interest to further explore how pyrimidine synthesis inhibition impacts the in vivo response of pathogen-specific T cells.

To explore this, we used well-defined model systems in which we transferred a low number ($10^4$) of CD45.1 congenic, T cell antigen receptor (TCR)-transgenic OT-1 T cells into CD45.2-positive C57BL/6 hosts. As OT-1 T cells are specific to the ovalbumin-derived H-$2K^b$-restricted SIINFEKL peptide, we challenged the host mice with recombinant, ovalbumin-expressing *Listeria monocytogenes* (Lm-Ova; Fig. 1a). We consistently noted that treated mice contained about 5–10 times lower frequencies of OT-1 T cells in spleen, blood and liver, and about 25-fold fewer absolute OT-1 T cell numbers in the spleen (Fig. 1b). Nonetheless, taking into consideration our input number of $10^4$ OT-1 T cells and the typically measured 10% engraftment rate, we concluded that the OT-1 cells had robustly expanded in treated mice, albeit not as prominently as in the untreated controls.

While a diminished T cell response is an expected outcome when applying an immunosuppressive drug, we were very surprised to note that this difference vanished with time and that memory OT-1 T cells reached comparable frequencies and absolute numbers at around 30 or 61 d after infection (Fig. 1c and Extended Data Fig. 2a). In line with this observation, the curve showing the frequency of OT-1 T cells among total $CD8^+$ T cells from leflunomide-treated mice remained quite flat over time, indicating the treated cells lack a prominent contraction phase (Fig. 1d). Subsequently, we transferred bona fide memory cells generated without leflunomide treatment and observed a similarly curtailed effector response in treated animals compared to control mice (Fig. 1e). Again, even these cells formed similar frequencies of secondary memory T cells compared to cells re-expanded in untreated secondary host mice (Fig. 1e). When we reverted the strategy and transferred memory T cells generated with or without pyrimidine synthesis inhibitors into untreated host mice, we saw that both types of memory T cells had a similar capacity to undergo secondary expansion (Fig. 1f) and survived long-term as secondary memory T cells (Extended Data Fig. 2b). Most notably, leflunomide-treated memory cells conferred comparable protective capacity against high-dose Lm-Ova challenge (Fig. 1g).

Similar observations were made following acute infections with ovalbumin-expressing influenza and vesicular stomatitis virus; and with P14 TCR-transgenic T cells in lymphocytic choriomeningitis virus (LCMV) infections (Extended Data Fig. 2c). This underlines that the leflunomide-induced partial block of effector T cell expansion occurs across different infections. Next, we tested how the treatment alters the T cell response to lower-affinity ligands. For example, the altered peptide ligand SIITFEKL (T4Ova) induces a ~tenfold reduced T cell expansion magnitude[34] compared to the wild-type SIINFEKL peptide (N4Ova). Notably, we observed that leflunomide treatment resulted in a similar fold reduction in OT-1 expansion compared to untreated controls, for both high-affinity (N4Ova) and low-affinity (T4Ova) stimulated T cells (Extended Data Fig. 2d). Thus, leflunomide reduces T cell expansion independently of the strength of TCR stimulation.

Leflunomide becomes metabolized in vivo into its active compound teriflunomide. While leflunomide was the first licensed DHODH inhibitor, teriflunomide is now more frequently given to patients than leflunomide. Therefore, we repeated our key experiments using teriflunomide instead of leflunomide. This revealed a similar selective reduction of effector T cell frequencies in mice treated with or without teriflunomide, compared to leflunomide treatments (Extended Data Fig. 2e). Subsequently, several experiments were therefore performed with teriflunomide instead of leflunomide. As a further control, we also determined the plasma levels of teriflunomide that can be detected in our leflunomide-treated animals. Here we took advantage of routine screening procedures installed to monitor drug levels in patients. The detected ~50 μg $ml^{-1}$ is within the therapeutic margin that is recommended for the treatment of individuals with rheumatoid arthritis or multiple sclerosis[35] (Extended Data Fig. 2f). A pharmacokinetic study of orally applied leflunomide revealed that similar peak levels of the active compound teriflunomide were reached following a single-dose injection or upon injecting the mice for 7 d every other day (Extended Data Fig. 2g). In both cases, the concentration substantially decayed after reaching the peak—underlining the need for repetitive injections.

https://doi.org/10.1038/s41590-023-01436-x

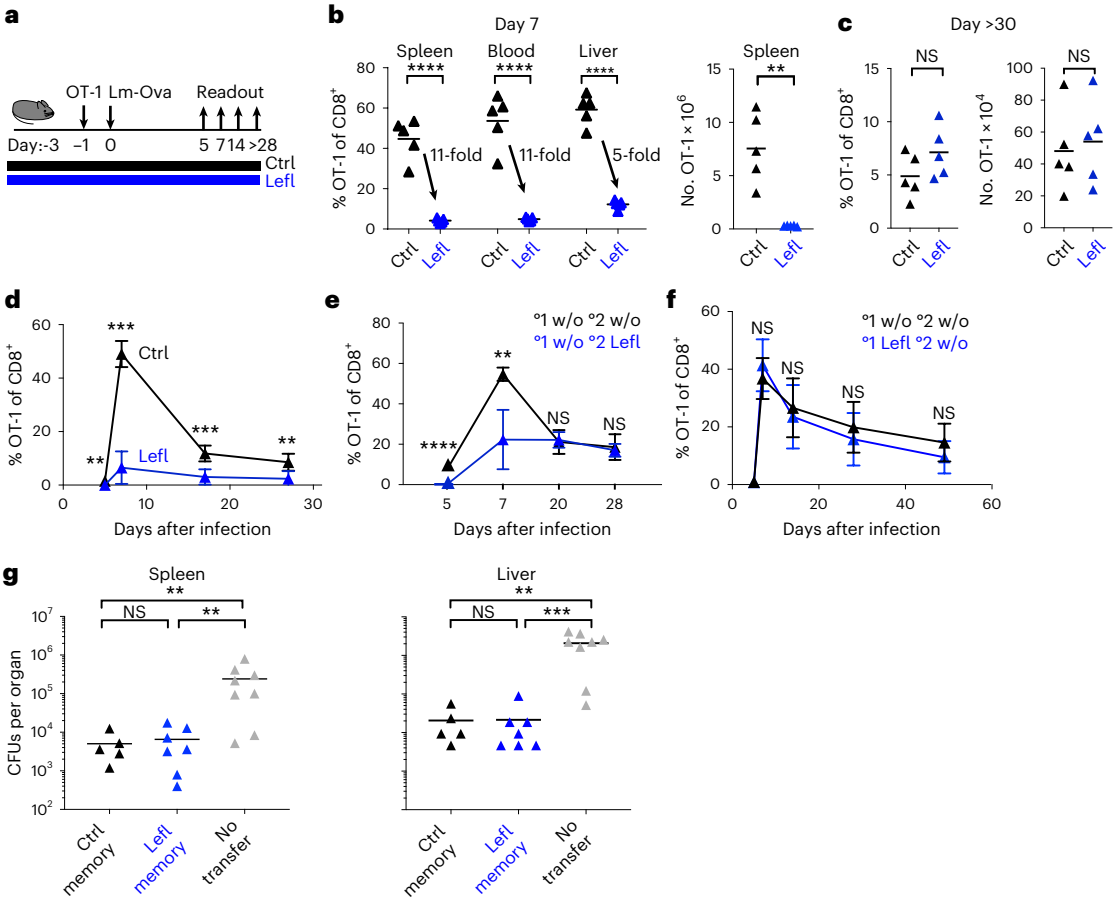


**Fig. 1 | Pyrimidine nucleotide starvation selectively reduces effector but not memory T cell numbers. a**, Naïve OT-1 T cells were transferred into naïve host mice 1 d before infection with recombinant, ovalbumin-expressing *L. monocytogenes* (Lm-Ova). Hosts were treated with leflunomide (Lefl) or carboxymethylcellulose vehicle control (Ctrl) every other day starting 3 d before until 7 d after the infection and every third day thereafter. **b**, Frequency of OT-1 among total splenic CD8$^+$ T cells in spleen, blood and liver and total OT-1 numbers in the spleen 7 d after infection. **c**, Frequency and absolute quantification of OT-1 in the spleen >30 d after infection. **d**, Representative OT-1 expansion kinetics in control (Ctrl) or leflunomide (Lefl)-treated hosts. **e**, $2 \times 10^4$ splenic memory OT-1 T cells generated without leflunomide (°1 w/o) were transferred into naïve host mice, which were then infected with Lm-Ova. Shown are OT-1 response kinetics in hosts without (°1 w/o °2 w/o) or with (°1 w/o °2 Lefl) leflunomide treatment. **f**, Similarly, $2 \times 10^4$ memory OT-1 cells were obtained from mice treated with (°1 Lefl) or without (°1 w/o) leflunomide and transferred into new naïve hosts. Hosts were challenged with Lm-Ova but remained free from leflunomide. **g**, $10^5$ memory OT-1 T cells generated without (Ctrl) or with (Lefl) leflunomide were transferred into new host mice. Hosts were challenged with a high Lm-Ova dose. Lm-Ova colony-forming units (CFUs) were determined in spleen and liver 4 d after infection in mice that received the two types of donor OT-1 or no cell graft. Symbols represent individual mice and the lines indicate the mean of the group. Symbols in **d**–**f** represent the mean of the group and error bars show the s.d. $n = 5$–7 mice per group and data show one representative of 2–3 individual experiments. Two-tailed, unpaired *t*-tests were performed to calculate significance with $^{**}P < 0.01$, $^{***}P < 0.001$, $^{****}P < 0.0001$; NS, not significant ($P > 0.05$). Supplementary Fig. 1 contains gating information.

Together, our observations strongly contrast with the prior view that pyrimidine synthesis inhibition causes a global suppression of T cell differentiation and proliferation. Instead, it induces a selective block in effector T cell formation without impacting primary or secondary memory T cell differentiation across different infection and stimulation conditions.

## Leflunomide selectively reduces the formation of effector T cells

The massive reduction in the peak numbers of pathogen-specific T cells under leflunomide treatment prompted us to compare the T cell phenotype that forms with and without leflunomide treatment. We saw a major loss of KLRG1$^+$CD127$^-$ terminally differentiated effector cells on day 7 (Fig. 2a,b) and this occurs in different infections and in different organs (Extended Data Fig. 2h,i). In contrast, the number of day 7 CD127$^+$KLRG1$^-$ memory precursor cells (Fig. 2b, right plot), the number of memory T cells found >30 d after infection (Fig. 1c and 2c, far right), and their phenotype remained largely unchanged (Fig. 2c). Interestingly, pyrimidine synthesis inhibition caused a significant delay in *Listeria* clearance in spleen and liver (Extended Data Fig. 2j), owing to the lack of effector cells. However, despite this pathogen persistence and continuous antigen presentation, pyrimidine synthesis inhibition potently suppresses the generation of effector cells while sparing memory precursor T cells. Analogous to this treatment-induced phenotypic bias toward memory precursor cells, histological analysis and absolute quantification of OT-1 T cells per area revealed a major loss of T cells in the red pulp, while their numbers remained similar in the T cell zone of the white pulp (Extended Data Fig. 3a,b). Following the kinetics of KLRG1$^+$CD127$^-$ T cells more closely beyond the expansion peak, we detected that their frequencies in control and leflunomide-treated animals became similar as early as 11 d after infection (Extended Data Fig. 4a). This suggests that leflunomide blocks terminally differentiated KLRG1$^+$ T cells, but possibly not the type of longer-lived KLRG1$^+$ cells with high plasticity that were described previously[7]. Moreover, the data also show that interrupting the leflunomide treatment on day 7 after infection caused similar KLRG1 response kinetics as continuous treatment.

Matching the pyrimidine nucleotide starvation-induced phenotypic bias toward a memory precursor T cell phenotype, we found higher frequencies of OT-1 expressing Eomes, Tcf-1 and CD62L (Fig. 2d–f) and lower frequencies of OT-1 expressing granzyme B and T-bet at 5 d or 7 d after infection in treated mice (Fig. 2g,h). Notably, absolute numbers of CD62L$^+$ OT-1 were similar at 7 d and >30 d after infection (Fig. 2f,i). While the expression of effector cytokines such as tumor necrosis factor (TNF) and interferon (IFN)-γ remained very similar at all times (Fig. 2j and Extended Data Fig. 4b,c), there was a higher frequency of interleukin (IL)-2-producing cells upon the treatment in the acute infection phase (Fig. 2k), while both frequencies and absolute numbers reached similar levels upon transition into the memory phase (Fig. 2l). Interestingly, leflunomide-treated and control mice showed equal frequencies and absolute numbers of CXCR6$^+$CD69$^+$ memory cells in the liver (Extended Data Fig. 4d–f). Of note, we also investigated the endogenous T cell responses under leflunomide treatment. Here we compared gp33-Tetramer-positive CD8$^+$ T cells following LCMV infection. Here we found again on day 7 a reduction of the frequency and total numbers of Tetramer-positive CD8$^+$ T cells (Extended Data Fig. 5a) and a more than 600-fold loss of KLRG1$^+$CD127$^-$ cells compared to only a 7-fold reduction in the number of CD127$^+$KLRG1$^-$ memory precursor T cells (Extended Data Fig. 5b,c). In contrast, both groups of mice contained similar numbers of Tetramer-positive T cells on day 29 after infection and the phenotype of the cells was similar (Extended Data Fig. 5d–h). This highlights that the selective sensitivity of effector cells—compared to memory precursors—to pyrimidine de novo biosynthesis inhibition also applies to endogenous T cells.

To further characterize the OT-1 compartment upon leflunomide treatment, we assessed global RNA expression profiles 7 d after infection in mice treated with a pyrimidine synthesis inhibitor. When comparing total OT-1 population from treated and untreated mice, we noted major differences in *Prf1*, *Gzma*, *Gzmk* and *Fasl* (Fig. 3a, b) and reductions in the transcriptional regulators *Prdm1* and *Klf3* in treated mice at the mRNA level, while L-selectin CD62L (*Sell*), *CCR7*, IL-2 receptor subunit alpha (*Il2ra*), the transcriptional regulator *Id3*, *Ezh2*—encoding a histone-lysine *N*-methyltransferase enzyme—and *Myb* were increased in the treated group. In contrast, there were only very few differentially expressed genes when day 7 memory precursor OT-1 T cells (CD127$^+$KLRG1$^-$; Fig. 3c) or total day 28 memory OT-1 T cells were compared (Fig. 3d).

Since memory OT-1 T cells from treated and untreated mice were phenotypically indistinguishable, we also wanted to test if this held true for secondary effector T cells derived from these memory T cells. We therefore transferred memory cells originating from control or treated mice into naïve host mice, which were then infected with Lm-Ova (Extended Data Fig. 6a). We detected only minor changes in the frequency of OT-1 T cells on day 7 after infection (Extended Data Fig. 6b), and overall similar frequencies and absolute numbers of cells expressing KLRG1 or CD127 (Extended Data Fig. 6c, d) and identical IFN-γ and TNF cytokine secretion profiles (Extended Data Fig. 6e).

Furthermore, we also tested how leflunomide impacts T cell responses in infections that develop into a persisting infection. Here we used infection with LCMV clone 13 and LCMV docile—two prototypic models for chronic infections in mice[36–38]. Again, we saw a strong reduction in total P14 numbers in the spleen and liver of treated mice (Extended Data Fig. 7a). Analogous to the other infection we tested, this reduction correlated again with a loss of terminally differentiated TCF-1$^-$ T cells, while TCF-1$^+$ precursors of exhausted T cells were retained (Extended Data Fig. 7b,c). This indicates that resistance of memory precursors to the treatment applies also to precursors of exhausted T cells. Interestingly, we also noted that the short treatment duration until day 5 after infection significantly reduced the magnitude of the weight loss that occurred in response to the infection (Extended Data Fig. 7d).

Finally, we also tested the effect of pyrimidine de novo biosynthesis inhibition on adoptively transferred CD4$^+$ SMARTA T cells following acute LCMV infection (Extended Data Fig. 7e). We detected a clear reduction of both frequencies and absolute numbers of SMARTA T cells at the peak of infection (Extended Data Fig. 7f), but this applied to both $T_H1$ and $T_{FH}$ subsets as their relative frequencies were maintained while their absolute numbers were reduced (Extended Data Fig. 7g,h). Most importantly, SMARTA T cells in treated animals showed higher IL-2 production capacity compared to untreated controls at the peak of the effector response, again suggesting that memory precursor cells were enriched in leflunomide-treated mice (Extended Data Fig. 7i).

Altogether, we concluded from these observations that cells with a memory precursor phenotype are resistant to leflunomide-induced pyrimidine nucleotide starvation. Most importantly, the selective reduction of effector cells and the unchanged number of memory cells indicate that the memory T cell trajectory is uncoupled from the cell trajectory that generates typical effector T cells.

## Leflunomide reduces effector T cell numbers in a narrow time window

As a next step, we sought to identify the time point at which leflunomide affects T cell expansion following the infection. To ensure a successful recovery in the early T cell expansion phase, we adjusted the number of naïve OT-1 T cells engrafted into the host mice to the harvest time point such that day 1.5 mice received the highest and day 5 mice the lowest number of donor OT-1 T cells. This analysis revealed that pyrimidine synthesis inhibition starts to impact the expansion of activated OT-1 T cells at day 3 after infection (Fig. 4a), while a loss of KLRG1-expressing cells is clearly detectable on day 4 after infection (Extended Data Fig. 8a). Notably, OT-1 T cells started to proliferate between 36 and 60 h after infection (Extended Data Fig. 8b).

Next, we asked what happens if we delay the treatment until day 4 after infection. This time point is beyond the day 3 time point when the treatment otherwise begins to impact cell expansion and differentiation. Interestingly, we noted that delaying the treatment resulted in similar expansion (Fig. 4b, c) and similar phenotypes without and with the late leflunomide application (Fig. 4d). This suggests that T cells are primarily receptive to leflunomide treatment when they begin to proliferate and when they are undergoing their first rounds of division. Hence, our data indicate that there is a time window spanning the first rounds of division, during which effector cells, or their precursors, are

**Fig. 2 | Pyrimidine nucleotide starvation blocks formation of terminal effector T cells.** CD45.1 congenic OT-1 T cells were obtained from treated and untreated mice (Fig. 1a) on days 5–7 or 41 after a *Listeria* infection. **a**–**c**, Splenocytes were extracellularly stained and analyzed for CD127 and KLRG1. Representative flow cytometry dot plots and data graphs showing the phenotype and frequency (**a**) and total numbers (**b**) of indicated populations 7 d after infection, and the phenotype, frequency and total number of CD127$^+$KLRG1$^-$ OT-1 cells 41 d after infection (**c**). **d**–**i**, Splenocytes were stained intracellularly for Eomes, TCF-1, T-bet and GzmB and surface strained for CD62L. Representative flow cytometry dot plots, histograms and data graphs showing the frequency of Eomes$^+$ OT-1 (**d**), Tcf-1$^+$ OT-1 (**e**) and CD62L (**f**) all on day 7, GzmB on day 5 (**g**), T-bet on day 7 (**h**) and CD62L also on day 41 after infection (**i**). **j**–**l**, Splenocytes were briefly ex vivo restimulated with ova-peptide in the presence of brefeldin A and then stained intracellularly for IFN-γ and IL-2. Time points indicate when cells were harvested. Shown are scatterplots depicting the frequency of IFN-γ$^+$ OT-1 on day 7 (**j**), representative dot plots for IFN-γ and IL-2 co-production and scatterplots of the frequency and number of IL-2-producing cells at 7 d (**k**) and 41 d (**l**) after infection. The scatterplots depict all mice per group in the shown representative experiment. Symbols represent individual mice and the line is the mean of a group. Data are representative of 2–3 individual experiments with $n = 5$–10 mice per group. Two-tailed, unpaired *t*-tests were performed to calculate significance with $^*P < 0.05$, $^{***}P < 0.001$, $^{****}P < 0.0001$. Supplementary Fig. 2 contains gating information.

https://doi.org/10.1038/s41590-023-01436-x

sensitive to pyrimidine nucleotide starvation. Beyond this checkpoint, cells committed to become effector cells continue to develop despite the treatment.

To rule out that leflunomide causes this block in effector T cell formation through mechanisms other than DHODH inhibition, we used a short hairpin RNA (shRNA) that reduces DHODH in primary CD8$^+$ T cells to about 30% of the normal expression level (Extended Data Fig. 8c). Here we transduced the cells at ~30 h after ex vivo activation and transferred them immediately into infected host mice. Expression of this shRNA in T cells resulted in a similar phenotype as

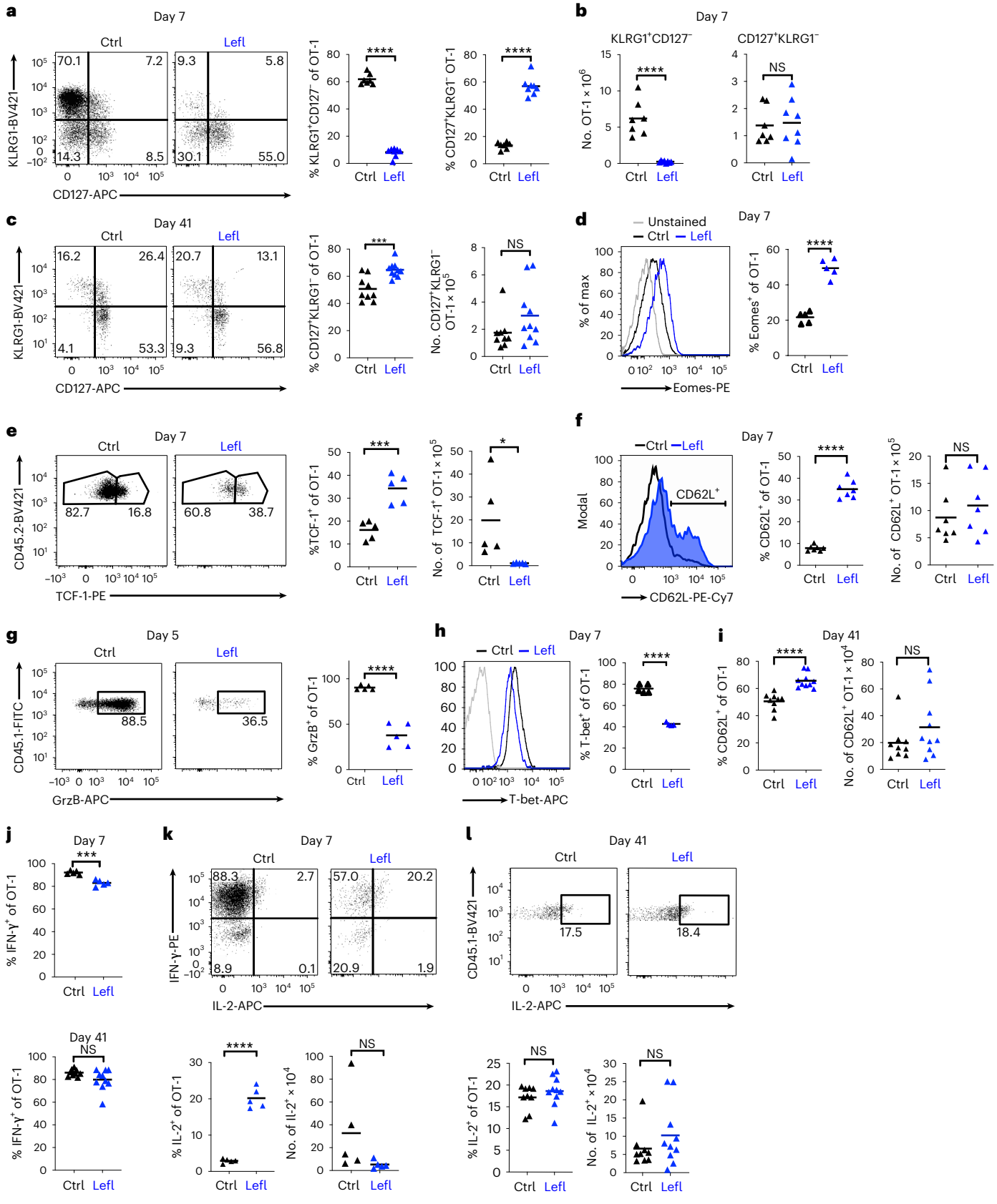

https://doi.org/10.1038/s41590-023-01436-x

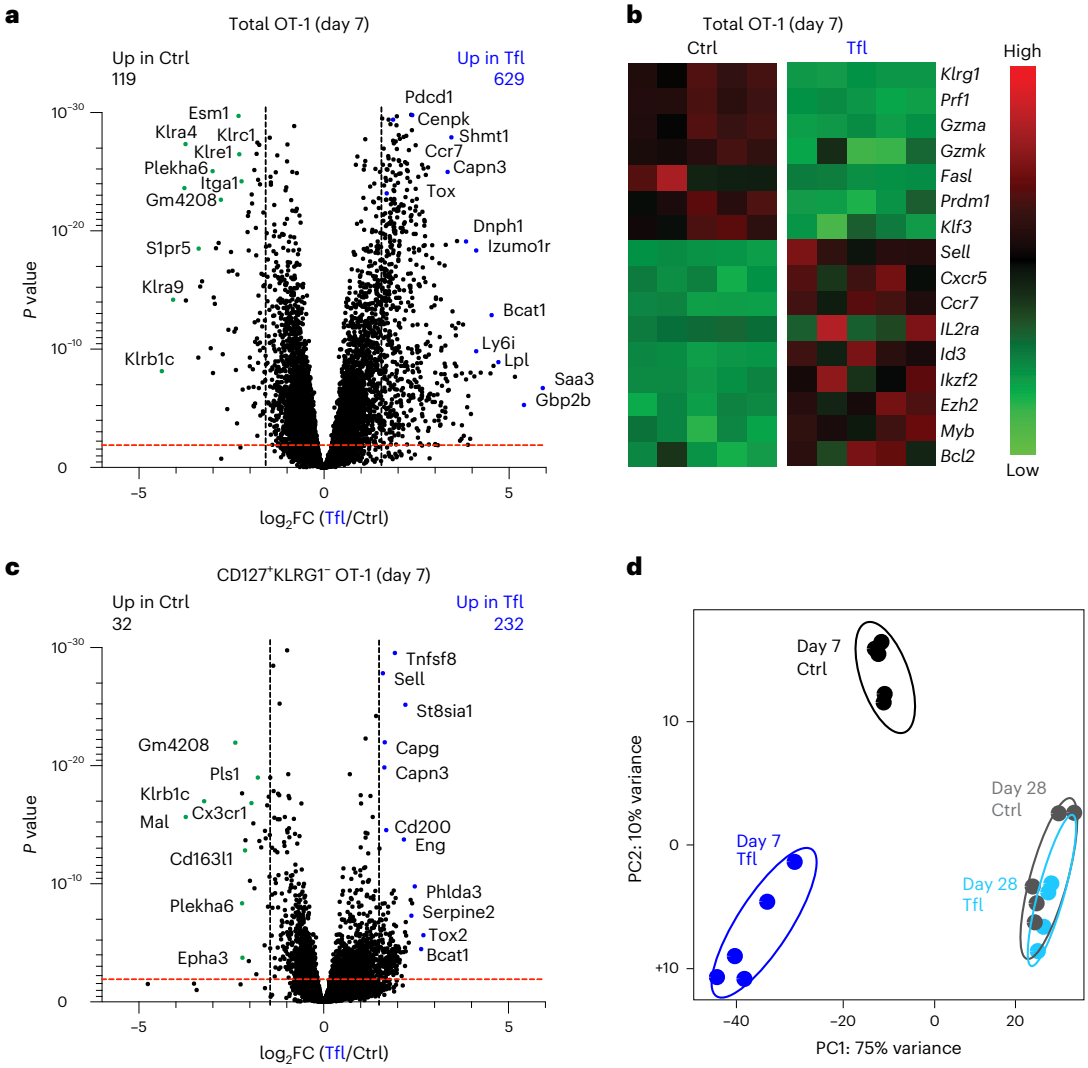


**Fig. 3 | RNA expression profiles of T cells exposed to pyrimidine synthesis inhibition.** OT-1 T cells were obtained on day 7 and day 28 after infection from an experimental setup as shown in Fig. 1. OT-1 T cells (or their indicated subset) were analyzed for global gene expression profiles using next-generation sequencing. **a**, Volcano plot showing $\log_2$ fold change versus *P* value for total splenic day 7 OT-1 T cells obtained from teriflunomide treated (Tfl) and untreated (Ctrl) hosts. **b**, Corresponding heat map highlighting the expression *z*-scores of selected genes in all analyzed samples. **c**, Volcano plot comparing CD127$^+$ KLRG1$^-$ OT-1 T cells that were sorted by flow cytometry from OT-1 populations obtained 7 d after infection. **d**, Principal-component analysis (PCA) of OT-1 T cells harvested 7 or 28 d after infection from control (Ctrl) and teriflunomide (Tfl)-treated hosts. *P* values in **a** and **c** were adjusted using the Benjamini–Hochberg method.

the leflunomide or teriflunomide treatment. It reduced the numbers of effector cells and caused a clear bias toward memory precursor cells at the peak of infection (Fig. 4e–g), supporting that T cell-intrinsic and DHODH-restricted mechanisms impair the formation of a functional effector T cell compartment.

Having confirmed that reduced DHODH levels alter T cell differentiation, we subsequently tested, if leflunomide may also interfere with the initial T cell activation and possibly with programming the generation of effector T cells. We therefore addressed the level of CD69 upregulation following in vivo T cell activation under leflunomide treatment and used Nur77 (Nr4a1) reporter mice to monitor TCR-induced transcriptional activity. Interestingly, both the Nur77 reporter and CD69 were similarly upregulated with and without the treatment (Extended Data Fig. 8d,e). Alongside, CD62L downregulation (Extended Data Fig. 8f) and dendritic cell maturation status were similar in both conditions (Extended Data Fig. 8g). All this indicates that TCR signaling and dendritic cells remain unaltered under the leflunomide treatment.

## Leflunomide selectively deprives effector-committed T cells

To better understand the impact of pyrimidine synthesis inhibition on the diversification of recently activated naïve T cells, we generated single-cell resolved RNA expression profiles for T cells isolated from control and leflunomide-treated host mice on day 4 after *L. monocytogenes* infection. Using *k*-nearest-neighbor (KNN) clustering (Seurat), we found that five clusters optimally represent the diversity when treated and untreated cells are jointly analyzed (Fig. 5a and Supplementary Fig. 4). Percentagewise, we noted a large bias such that clusters 1 and 2 were dominated by cells from treated mice and clusters 4 and 5 from untreated mice, while cluster 3 contained cells from both setups (Fig. 5a,b). The mRNA levels of markers of memory cells such as *Tcf7*, *Ccr7*, *Slamf6* and *Id3* were increased in clusters 1, 2 and 3, while the levels of effector cell markers such as *Gzma* or *Prf1* were increased in clusters 4 and 5 (Fig. 5c and Extended Data Fig. 9a–c). Moreover, gene-set enrichment and regulatory network analysis revealed differential activity across the clusters that match their commitment to generate effector or memory precursor cells (Extended Data Fig. 9c,d).

https://doi.org/10.1038/s41590-023-01436-x

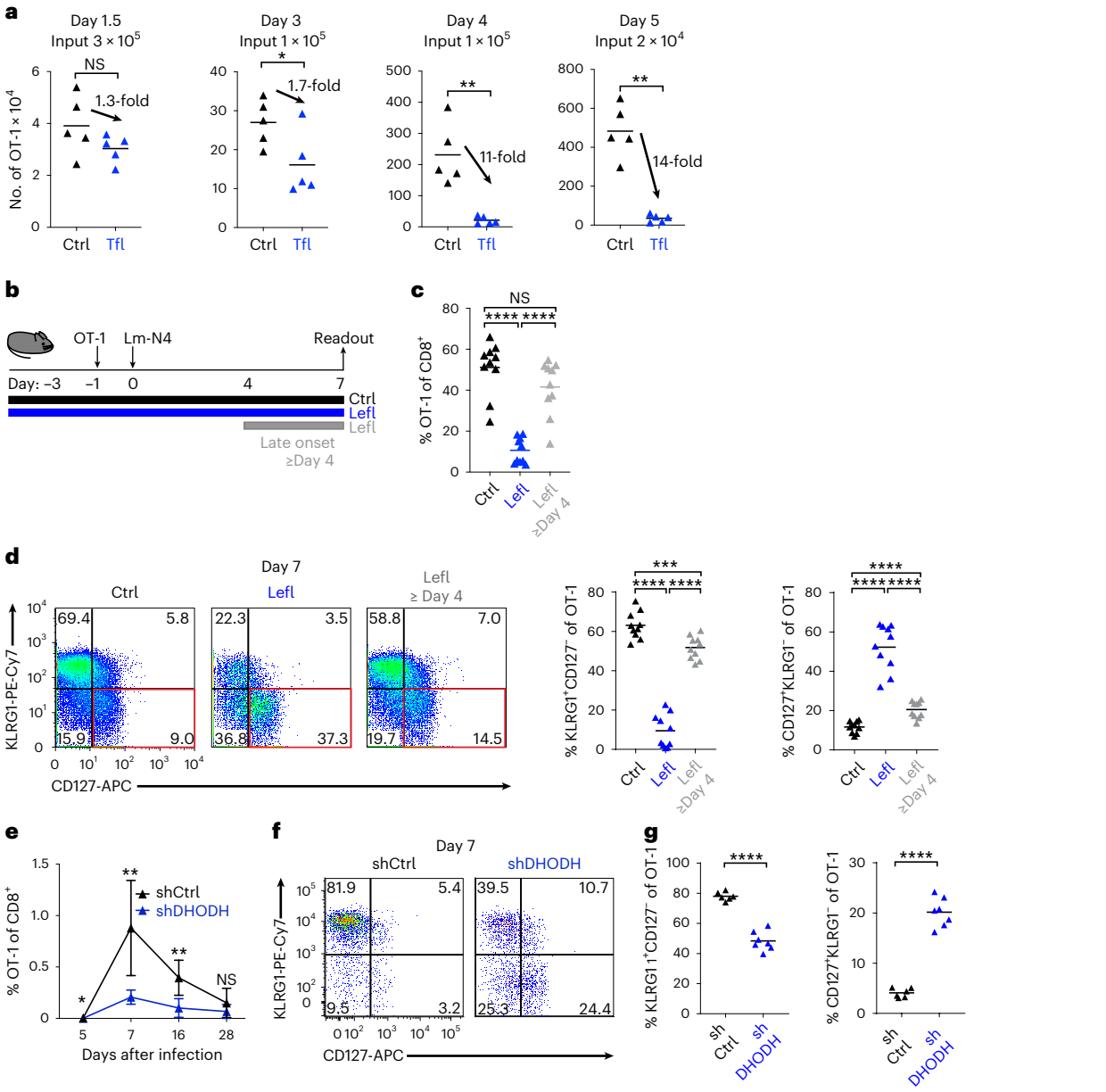


**Fig. 4 | Pyrimidine synthesis inhibits effector T cell formation during a narrow time window. a**, Naïve host mice received $3 \times 10^5$ (day 1.5 time point), $1 \times 10^5$ (days 3 and 4) or $2 \times 10^4$ (day 5) naïve OT-1 T cells and the hosts were infected with Lm-Ova. Absolute numbers of OT-1 were determined at the indicated time points in control (Ctrl) or teriflunomide (Tfl)-treated hosts. **b**, Experimental scheme; mice received OT-1 and were treated with leflunomide as indicated in Fig. 1a. One additional group of mice received leflunomide starting 4 d after infection. **c**, Frequencies of OT-1 among total $CD8^+$ T cells. **d**, Representative flow cytometry dot plots and data graphs showing the frequencies of OT-1 T cells expressing KLRG1 and CD127 on day 7 after infection. **e**–**g**, Naïve OT-1 T cells were briefly ex vivo activated and then transduced with retroviral vector encoding DHODH downregulating or control small interfering RNAs. After transduction, cells were immediately transferred into host mice infected with Lm-Ova 1 d before the transfer. Shown are frequencies of transduced OT-1 among total $CD8^+$ T cells on days 5, 7, 16 and 28 after primary infection with Lm-Ova (**e**), representative flow cytometry dot plots (**f**) and data graphs, which illustrate the frequency of ametrine-positive $KLRG1^+$ and $CD127^+$ OT-1 T cells for all analyzed mice (**g**). Symbols represent individual mice and the lines the mean of a group. Symbols in **e** are the mean of the group. Data are representative of at least two independent experiments. Error bars in **e** represent the s.d., $n = 7$ mice per group. Two-tailed, unpaired *t*-tests were performed to calculate significance with $^*P < 0.05$, $^{**}P < 0.01$, $^{***}P < 0.001$, $^{****}P < 0.0001$; NS, $P > 0.05$. Supplementary Fig. 3 contains gating information.

This includes upregulation of *Myc* mRNA in the memory-committed, treatment-resistant clusters 1 and 2 and upregulation of the activity of Rictor in the treatment-sensitive effector cluster 4 (Extended Data Fig. 9d). Interestingly, a calculation of absolute numbers revealed that treated and control mice contain similar total numbers of cells that would fall into clusters 1 and 2 (Fig. 5d). In contrast, there was a massive loss of cells from treated mice in clusters 4 and 5 (Fig. 5d). We subsequently repeated this experiment using the 10x Genomics platform. We identified seven representative clusters (Extended Data Fig. 10a,b), which we assigned based on transcriptional similarity with the clusters shown in Fig. 5 and Extended Data Fig. 9. Again, we observed that the clusters 1 and 2, which did not or only slightly declined, expressed typical memory markers, while the population that most prominently diminished in response to the treatment (cluster 5) showed a clear effector signature (Extended Data Fig. 10c,d). Alongside, we saw again a correlation in the mRNA expression levels of pyrimidine synthesis

genes (*Dhodh*, *Cad* and *Umps*) and sensitivity to leflunomide treatment, as the most resistant cluster (cluster 2) expressed the highest levels and the most sensitive cluster (cluster 5) expressed the lowest levels of these enzymes (Extended Data Fig. 10d,e). We also grouped the *Dhodh* mRNA expression levels detected in the single-cell data into five distinct intensities and compared the distribution of OT-1 T cells obtained from treated mice within these groups. This analysis revealed a loss of cells expressing low DHODH levels in the treated group. However, the maximum expression and the expression pattern in these groups remained similar to those in untreated groups, indicating that leflunomide treatment did not upregulate *Dhodh* mRNA expression. Overall, these data reveal a selection against cells with lower DHODH expression levels (Extended Data Fig. 10f).

To further infer cell population dynamics at this stage, both with and without leflunomide treatment, we performed an RNA velocity analysis. It revealed two endpoints in the untreated group (Fig. 5e), which in terms of gene expression corresponded to clusters 1–3 or clusters 4 and 5, respectively (Extended Data Fig. 9a). Alongside, we noted a selective increase in the expression of markers such as Zeb2 in the effector trajectory or Sell in the memory branch (Fig. 5e). In contrast, treated cells lacked the effector endpoint and the branching point seen in the untreated group (Fig. 5f). Similar findings were made after a transcriptional trajectory analysis on the data derived from the 10x Genomics platform (Extended Data Fig. 10g). Accordingly, the single-cell sequencing data confirmed that pyrimidine synthesis inhibition induces a block in effector T cell differentiation and an early loss of effector-committed T cells and of the trajectory that forms the effector T cell population. Moreover, the selective loss of the effector populations unmasks and allows profiling of the earliest progenitors of cells committed to become memory T cells. Without the leflunomide treatment, these could be hard to identify given their rare numbers within the population of activated and expanding T cells and because of the lack of specific markers to identify them. Our data therefore also reveal that critical memory signature genes are detectable as early as after 3–5 rounds of division.

## Memory precursors upregulate pyrimidine synthesis capacity

Leflunomide-induced pyrimidine starvation was shown to result in cell cycle arrest and apoptosis in proliferating ex vivo-stimulated T cells. What remained largely unclear is why leflunomide selectively blocks proliferating effector T cells and not precursors of memory T cells. Here, one needs to consider also that these cells undergo a substantial level of proliferation and expansion. Our single-cell profiling data show that actively dividing *Mki67* mRNA-positive cells are confined to the leflunomide-resistant cluster 1 and to the leflunomide-sensitive clusters 4 and 5 (Fig. 6a,b). Interestingly, the resistant clusters 1 and 2 contained significantly higher frequencies of *Dhodh* mRNA-positive cells than the sensitive clusters 3–5. (Fig. 6a,b). Similarly, gene-set enrichment and specific pyrimidine synthesis pathway analyses revealed significantly higher expression of genes involved in pyrimidine synthesis and metabolism in the treatment-resistant clusters 1 and 2 compared to the treatment-sensitive clusters 3–5 (Fig. 6c,d). We therefore conclude that cells within the memory-committed clusters have a higher capacity to produce pyrimidine nucleotides than cells in the effector clusters and that this renders the memory-committed populations resistant to the treatment. To formally demonstrate the dependency on DHODH-mediated de novo pyrimidine synthesis, we reasoned that the leflunomide-induced phenotype should be rescuable upon the provision of orotate—the metabolite synthesized by DHODH (see pathway in Fig. 6d). We therefore supplemented leflunomide-treated mice with orotate and took note that orotate significantly restored the KLRG1$^+$ population (Fig. 6e,f). This underlines that pyrimidine nucleotide starvation is responsible for the loss of effector cells following leflunomide treatment.

We subsequently addressed in more detail how the leflunomide treatment impacts early T cell expansion kinetics by injecting carboxyfluorescein diacetate succinimidyl ester (CFSE)-labeled OT-1 T cells into Lm-Ova-infected and leflunomide-treated or untreated host mice. Here we found that the majority of OT-1 T cells in untreated mice were in their 3rd–6th division at 2.75 d after infection, while cells in treated mice had reached only 1–3 divisions (Fig. 7a). These data imply at first glance that leflunomide slows down the entry into or the pace of proliferation of the responding cells. However, a population analysis of the day 2.75 dataset revealed that, while treated cells had a lower proliferation index (Fig. 7b), equal numbers of OT-1 T cells from both treated and untreated mice began to proliferate (Fig. 7c), which indicates a similar recruitment and transition into proliferating cells in both groups. We also analyzed absolute cell numbers per round of division at this time point. Here, we found that treated and untreated mice contained equal numbers of OT-1 T cells that are in their 1st and 2nd division and that differences arose only beyond the 3rd division (Fig. 7d). We also noted similar expression of CD69 and CD62L among the cells in the 1st–3rd division (Fig. 7e). This indicates that the type of slowly dividing T cells seen in treated mice is also present in the untreated group. Accordingly, untreated mice contain slowly and rapidly dividing T cells, while the rapidly dividing T cells are selectively lost in the treated group. Thus, the leflunomide treatment unmasked these slowly proliferating, memory-committed cells that are otherwise outnumbered by the larger and more rapidly proliferating effector-committed population. We therefore conclude that treatment with leflunomide reveals the in vivo proliferation kinetics of memory precursor cells.

To gain a better quantitative understanding of the proliferation rates and the proposed model, we modeled T cell activation mathematically, with an early branching of activated T cells (blasts) into either effector or memory differentiation (model 1; Fig. 7f–h) or with common precursors for effector and memory T cells (model 2; Fig. 7f–h). Experimental data on total cell numbers as well as fractions of CD127$^+$ KLRG1$^-$ memory precursor cells and KLRG1$^+$CD127$^-$ terminally differentiated effector cells were only reproduced by the first model, in which leflunomide selectively inhibited the formation of effector

**Fig. 5 | Transcriptional profile of pyrimidine starvation sensitive and resistant T cells. a**, Schematic of the experimental procedure. Mice were treated with (Tfl) or without (Ctrl) teriflunomide starting on day −3 followed by infection with Lm-Ova. OT-1 cells were harvested 4 d after infection and subjected to single-cell resolved RNA-sequencing analysis. All plots were generated using a nonlinear dimensional reduction *t*-SNE (*t*-distributed stochastic neighborhood embedding). Each circle represents a cell. Left, *t*-SNE distribution of OT-1 from control (red) and teriflunomide (blue)-treated mice. Right, Seurat cluster analysis (cell color) overlaying the *t*-SNE cell distribution (cell location). Five clusters were identified (green, cluster 1; yellow, cluster 2; red, cluster 3; orange, cluster 4; blue, cluster 5). **b**, Pie chart representing scaled distribution of control (Ctrl) and teriflunomide (Tfl)-treated OT-1 T cells among the identified clusters. **c**, *t*-SNE plots with overlaid expression of selected genes involved in memory or effector CD8$^+$ differentiation and function. **d**, Scatterplots with calculated absolute numbers of splenic OT-1 T cells from control (Ctrl) and teriflunomide (Tfl)-treated mice corresponding to each of the identified clusters. The calculation is based on the percentagewise representation of each cluster among total OT-1 T cells (Methods). **e**,**f**, Trajectory analysis based on RNA velocity. The differentiation trajectory of control OT-1 T cells bifurcated into an effector (green) and memory (orange) branch. Circles represent single cells. Arrows indicate the direction of gene expression change. The branches were characterized using classical effector or memory gene expression signatures, as shown for *Zeb2* and *Sell* (**e**). The OT-1 T cells recovered from teriflunomide-treated animals formed only the memory but not the effector branch (**f**). Symbols in **d** represent individual mice, or the mean of $n = 5$ mice per group and the lines represent the mean of a group. Two-tailed, unpaired *t*-tests were performed to calculate significance with $^*P < 0.05$ and $^{****}P < 0.0001$.

https://doi.org/10.1038/s41590-023-01436-x

T cells (Fig. 7g,h). The alternative model 2, with memory precursors originating from a common precursor, did not fit the data. The fit of model 1 to the data dictated slow proliferation of memory precursors and rapid proliferation of effector cells (with an approximately twofold ratio of proliferation rates between both types of cells; 'Mathematical modeling'). We conclude that the slower division rate of memory

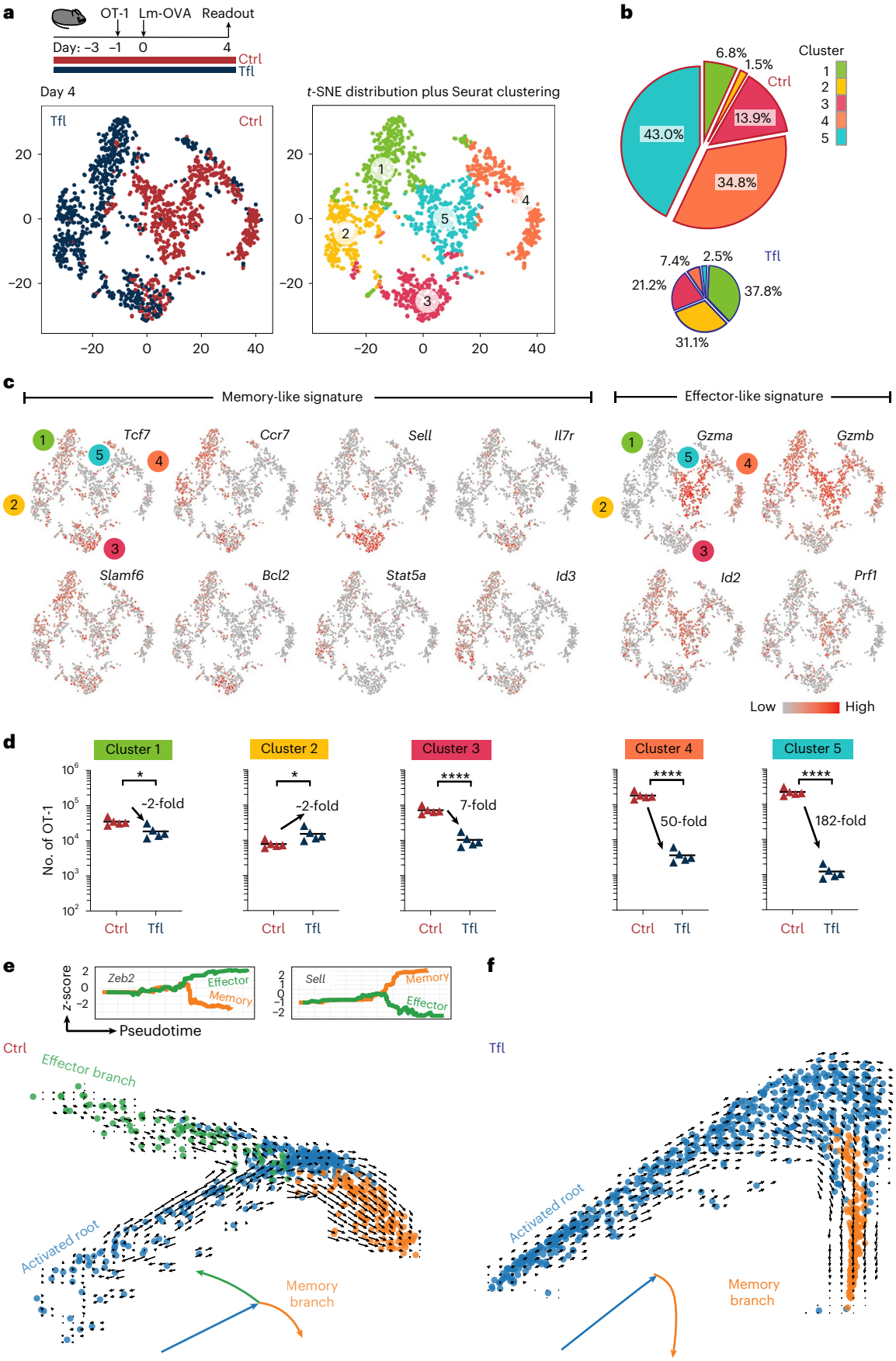

https://doi.org/10.1038/s41590-023-01436-x

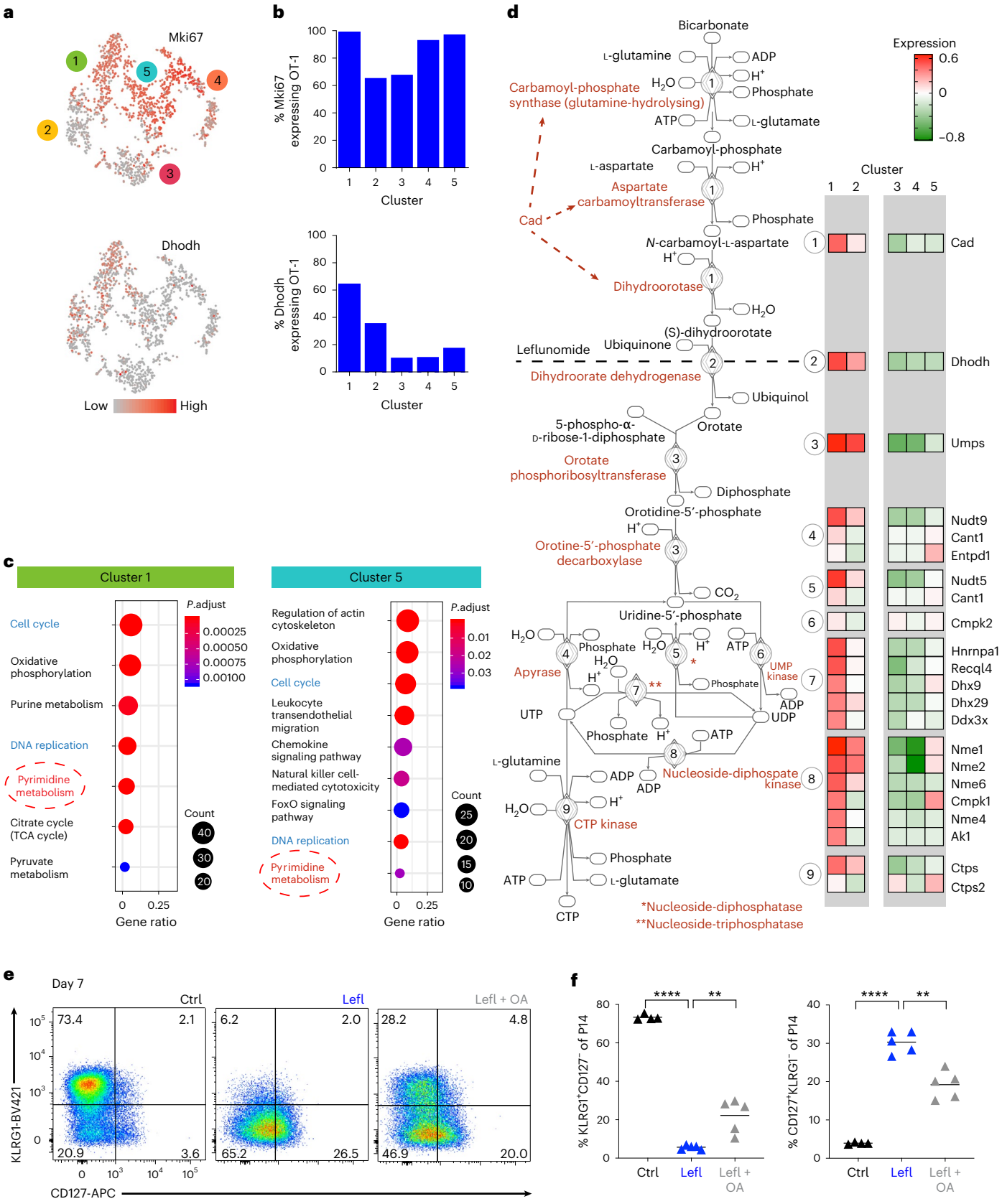


**Fig. 6 | Effector T cells have lower expression of pyrimidine synthesis pathway genes. a–d**, Further analysis of the single-cell sequencing data explained in Fig. 5. Shown are additional feature plots depicting expression of the indicated factors (**a**), bar plots indicating the percentage of marker-positive cells per cluster (**b**), pathway analysis for clusters 1 and 5 and (**c**) and cluster-specific expression activity of the genes involved in the pyrimidine synthesis pathway (**d**). **e**,**f**, Mice received $10^4$ CD45.1 congenic P14 T cells and were infected with LCMV Armstrong. Mice were left untreated (Ctrl), received leflunomide (Lefl) or leflunomide and orotic acid (Lefl + OA). Shown are representative flow cytometry dot plots (**e**) or data graphs showing the frequency of KLRG1 and CD127 expressing P14 for all individual mice (**f**). Symbols in **f** represent individual mice, the line indicates the mean of the group; $n = 4$ (Ctrl, Lefl) and $n = 5$ (Lefl + OA) mice per group were analyzed. Two-tailed, unpaired *t*-tests were performed to calculate significance with $^{**}P < 0.01$, $^{***}P < 0.001$ and $^{****}P < 0.0001$. Supplementary Fig. 5 contains gating information.

precursor T cells, as described previously[39], synergizes with their higher pyrimidine synthesis capacity and that both processes render memory-committed T cells more resistant to leflunomide treatment. In contrast, effector T cells are very sensitive to pyrimidine starvation given their lower pyrimidine production capacity and their larger need for nucleotides as a consequence of their higher proliferation velocity.

## Discussion

In summary, we demonstrated in various types of primary infections and during recall responses the existence of an early kinetic window, when effector-committed but not memory-committed cells are vulnerable to pyrimidine nucleotide starvation. Our observations help to better understand the therapeutic effects caused by pyrimidine synthesis inhibitors approved for treating autoimmune diseases. We anticipate that knowledge of this cell fate-determining checkpoint will inspire the development of new approaches to selectively influence effector T cell responses in various clinically relevant situations. This selective action of leflunomide against effector T cells contrasts with effects observed with other nucleotide synthesis or metabolism inhibitors. Mycophenolat mofetil and Methotrexate, which both block purine synthesis, and 5-fluorouracil, an antimetabolite to pyrimidines, reduce both effector and memory T cells numbers[40]. Similarly, FK506/tacrolimus also blocks effector and memory T cells[41].

The elevated demands for nucleotides following T cell activation and proliferation makes it very intuitive to grasp that manipulations of nucleotide metabolism perturb T cell differentiation. For leflunomide, it was well established that it induces fulminant apoptosis of the entire population of ex vivo activated T cells. This profound ex vivo effect contrasts with the selective action against effector T cells in vivo. A possible explanation is that in vitro anti-CD3/CD28 and IL-2 stimulation drives cells toward becoming terminally differentiated effector cells, which according to our results are very sensitive to leflunomide treatment.

The selective action against effector T cells distinguishes leflunomide also from other manipulations known to impact both effector and memory formation or only memory T cells. For instance, the elimination of Id2, T-bet, Blimp-1, FoxO3, Tcf-1 or Lef-1 alters effector and memory numbers[14,22,27,42–45]. Similarly, Akt–mTOR signaling manipulation induces a memory bias but also impacts the effector response[46–50]. Removing FoxO1, Eomes, Id3 or alterations in TCR signaling goes along with reductions in the numbers of memory T cells without a major impact on the effector response[14,17,19,22,27,42–45,51–53]. In strong contrast, we have observed a selective elimination of effector T cells, without a detectable impact on memory T cells.

A decreased effector response and normal memory formation were also observed after early termination of bacterial and viral infections, or after shortening the extent or duration of inflammation and antigen presentation[54,55]. We can exclude that our observations are due to such effects, as leflunomide prolonged the clearance of *L. monocytogenes* and yet effector T cell numbers were strongly reduced. Moreover, shRNA-mediated downregulation of DHODH caused similar effects as treating mice with leflunomide, indicating that a T cell-intrinsic reduction in DHODH activity and not effects in other cells or compartments caused the leflunomide effect.

Several factors contribute to the pyrimidine starvation resistance of developing memory T cells. Our experiments with CFSE-labeled OT-1 T cells revealed lower cell division numbers following leflunomide treatment. This outcome suggests at first glance that the treatment slows down or delays the onset of proliferation. However, we abandoned the idea that leflunomide reduces the proliferation rate of memory precursor cells, because such a slowdown should result in reduced memory T cell numbers and reduced day 7 memory precursors—both of which we did not observe. Instead, we favor the interpretation that the lower division numbers in the CFSE profiles of leflunomide-treated T cells stem from the absence of the rapidly proliferating, effector-committed T cells, and that the CFSE profiles seen in leflunomide-treated mice reveal the physiologically slower proliferation speed of memory-committed T cells. Accordingly, we think that the leflunomide treatment unmasks the proliferation kinetics of memory-committed T cells that are normally covered up by the high abundance of rapidly proliferating effector-committed T cells. Such reduced proliferation pace of memory precursor cells was also concluded from in vitro studies[6]. This slower division presumably results in a lower per-time demand in nucleotides and this renders memory-committed cells more resistant to the treatment. Moreover, we also observed in our single-cell expression profiles that memory precursor cells express higher levels of key enzymes involved in pyrimidine biosynthesis than effector cells including DHODH. This augmented synthesis capacity likely reinforces the resistance to leflunomide.

We became originally interested in studying leflunomide and teriflunomide, because patients treated with these drugs still handle many infection challenges without major complications[56]. Here we were puzzled how a drug that inhibits the proliferation of autoreactive T cells still permits a substantial level of pathogen control. In fact, we found similar numbers of EBV-specific and CMV-specific memory T cells in leflunomide-treated participants and in controls. To explain the different outcomes, we were initially considering that the responses could be driven by a different quality of T cells[57]. Autoimmunity is often caused by central and peripheral tolerance evading low-affinity self-reactive T cells[58], while T cells with high-affinity receptors dominate during infections[34]. We observed, independently of the affinity, a tenfold

**Fig. 7 | Pyrimidine starvation effect on CD8$^+$ T cell differentiation.** Mice received OT-1, leflunomide treatment and an Lm-Ova infection (1a and 4b). Numbers of bulk OT-1 cells and fractions of CD127$^+$KLRG1$^-$ and CD127$^-$KLRG1$^+$ OT-1 cells T were analyzed between 1.5 and 28 d after infection. Data were used for mathematical modeling. **a**, Fits of the Gaussian mixture model (black line) to the CFSE intensity distribution in OT-1 (red line) on days 2.75 and 3.75 under control (Ctrl) and leflunomide (Lefl)-treated conditions. Mean division numbers were extracted from five biological replicates. **b**,**c**, Proliferation analysis of day 2.75 data using FlowJo. Symbols represent individual mice and lines indicate the mean of a group. $n = 5$ mice per group. Two-tailed, unpaired *t*-tests were performed to calculate significance with ****$P < 0{,}0001$; NS, $P > 0.05$. **d**, Graph depicts total cell numbers per division in the day 2.75 dataset with $n = 5$ mice per group. Symbols represent the mean of a group and lines the s.e.m. **e**, Flow cytometry diagrams showing CD69 (left) and CD62L (right) surface expression and CFSE of one representative sample per group. **f**, Model 1 describing the experimental data, with activating cells passing through a blast stage and differentiating into memory precursor T cells ($TM_p$), or effector precursor ($TEF_p$) and then effector T cells (TEF). Leflunomide inhibits the differentiation into $TEF_p$ cells. Model 2 with a later branching point. **g**, Model fits for the number of splenic OT-1 T cells under control and leflunomide-treated conditions. 95% confidence bands are depicted in gray. **h**, Model fits for fractions of CD127$^+$KLRG1$^-$ and KLRG1$^+$CD127$^-$ OT-1 on day 7 under control (Ctrl), leflunomide (Lefl) and leflunomide given from day 4 (Lefl D4) conditions indicated in Fig. 4b. $n = 5$ mice per group in **b**–**d**, **g** and **h**. Horizontal lines in **b**–**d** represent the mean of the group. Two-tailed, unpaired *t*-tests were performed in **b** and **c** to calculate significance with ****$P < 0.0001$ and NS ($P > 0.05$). Error bars in **d** represent the s.d. In **g** and **h**, error bars represent the s.e.m. and the center indicates the mean of at least five biological replicates. The median estimates for proliferation rates of $TM_p$ and $TEF_p$ cells were 1.7 and 3.5 per day, respectively. **i**,**j**, Illustrations of an early bifurcation model of T cell differentiation. Early after activation, naïve T cells developed into a pool of precursor cells, which have differential sensitivities to pyrimidine starvation. These early precursor T cells differed in the expression levels of DHODH, a rate-limiting enzyme in the pyrimidine nucleotide de novo biosynthesis pathway (**I**). DHODH levels were high among the resistant cells, compared to treatment-sensitive effector-committed cells. The elimination of effector cells would be in line with this early effector-committed and memory-committed bifurcation model, whereby leflunomide selectively impaired the effector arm (**j**). Supplementary Fig. 6 contains gating information.

https://doi.org/10.1038/s41590-023-01436-x

reduction of the peak numbers of effector T cells, which excluded the possibility that low-affinity cells are more sensitive to leflunomide treatment than high-affinity T cells.

Overshooting or impaired effector T cell responses contribute to disease severity in hyperacute infections, autoimmune diseases or chronic viral infection. We found that the treatment of mice with chronic infection causing LCMV clone 13 virus prevented the type of cachexia that was described for this infection[59]. Interestingly, the weight-loss reduction in leflunomide-treated mice was accompanied by a reduction in the number of total P14 T cells, while TCF-1$^+$ precursors of exhausted T cells were retained within this population (Extended Data Fig. 7). Thus, the differential sensitivity to pyrimidine starvation applies not only to effector versus memory T cells in acute infection, but also to terminally differentiated and precursor T cells in infections that become chronic.

The observations we made after leflunomide treatment also have implications for our understanding of the kinetics and cellular trajectories leading to the formation of effector and memory T cell populations. Our data support that memory development occurs independently of the formation of effector cells. Moreover, our RNA velocity and pseudotime analysis imply an early bifurcation of the trajectory leading to effector and memory T cells (Fig. 7i,j). Our observations are compatible with the early bifurcation but also with the progressive differentiation model[60] in the early phase of infection. At this early time

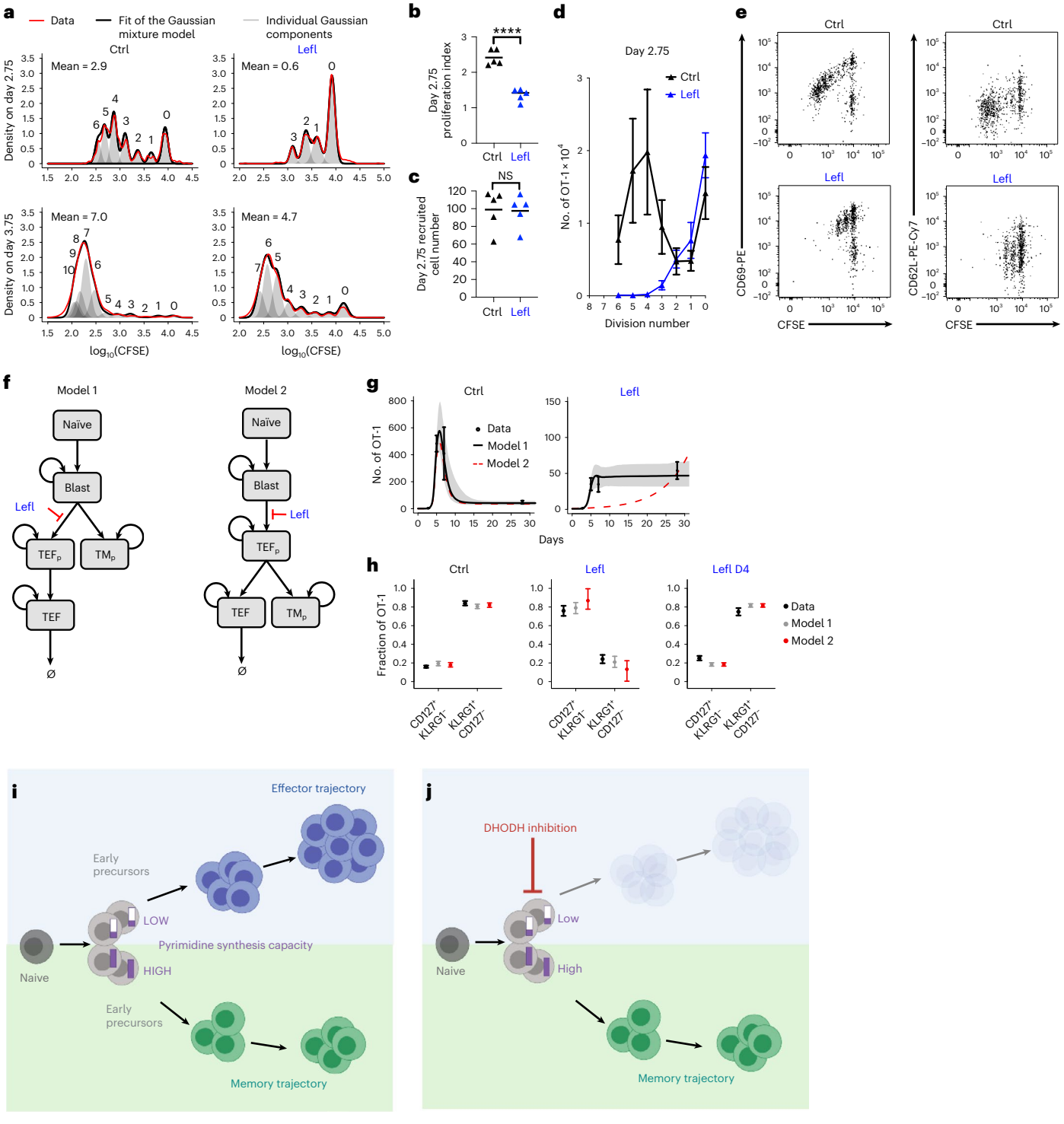

point, leflunomide could inhibit the more extensive proliferation of effector-committed cells compared to T cells, which are less engaged in proliferation and become memory T cells. Finally, our data do not exclude that memory-committed cells acquire features of effector T cells including GrzB secretion (Fig. 5c and Extended Data Fig. 10d) (refs. [61,62]). In fact, our single-cell sequencing data show the expression of granzyme B in the memory-committed cluster (Fig. 5c and Extended Data Fig. 10d), and a loss of CD62L expression within the cluster with a memory signature.

Altogether, we have identified a particularity in the sensitivity to pyrimidine nucleotide starvation that distinguishes developing memory T cells from expanding effector T cells and constitutes a new and targetable metabolic checkpoint of high clinical relevance.

## Online content

Any methods, additional references, Nature Portfolio reporting summaries, source data, extended data, supplementary information, acknowledgements, peer review information; details of author contributions and competing interests; and statements of data and code availability are available at https://doi.org/10.1038/s41590-023-01436-x.

## References


1. Murali-Krishna, K. et al. Counting antigen-specific CD8 T cells: a reevaluation of bystander activation during viral infection. *Immunity* **8**, 177–187 (1998).
2. Best, J. A. et al. Transcriptional insights into the CD8$^+$ T cell response to infection and memory T cell formation. *Nat. Immunol.* **14**, 404–412 (2013).
3. Lugli, E., Galletti, G., Boi, S. K. & Youngblood, B. A. Stem, effector and hybrid states of memory CD8$^+$ T cells. *Trends Immunol.* **41**, 17–28 (2020).
4. Pace, L. et al. The epigenetic control of stemness in CD8$^+$ T cell fate commitment. *Science* **359**, 177–186 (2018).
5. Geltink, R. I. K., Kyle, R. L. & Pearce, E. L. Unraveling the complex interplay between T cell metabolism and function. *Annu Rev. Immunol.* **36**, 461–488 (2018).
6. Buchholz, V. R. et al. Disparate individual fates compose robust CD8$^+$ T cell immunity. *Science* **340**, 630–635 (2013).
7. Herndler-Brandstetter, D. et al. KLRG1$^+$ effector CD8$^+$ T cells lose KLRG1, differentiate into all memory T cell lineages, and convey enhanced protective immunity. *Immunity* **48**, 716–729 (2018).
8. Jameson, S. C. & Masopust, D. Understanding subset diversity in T cell memory. *Immunity* **48**, 214–226 (2018).
9. Sallusto, F., Lenig, D., Forster, R., Lipp, M. & Lanzavecchia, A. Two subsets of memory T lymphocytes with distinct homing potentials and effector functions. *Nature* **401**, 708–712 (1999).
10. Thome, J. J. et al. Spatial map of human T cell compartmentalization and maintenance over decades of life. *Cell* **159**, 814–828 (2014).
11. Urban, S. L. et al. Peripherally induced brain tissue-resident memory CD8$^+$ T cells mediate protection against CNS infection. *Nat. Immunol.* **21**, 938–949 (2020).
12. Arens, R. & Schoenberger, S. P. Plasticity in programming of effector and memory CD8 T cell formation. *Immunol. Rev.* **235**, 190–205 (2010).
13. Gattinoni, L. et al. Wnt signaling arrests effector T cell differentiation and generates CD8$^+$ memory stem cells. *Nat. Med.* **15**, 808–813 (2009).
14. Joshi, N. S. et al. Inflammation directs memory precursor and short-lived effector CD8$^+$ T cell fates via the graded expression of T-bet transcription factor. *Immunity* **27**, 281–295 (2007).
15. Kaech, S. M. et al. Selective expression of the interleukin-7 receptor identifies effector CD8 T cells that give rise to long-lived memory cells. *Nat. Immunol.* **4**, 1191–1198 (2003).
16. Martin, M. D. & Badovinac, V. P. Defining memory CD8 T cell. *Front Immunol.* **9**, 2692 (2018).
17. Hess Michelini, R., Doedens, A. L., Goldrath, A. W. & Hedrick, S. M. Differentiation of CD8 memory T cells depends on Foxo1. *J. Exp. Med.* **210**, 1189–1200 (2013).
18. Jeannet, G. et al. Essential role of the Wnt pathway effector Tcf-1 for the establishment of functional CD8 T cell memory. *Proc. Natl Acad. Sci. USA* **107**, 9777–9782 (2010).
19. Kim, M. V., Ouyang, W., Liao, W., Zhang, M. Q. & Li, M. O. The transcription factor Foxo1 controls central-memory CD8$^+$ T cell responses to infection. *Immunity* **39**, 286–297 (2013).
20. Milner, J. J. et al. Heterogenous populations of tissue-resident CD8$^+$ T cells are generated in response to infection and malignancy. *Immunity* **52**, 808–824 (2020).
21. Zhao, D. M. et al. Constitutive activation of Wnt signaling favors generation of memory CD8 T cells. *J. Immunol.* **184**, 1191–1199 (2010).
22. Zhou, X. et al. Differentiation and persistence of memory CD8$^+$ T cells depend on T cell factor 1. *Immunity* **33**, 229–240 (2010).
23. Raczkowski, F. et al. The transcription factor Interferon regulatory factor 4 is required for the generation of protective effector CD8$^+$ T cells. *Proc. Natl Acad. Sci. USA* **110**, 15019–15024 (2013).
24. Starbeck-Miller, G. R., Xue, H. H. & Harty, J. T. IL-12 and type I interferon prolong the division of activated CD8 T cells by maintaining high-affinity IL-2 signaling in vivo. *J. Exp. Med.* **211**, 105–120 (2014).
25. Sullivan, B. M., Juedes, A., Szabo, S. J., von Herrath, M. & Glimcher, L. H. Antigen-driven effector CD8 T cell function regulated by T-bet. *Proc. Natl Acad. Sci. USA* **100**, 15818–15823 (2003).
26. Xue, L., Chiang, L., He, B., Zhao, Y. Y. & Winoto, A. FoxM1, a forkhead transcription factor is a master cell cycle regulator for mouse mature T cells but not double positive thymocytes. *PLoS ONE* **5**, e9229 (2010).
27. Yang, C. Y. et al. The transcriptional regulators Id2 and Id3 control the formation of distinct memory CD8$^+$ T cell subsets. *Nat. Immunol.* **12**, 1221–1229 (2011).
28. Broen, J. C. A. & van Laar, J. M. Mycophenolate mofetil, azathioprine and tacrolimus: mechanisms in rheumatology. *Nat. Rev. Rheumatol.* **16**, 167–178 (2020).
29. Aly, L., Hemmer, B. & Korn, T. From leflunomide to teriflunomide: drug development and immunosuppressive oral drugs in the treatment of multiple sclerosis. *Curr. Neuropharmacol.* **15**, 874–891 (2017).
30. Thoenes, G. H., Sitter, T., Langer, K. H., Bartlett, R. R. & Schleyerbach, R. Leflunomide (HWA 486) inhibits experimental autoimmune tubulointerstitial nephritis in rats. *Int. J. Immunopharmacol.* **11**, 921–929 (1989).
31. Herrmann, M. L., Schleyerbach, R. & Kirschbaum, B. J. Leflunomide: an immunomodulatory drug for the treatment of rheumatoid arthritis and other autoimmune diseases. *Immunopharmacology* **47**, 273–289 (2000).
32. Cherwinski, H. M. et al. The immunosuppressant leflunomide inhibits lymphocyte proliferation by inhibiting pyrimidine biosynthesis. *J. Pharmacol. Exp. Ther.* **275**, 1043–1049 (1995).
33. Chong, A. S. et al. Leflunomide, a novel immunosuppressive agent. The mechanism of inhibition of T cell proliferation. *Transplantation* **55**, 1361–1366 (1993).
34. Zehn, D., Lee, S. Y. & Bevan, M. J. Complete but curtailed T cell response to very low-affinity antigen. *Nature* **458**, 211–214 (2009).
35. Chan, V., Charles, B. G. & Tett, S. E. Population pharmacokinetics and association between A77 1726 plasma concentrations and disease activity measures following administration of leflunomide to people with rheumatoid arthritis. *Br. J. Clin. Pharm.* **60**, 257–264 (2005).

36. Ahmed, R., Salmi, A., Butler, L. D., Chiller, J. M. & Oldstone, M. B. Selection of genetic variants of lymphocytic choriomeningitis virus in spleens of persistently infected mice. Role in suppression of cytotoxic T lymphocyte response and viral persistence. *J. Exp. Med.* **160**, 521–540 (1984).
37. Moskophidis, D., Lechner, F., Pircher, H. & Zinkernagel, R. M. Virus persistence in acutely infected immunocompetent mice by exhaustion of antiviral cytotoxic effector T cells. *Nature* **362**, 758–761 (1993).
38. Zehn, D. & Wherry, E. J. Immune memory and exhaustion: clinically relevant lessons from the LCMV model. *Adv. Exp. Med Biol.* **850**, 137–152 (2015).
39. Kretschmer, L. et al. Differential expansion of T central memory precursor and effector subsets is regulated by division speed. *Nat. Commun.* **11**, 113 (2020).
40. Quéméneur, L. et al. Restriction of de novo nucleotide biosynthesis interferes with clonal expansion and differentiation into effector and memory CD8 T cells. *J. Immunol.* **173**, 4945–4952 (2004).
41. Araki, K. et al. Pathogenic virus-specific T cells cause disease during treatment with the calcineurin inhibitor FK506: implications for transplantation. *J. Exp. Med.* **207**, 2355–2367 (2010).
42. Cannarile, M. A. et al. Transcriptional regulator Id2 mediates $CD8^+$ T cell immunity. *Nat. Immunol.* **7**, 1317–1325 (2006).
43. Intlekofer, A. M. et al. Requirement for T-bet in the aberrant differentiation of unhelped memory $CD8^+$ T cells. *J. Exp. Med.* **204**, 2015–2021 (2007).
44. Kallies, A., Xin, A., Belz, G. T. & Nutt, S. L. Blimp-1 transcription factor is required for the differentiation of effector $CD8^+$ T cells and memory responses. *Immunity* **31**, 283–295 (2009).
45. Rutishauser, R. L. et al. Transcriptional repressor Blimp-1 promotes $CD8^+$ T cell terminal differentiation and represses the acquisition of central memory T cell properties. *Immunity* **31**, 296–308 (2009).
46. Prlic, M., Hernandez-Hoyos, G. & Bevan, M. J. Duration of the initial TCR stimulus controls the magnitude but not functionality of the $CD8^+$ T cell response. *J. Exp. Med.* **203**, 2135–2143 (2006).
47. Sarkar, S. et al. Functional and genomic profiling of effector CD8 T cell subsets with distinct memory fates. *J. Exp. Med.* **205**, 625–640 (2008).
48. Snell, L. M. et al. $CD8^+$ T cell priming in established chronic viral infection preferentially directs differentiation of memory-like cells for sustained immunity. *Immunity* **49**, 678–694 (2018).
49. Araki, K. et al. mTOR regulates memory CD8 T cell differentiation. *Nature* **460**, 108–112 (2009).
50. Zhang, L. et al. Mammalian target of rapamycin complex 2 controls CD8 T cell memory differentiation in a Foxo1-dependent manner. *Cell Rep.* **14**, 1206–1217 (2016).
51. Banerjee, A. et al. Cutting edge: the transcription factor eomesodermin enables $CD8^+$ T cells to compete for the memory cell niche. *J. Immunol.* **185**, 4988–4992 (2010).
52. Cui, W., Liu, Y., Weinstein, J. S., Craft, J. & Kaech, S. M. An interleukin-21–interleukin-10–STAT3 pathway is critical for functional maturation of memory $CD8^+$ T cells. *Immunity* **35**, 792–805 (2011).
53. Teixeiro, E. et al. Different T cell receptor signals determine $CD8^+$ memory versus effector development. *Science* **323**, 502–505 (2009).
54. Badovinac, V. P., Porter, B. B. & Harty, J. T. $CD8^+$ T cell contraction is controlled by early inflammation. *Nat. Immunol.* **5**, 809–817 (2004).
55. Bird, N. L. et al. Oseltamivir prophylaxis reduces inflammation and facilitates establishment of cross-strain protective T cell memory to influenza viruses. *PLoS ONE* **10**, e0129768 (2015).
56. Confavreux, C. et al. Oral teriflunomide for patients with relapsing multiple sclerosis (TOWER): a randomised, double-blind, placebo-controlled, phase 3 trial. *Lancet Neurol.* **13**, 247–256 (2014).
57. Klotz, L. et al. Teriflunomide treatment for multiple sclerosis modulates T cell mitochondrial respiration with affinity-dependent effects. *Sci. Transl. Med.* **11**, eaa05563 (2019).
58. Enouz, S., Carrié, L., Merkler, D., Bevan, M. J. & Zehn, D. Autoreactive T cells bypass negative selection and respond to self-antigen stimulation during infection. *J. Exp. Med.* **209**, 1769–1779 (2012).
59. Baazim, H. et al. $CD8^+$ T cells induce cachexia during chronic viral infection. *Nat. Immunol.* **20**, 701–710 (2019).
60. Kaech, S. M. & Cui, W. Transcriptional control of effector and memory $CD8^+$ T cell differentiation. *Nat. Rev. Immunol.* **12**, 749–761 (2012).
61. Bannard, O., Kraman, M. & Fearon, D. T. Secondary replicative function of $CD8^+$ T cells that had developed an effector phenotype. *Science* **323**, 505–509 (2009).
62. Youngblood, B. et al. Effector CD8 T cells dedifferentiate into long-lived memory cells. *Nature* **552**, 404–409 (2017).




[1]Division of Animal Physiology and Immunology, School of Life Sciences Weihenstephan, Technical University of Munich, Freising, Germany. [2]Formerly Division of Immunology and Allergy, Department of Medicine, Lausanne University Hospital, Lausanne, Switzerland. [3]Max Planck Institute of Immunobiology and Epigenetics, Freiburg, Germany. [4]Institute for Experimental Neuroimmunology, Technical University of Munich School of Medicine, Munich, Germany. [5]Department of Neurology, Technical University of Munich School of Medicine, Munich, Germany. [6]Division of Theoretical Systems Biology, German Cancer Research Center (DKFZ), Heidelberg, Germany. [7]Marianne-Strauß-Klinik, Behandlungszentrum Kempfenhausen für Multiple Sklerose Kranke, Berg, Germany. [8]Department of Neurology, St. Josef-Hospital, Ruhr-University Bochum, Bochum, Germany. [9]Department of Internal Medicine, Infectious Diseases, University Hospital Frankfurt, Goethe University Frankfurt, Frankfurt, Germany. [10]Neurologische Gemeinschaftspraxis am Kaiserplatz, Frankfurt, Germany. [11]Institute of Molecular Immunology, School of Medicine, Technical University of Munich (TUM), Munich, Germany. [12]German Center for Infection Research (DZIF), Munich, Germany. [13]Institute of Molecular Immunology, School of Life Science, Technical University of Munich (TUM), Munich, Germany. [14]Chair for Molecular Nutritional Medicine, School of Life Sciences, Technical University of Munich, Freising, Germany. [15]Division of Immunology, Transplantation and Infectious Diseases, IRCCS San Raffaele Scientific Institute, Milan, Italy. [16]Vita-Salute San Raffaele University, Milan, Italy. [17]Fred Hutchinson Cancer Research Center, Vaccine and Infectious Disease Division, Seattle, WA, USA. [18]Department of Global Health, University of Washington, Seattle, WA, USA. [19]Munich Cluster for Systems Neurology (SyNergy), Munich, Germany. [20]Present address: Sanofi Genzyme,

Baar, Switzerland. [21]Present address: Medpace Germany, Munich, Germany. [22]Present address: Spatial Transcriptomics AB, Stockholm, Sweden. [23]Present address: Bloomberg-Kimmel Institute for Cancer Immunotherapy, Department of Oncology, Johns Hopkins University School of Medicine, Baltimore, MD, USA. [24]Present address: Department of Biochemistry and Molecular Biology, Johns Hopkins University Bloomberg School of Public Health, Baltimore, MD, USA. [25]These authors contributed equally: Stefanie Scherer, Susanne G. Oberle, Kristiyan Kanev. [26]These authors jointly supervised this work: Anna M. Schulz, Dietmar Zehn. ✉e-mail: anna.schulz@tum.de; dietmar.zehn@tum.de

# Methods

## Mice

C57BL/6 mice were obtained from Charles River and C57BL/6.SJL from Jackson Laboratory. Both lines were maintained by intercrossing. Nur77 and OT-1 TCR-transgenic mice (both Jackson Laboratory) and P14 TCR and SMARTA transgenic mice obtained from A. Oxenius (ETHZ, Switzerland) are on a C57BL/6 background. Lines were maintained by crossing them with C57BL/6 and C57BL/6.SJL mice. Mice were bred and maintained in specific-pathogen-free facilities and infected in conventional or specific-pathogen-free animal facilities. A maximum of five mice per cage were housed with unlimited access to food (Ssnif V1124-300) and water. Experiments performed with at least 6-week-old male and female mice were approved by the veterinarian authorities of the Swiss canton of Vaud and the 'Regierung von Oberbayern' in Germany. Experimental groups were randomly assigned and not blinded.

## Administration of leflunomide, teriflunomide and orotate

A total of 100 mg leflunomide (Arava) or 14 mg teriflunomide (Aubagio) tablets were grinded and resolved in 0.5% carboxymethylcellulose. Solutions were gavaged orally starting 3 d before and until 7 d after infection every other day and thereafter every third day. Orotate rescue experiments were performed by gavaging mice every 24 h between 3 d before and 7 d after the infection with 500 mg per kg body weight orotic acid (Sigma) in PBS. The teriflunomide pharmacokinetic, approved by the 'Regierungspräsidium Tübingen', was performed by Immunic Therapeutics on mice that received leflunomide every other day using blood collected on day 1 (at 0.5, 1, 2, 4, 8 and 24 h) and on day 7 (at 0.5, 1, 2, 4 and 8 h).

## T cell purifications and transfers

Single-cell suspensions from spleen, liver and lymph nodes were obtained by mashing organs through 100-µm cell strainers. Red blood cells were removed with hypotonic ACK buffer. Spleen or lymph node cells suspensions were directly used. Cells from the liver were separated by overlying a 35% physiological Percoll/DMEM cell suspension on top of a 65% Percoll/PBS solution.

Donor OT-1 or P14 T cells were enriched using a $CD8^+$ T cell isolation kit II (Miltenyi) and SMARTA T cells with the $CD4^+$ T cell isolation kit (Miltenyi). Unless stated otherwise, $1–2 \times 10^4$ $CD45.1^+$ congenic OT-1 were transferred into $CD45.2^+$ hosts. Mice received $1–2 \times 10^4$ P14 T cells for LCMV experiments. For the single-cell sequencing experiment on day 4.5, $2 \times 10^5$ naïve OT-1 T cells were transferred. Biotinylated anti-CD45.1, anti-biotin microbeads (Miltenyi) and LS separation columns were used to isolate memory OT-1 T cells for adoptive retransfers.

## Infection and pathogen quantifications

Infections were performed ≥1 d after cell transfers. Mice were infected intravenously (i.v.) with 1,000–2,000 CFUs of recombinant, mid-log-phase recombinant ovalbumin-expressing *L. monocytogenes*. Strains were used that contain the original OT-1 ligand SIINFEKL (Lm-N4 or Lm-OVA) or the altered peptide ligand SIITFEKL (Lm-T4) (ref. [34]). Pathogen load was determined by mashing spleens and livers of day 4 or 7 infected mice in 0.1% NP-40 Tergitol PBS. Serial dilutions were plated on brain–heart infusion agarose plates containing 200 µg $ml^{-1}$ streptomycin and 3 µg $ml^{-1}$ chloramphenicol and counted 48 h later. Mice were infected i.v. with $2 \times 10^6$ plaque-forming units (PFUs) of recombinant vesicular stomatitis virus expressing SIINFEKL (VSV-N4, originally provided by L. Lefrançois[63]). VSV-N4 was expanded and titrated on BHK-21 cells. Mice were infected intraperitoneally with $2 \times 10^5$ PFUs LCMV Armstrong strain 53b (LCMVArm), or with $2 \times 10^6$ PFUs LCMV clone 13 i.v. or with $2 \times 10^4$ PFUs Docile strain i.v., and LCMV was expanded in BHK cells and titered with Vero cells using a focus-forming essay[64]. Influenza virus was applied at $2 \times 10^5$ PFUs Flu-Ova intranasally[65].

## Flow cytometry and sorting of mouse cells

Mouse cells were stained with anti-CD8 (53-6.7), anti-CD4 (RM4-4 or GK1.5), anti-CD45.1 (A20), anti-CD45.2 (104), anti-CD127 (A7R34 or eBioSB/199), anti-KLRG1 (2F1), anti-CD27 (LG.7F9), anti-CD62L (MEL-14), anti-CD69 (FN50, H1.2F3), anti-CD44 (IM7), anti-CD185 (CXCR5, SPRCL5 or 2G8), anti-CD186 (CXCR6, SA051D1 or 221002), anti-CD366 (TIM3, RMT3-23 or 8B.2C12), anti-CD150 (SLAM, DREG56 or MEL-14). Stained cells were washed twice and fixed for 15 min in PBS (1% formaldehyde, 2% glucose and 0.03% sodium azide). Cells were restimulated for intracellular cytokine staining in vitro with 5 mM SIINFEKL or KAVYNFATC peptide for the last 5 h, and 7 µg $ml^{-1}$ Brefeldin A was added 30 min later. Cells were fixed and permeabilized with Cytofix/Cytoperm Kit (BD) and stained with anti-IFN-γ (XMG1.2), anti-TNF (MP6-XT22) and anti-IL-2 (JES6-5H4, S4B6). Intracellular granzyme B staining (clone GB12, NGZB or 16G6) was performed similarly but without culturing and stimulating the cells. The Foxp3/transcription factor staining kit (eBioscience) was used for staining for TCF-1 (S33966 or C63D9), Eomes (Dan11mag) and T-bet (eBio4B10). Antibodies were obtained from BD Biosciences, BioLegend, Cell Signaling, eBioscience, Invitrogen/Thermo Fisher, R&D, Thermo Fisher, BD Biosciences and Tonbo Biosciences. A CytoFLEX (Beckman Coulter), LSR Fortessa or LSR-II instrument (both BD) were used for readouts and FlowJo (TreeStar, BD) was used for data analysis including a built-in routine for CFSE-based proliferation analysis. Live cells were stained in PBS, 2% FCS and sorted using a FACSAria Fusion instrument (BD).

## Preparation of human PBMCs and human T cell assays

For the EBV/CMV study, pentamer detection of EBV- and CMV-specific human T cells, patients with relapsing remitting multiple sclerosis (RRMS) under teriflunomide treatment and RRMS patients without teriflunomide were recruited from the Department of Neurology of the Technical University of Munich and the Marianne Strauß Klinik of Berg in Germany. The study was approved by the local ethics committee according to the Declaration of Helsinki under written informed patient consent. PBMCs were isolated from fresh EDTA blood using ficoll density gradient centrifugation (1.077 g/ml, GE Healthcare). Pentamer staining was performed in DPBS (Gibco) with 1% fetal calf serum (Sigma-Aldrich). Briefly, 5 µl PE-labeled Pro5 MHC Class I Pentamers (0.05 mg/ml, Proimmune) were incubated with 45 µl staining buffer at room temperature for 30 minutes. EBV BMLF-1259-267 (sequence GLCTLVAML) and CMV pp65 495–504 (sequence NLVPMVATV) pentamers were ordered from ProImmune. Cells were stained using anti-human CD127 (A019D5), CD62L (DREG-56), CD45RA (HI100), KLRG1 (SA231A2), CD8 (SK1), CCR7 (3D12) and 7-AAD purchased from Biolegend (San Diego, USA), BD Biosciences (Franklin lakes, USA) or Beckman Coulter (Brea, USA). For the assessment of antigen-specific T cell responses from SARS-CoV-2 vaccinated individuals, venous blood from ten teriflunomide-treated individuals and eight healthy donors was collected in Lithium Heparin or Natrium-Heparin tubes 14 d after giving the 2nd dose of Bnt162b2 (BioNTech/Pfizer) vaccine. Blood was diluted at a 1:1 ratio in PBS and PBMCs were separated using Ficoll Paque Plus (GE Healthcare). PBMCs were washed twice after centrifugation with PBS. Cells were either immediately used for T cell stimulations or cryopreserved in heat-inactivated FCS (Sigma-Aldrich) containing 10% dimethylsulfoxide (Sigma). Cryopreserved PBMCs were thawed at 37 °C, washed twice with RPMI 1640 supplemented with 10% FCS and Benzonase (50 U $ml^{-1}$), and stimulated using 1 µg $ml^{-1}$ overlapping peptide pools (PepMix, JPT) spanning the structural SARS-CoV-2 protein spike (vial 1 containing the receptor binding domain, vial 2 containing fusion peptide, transmembrane domain and cytoplasmic peptide), and controls remained without peptide. Cells were cultured in medium for 6 h (37 °C, 7% $CO_2$). In total, 10 µg $ml^{-1}$ Brefeldin A (Sigma) was added for the final 4 h. Cells were stained with purchased self-labeled anti-CD8 (OKT-8, BioXCell), anti-CD4 (RPA-T4, BioXCell), anti-CD3 (UCHT1, BioXCell), anti-CD45RA (HI100, BioLegend) and anti-CCR7 (G043H7,

BioLegend). Stained cells were washed and fixed for 30 min in PBS containing 2% formaldehyde. Cells were permeabilized in PBS with 10% saponin, 0.02% sodium azide and stained with anti-TNF (Mac11, BioLegend) and anti-IFN-γ (B27, BioXCell).

### Spleen cryosections and staining

Spleens from infected mice were harvested 7 d after infection and processed as described previously[66]. Sections were stained with anti-CD3 (17A2), anti-CD45.R/B220 (RA3-6B2) and anti-CD45.1 (A20; BioLegend). Spleen compartments were visualized by setting the density threshold of areas rich in CD3 (T cell zone) and B220 (B cell zone).

### Retroviral transduction of T cells

Two DHODH-targeting shRNA seed sequences were cloned into the pLMPd mAmetrine1.1 vector (transOMIC technologies),

Construct 1: 5′-CTCGAGTGCTGTTGACAGTGAGCGCCCCACTGTCTCTAGATCTAAATAGTGAAG

CCACAGATGTATTTAGATCTAGAGACAGTGGGATGCCTACTGCCTCGGAATTC-3′;

Construct 2: 5′-CTCGAGTGCTGTTGACAGTGAGCGCTCCCACTGTCTCTAGATCTAATAGTGAAG

CCACAGATGTATTAGATCTAGAGACAGTGGGATTGCCTACTGCCTCGGAATTC-3′; Control shRNA:

5′-TGCTGTTGACAGTGAGCGAAGGCAGAAGTATGCAAAGCATTAGTGAAGCCACA

GATGTAATGCTTTGCATACTTCTGCCTGTGCCTACTGCCTCGGA-3′.

Plasmids were transfected into Phoenix-E cells using FuGENE 6 (Promega) reagent. Retroviral particles were harvested 48 h later. OT-1 T cells were activated via anti-CD3/CD28 beads (Thermo Fisher), cultured in complete RPMI medium supplemented with 50 U $ml^{-1}$ IL-2 (Chiron) for 24–28 h, and spin-infected for 90 min at 32 °C 700*g* with polybrene. Cells were rested for 3–4 h at 37 °C in complete RPMI medium and injected into mice or kept in culture for an additional 48 h. Successfully transduced (Ametrine$^+$) cells were sorted by flow cytometry, RNA was isolated with the RNeasy Mini Kit (QIAGEN), cDNA was synthesized using the ProtoScript first-strand cDNA Synthesis Kit (New England BioLabs), and qPCR was performed using SsoAdvancedTM Universal SYBR Green Supermix, using an annealing temperature 60 °C. DHODH forward-TGTTTGAATGAGGCTTCAGTACTTTACAG, DODH reverse-GGTGCAGATGAACTTCAGGG; 18S forward-CTCAACACGGGAAACCTCAC, 18S reverse-CGCTCCACCAACTAAGAAGC.

### Bulk population RNA sequencing

OT-1 cells were pre-enriched using magnetic cell separation (Miltenyi) and were sorted by flow cytometry (purity > 95%). RNA extraction, sample processing, library preparation and sequencing were performed as described[66].

### Bulk population RNA-sequencing data analysis

Reads were processed using snakemake pipelines[67] as indicated under https://gitlab.lrz.de/ImmunoPhysio/bulkSeqPipe. Sequencing quality was assessed with FastQC (http://www.bioinformatics.babraham.ac.uk/projects/fastqc; version 0.11.6). Filtering was performed with trimmomatic (version 0.36) (ref. [68]), mapping using STAR (version 2.5.3a) (ref. [69]) with genome Mus_musculus.GRCm38, counting using htseq (version 0.9.1) (ref. [70]) and annotation with Mus_musculus.GRCm38.91. To supervise STAR and fastqc results we used multiqc (v1.2) (ref. [71]). Genes with total counts < 10 were discarded. Differential expression analysis used default parameters of DESeq2 (v1.24.0) (ref. [72]). Batch effects were eliminated with removeBatchEffect function provided by limma (v3.40.6) (ref. [73]) in PCA. Differences with a base mean > 50, an absolute $\log_2$ fold change > 1.5 and an adjusted *P* value < 0.05 were considered significant. Genes with average normalized counts of all samples (base mean) > 50 were selected for volcano plots. ggplot2 (v3.2.1) (ref. [74]) was used to generate PCA plots. Heat maps were generated by pheatmap (v1.0.12) (ref. [75]). Colors were encoded by the *z*-score based on rlog-transformed data obtained from DESeq2 (v1.24.0) (ref. [76]).

### Plate-based single-cell RNA-sequencing and analysis

Day 4 splenocytes from Lm-N4 infected mice were enriched via magnetic cell sorting (Miltenyi) followed by index sorting using a BD FACSaria Fusion sorter (100-µm nozzle, standard operation settings, single-cell purity, index sorting). Individual cells were sorted into low-binding PCR plates filled with lysis buffer. Plates were spun down, snap-frozen and stored at −80 °C. Single-cell libraries were generated using the previously described SCRB-seq protocol[77], with some modifications. After RNA purification and reverse transcription, single-cell cDNA was amplified for 20 cycles. Barcoded single-cell amplicons were double-purified with the use of (0.6×) Agencourt AMPure XP beads. Then, 1 ng of the resulting amplified cDNA was used for library preparation with the Illumina Nextera XT DNA Library reagents (FC-131-1024, Illumina). Fragmented libraries were purified with (0.6×) Agencourt AMPure XP beads and eluted in 10 µl of molecular-grade water. Library quality was assessed using Agilent High Sensitivity DNA Kit (5067-4626). Library quantification was performed based on Illumina recommendations (SY-930-1010) with the KAPA SYBR FAST qPCR Master Mix (KK4600, Kapa Biosystems). Samples were sequenced on an Illumina HiSeq 2500 system in high-output run mode, paired-end, 16-base pair (bp) read 1, 49 bp read 2, single-indexed sequencing resulting in 1 million reads per single cell. A total of 1,728 single cells were sequenced−864 from control and 864 from teriflunomide-treated mice. Cells were derived from three experimental animals (288 single cells per animal) per condition.

DropSeqPipe v0.4 (https://hoohm.github.io/dropSeqPipe/) was used for raw data processing. Parameters are provided in the Gene Expression Omnibus (GEO) series under accession GSE200359. Cutadapt v1.16 was used for trimming[78]. Trimming and filtering were done on both fastq files separately. Reads with a missing pair were discarded using bbmap v38.22. STAR (v2.5.3a) (ref. [69]) was used for mapping to annotation release no. 91 and genome build no. 38 from *Mus musculus* (Ensembl). Multimapped reads were discarded. Dropseq_tools v1.13 was used for demultiplexing and file manipulation[79]. A whitelist of cell barcodes with minimum distance of three bases was used. Cell barcodes and unique molecular identifiers (UMIs) with a hamming distance of 1 and 2, respectively, were corrected.

Features with a total UMI count < 1 were eliminated. A quality-control matrix was computed using calculateQCMetrics provided by scater (v1.12.2) (ref. [80]). Cells with total features by counts (number of genes) < 500 or total counts (number of UMI read counts) < 5,000 were excluded, yielding a matrix of 1,518 cells with 36,310 genes. Further analysis was implemented using Seurat (v2.3.4) (ref. [81]). Gene expression measurements for each cell were column-normalized, multiplied by the scaling factor 10,000 and transformed to log scale. Highly variable genes (8,751 genes) were detected by estimating the average expression and dispersion of each gene across all cells. PCA was applied for linear dimensional reduction. The top ten principal components and $K = 200$ were chosen for building KNN graphs followed by shared nearest-neighbor construction (ref. [82]). A modularity optimization-based algorithm was applied for cluster identification. The *t*-SNE technique was applied for illustration purposes. A Wilcoxon rank-sum test was applied for predicting marker genes with other default parameters using the function FindMarkers. Pheatmap (https://github.com/raivokolde/pheatmap) was used for heatmap visualization. Color was encoded by the *z*-score of normalized expression values derived from Seurat. Gene-set enrichment analysis was performed using clusterProfiler[83] based on the reference databases downloaded from the Molecular Signature Database (v6.2) (ref. [84]). The number of splenic OT-1 cells predicted to be allocated into each KNN single-cell cluster was calculated by projecting the percentage distribution of the

respective cluster over the total number of splenic OT-1 cells in each animal used for single-cell RNA sequencing.

For trajectory and RNA velocity analysis, the data were realigned using STAR 2.7.3a to retain splicing information for RNA velocity computation and standard quality-control measures (library size, number of features and mitochondrial reads) were evaluated to remove low-quality cells. Variance in the expression of each gene was decomposed in technical and biological variance as described in the Bioconductor scRNAseq pipeline[85], and genes with positive biological variance were retained for downstream analysis. Thirty principal components were retained and used to compute diffusion map embeddings. The three-dimensional diffusion landscapes were rotated to facilitate the comparison across conditions. Pseudotime analysis was performed by first clustering cells using the Seurat implementation of the Louvain algorithm, then running Slingshot[86]. Branches were obtained by manually annotating previously computed clusters. Pseudotime-resolved expression of transcriptome markers was obtained using a moving quantile approach over 150 cells, in which the quantile selected for each gene is adapted based on its dropout rate. RNA velocity was computed by using the stochastic version of the RNA velocity algorithm, as described in ref. [87].

### 10x Genomics-based scRNA-sequencing sample preparation and analysis

Day 4 OT-1 T cells from Lm-Ova-infected mice were obtained as outlined in the plate-based protocol described above. Around 5,000 live OT-1 T cells were used for sequencing. Gene expression libraries were prepared using the Chromium Next GEM Single Cell 3′ Reagent Kit v3.1 and 10x Chromium Controller (10x Genomics) following the manufacturer's protocol (CG000204 Rev. D). Single Index Kit T Set A was used for multiplexing (i7 index read, 8 bp). Samples were sequenced in a paired-end run (read 1, 28 bp; read 2, 91 bp) on a NovaSeq 6000 platform using S1 v1.5 (100 cycles) sequencing kits (Illumina). Bcl2fastq software (v2.20.0.422) was used for demultiplexing and generation of .fastq files allowing zero barcode mismatches.

Read alignment and gene counting were performed with 10x Genomics Cell Ranger (v6.0.1) (ref. [88]), using default parameters and pre-built mouse reference v2020-A (10x Genomics) based on mm10 GENCODE vM23/Ensembl 98. Cells with >2,000 detected genes, less than 10% of mitochondrial genes and UMI counts <3 standard deviations above the mean were kept for downstream analysis. Only genes detected in at least three cells in each sample were kept. Contaminating cells were filtered based on cluster expression of *Cd14*, *Lyz2*, *Fcgr3*, *Ms4a7*, *Fcer1g*, *Cst3*, *H2-Aa*, *Ly6d*, *Ms4a1*, *Cd19* and mitochondrial genes. Raw read count data from treatment and control replicates were merged. Merged replicates were normalized separately using the R package sctransform (v0.3.2) (ref. [89]) with the glmGamPoi method. Downstream analysis was performed with the R package Seurat (v4.0.1) (ref. [90]). Anchors between replicates were identified on the top 1,000 highly variable genes and integration was performed on the first 20 dimensions. PCA was calculated on the top 1,000 highly variable genes, and KNN graphs and uniform manifold approximation projection were computed on the first 20 PCA dimensions. Clusters were identified using the Louvain algorithm with a resolution of 0.33. Diffusion maps were calculated using the R package destiny (v3.4.0) (ref. [91]). The top 1,000 highly variable genes and the first 50 principal components were used and maps were rotated for better visualization. Transcriptional trajectory was identified using the diffusion pseudotime algorithm.

### Statistical tests

No data points were excluded. Group size was determined using a Mann–Whitney *U* test. Unpaired, two-tailed Student's *t*-test were used to calculate significance. Data distribution was assumed to be normal but this was not formally tested. *P* values < 0.05 were considered significant; $^{*}P < 0.05$, $^{**}P < 0.01$, $^{***}P < 0.001$ and $^{****}P < 0.0001$. *P* values > 0.05 were not significant. Graphs and statistical analysis were generated using Prism (GraphPad).

### Mathematical modeling

Splenic OT-1 T cells and fractions of $CD127^{+}KLRG1^{-}$ and $KLRG1^{+}CD127^{-}$ OT-1 T cells isolated at indicated time points of control (Ctrl) and leflunomide (Lefl)-treated mice were used. A branched ordinary differential equation model of $CD8^{+}$ T cell differentiation in the acute immune response was fitted to splenic data from three experimental conditions: control, leflunomide given throughout the observed time window and leflunomide given from day 4 after infection. The model describes the dynamics of the following $CD8^{+}$ T cell subsets (Extended Data Fig. 8a): activated T cell blasts, memory precursors and effector precursors (both of which are $CD127^{+}KLRG1^{-}$) as well as effector cells ($KLRG1^{+}CD127^{-}$).

The model is initialized with a fitted number of activated OT-1 cells on day 1.5 after infection in the blast compartment ($B_0$), in which the cells can proliferate with rate $\lambda_B$. From the blast cell compartment, cells can commit to either the long-lived memory or the short-lived effector branch. Differentiation of blast cells into effector T cell precursors ($TEF_p$) and memory T cell precursors ($TM_p$) is characterized by rates $\delta_{B\text{-}TEFp}$ and $\delta_{B\text{-}TMp}$, respectively. Cells in the $TEF_p$ and $TM_p$ compartments proliferate with the rates $\lambda_{TEF}$ and $\lambda_{TMp}$, respectively, until a fitted time point τ. Termination of proliferation is modeled as a logistic function $f_{AG}(t, k_m)$ and $f_{AG}(t, k_e)$ for $TEF_p$ and $TM_p$, respectively ($k_e = 10\ d^{-1}$). $TEF_p$ cells differentiate with the rate $\delta_{TEFp\text{-}TEF}$ to become effector T cells (TEF). Effector cells have a limited lifespan modeled by progression through a fixed number of 'age' states (i = 1,…6). The effect of leflunomide is modeled as a stepwise decrease in $\delta_{B\text{-}TEFp}$ with a fitted efficacy $1\text{-}\alpha_{lefl}$ and a delay of 1 d. Different modes of action of leflunomide were tested, and the best agreement with the experimental data was achieved by having leflunomide inhibit the development of effector precursors from blasts (indicated by lefl (t)). The cell numbers are described by the following set of ordinary differential Eqs. 1–7:

$$\frac{dB}{dt} = \lambda_B B - \delta_{B-TMp} B - lefl(t)\delta_{B-TEFp} B \tag{1}$$

$$\frac{dTM_p}{dt} = f_{AG}(t, k_m)\lambda_{TMp} TM_p + \delta_{B-TMp} B \tag{2}$$

$$\frac{dTEF_p}{dt} = f_{AG}(t, k_e)\lambda_{TEFp} TEF_p + lefl(t)\,\delta_{B-TEFp} B - \delta_{TEFp-TEF} TEF_p \tag{3}$$

$$\frac{dTEF_1}{dt} = \lambda_{TEF} TEF_1 + \delta_{TEFp-TEF} TEF_p - \delta_{TEF-TEF} TEF_1 \tag{4}$$

$$\frac{dTEF_i}{dt} = \lambda_{TEF} TEF_i + \delta_{TEF-TEF} TEF_{i-1} - \delta_{TEF-TEF} TEF_i \tag{5}$$

$$f_{AG}(t, k) = \frac{1}{1 + e^{k(t-\tau)}} \tag{6}$$

$$lefl(t) = \begin{cases} 1 \text{ if Ctrl} \\ \alpha_{lefl} \text{ if Lefl} \\ 1 \text{ if Lefl D4 and } t < 5 \\ \alpha_{lefl} \text{ if Lefl D4 and } t \geq 5 \end{cases} \tag{7}$$

Using Bayesian inference, the rates of cell proliferation (λs) and differentiation (δs) in the different populations were determined by fitting the model to the following experimental data: the total cell

**Table 1 | Overview of parameters for modeling data in Fig. 7**

| Parameter | Median | 95% confidence interval |
|---|---|---|
| $B_0$ | $0.8\times10^4$ | $[0.3\times10^4–4.1\times10^4]$ |
| $\lambda_B$ | $1.19\,d^{-1}$ | [0.18–1.96] |
| $\lambda_{TMp}$ | $1.76\,d^{-1}$ | [1.41–2.50] |
| $\lambda_{TEFp}$ | $3.53\,d^{-1}$ | [3.03–3.97] |
| $\lambda_{TEF}$ | $2.61\,d^{-1}$ | [0.28–3.94] |
| $\delta_{B\text{-}TMp}$ | $0.50\,d^{-1}$ | [0.03–0.97] |
| $\delta_{B\text{-}TEFp}$ | $0.22\,d^{-1}$ | [0.04–0.72] |
| $\delta_{TEFp\text{-}TEF}$ | $0.80\,d^{-1}$ | [0.4–0.9] |
| $\delta_{TEF\text{-}TEF}$ | $7.27\,d^{-1}$ | [2.8–9.9] |
| $\tau$ | 4.62 d | [4.0–5.0] |
| $\alpha_{lefl}$ | 0.03 | [0.02–0.05] |
| $\beta$ | $426\times10^4$ | $[255\times10^4–674\times10^4]$ |
| $\kappa_m$ | $0.87\,d^{-1}$ | [0.48–1.89] |

numbers (Eq. 8), the fraction of $KLRG1^+CD127^-$ cells (Eq. 9), the complementary fraction of $CD127^+KLRG1^-$ cells, and the frequency of OT-1 cells among all $CD8^+$ T cells ($N_{OTI}\beta$). Modeling was performed using Turing.jl library for probabilistic programming[92]. The parameter estimates are listed in Table 1.

$$(N_{OTI} = B + TM_p + TEF_p + \sum_{i=1}^{6} TEF_i \tag{8}$$

$$\left(\sum_{i=1}^{6} TEF_i/N_{OTI}\right) \tag{9}$$

To quantify the CFSE data, a Gaussian mixture model was fit to the kernel density estimates of log-transformed CFSE intensity distributions under control and leflunomide conditions at 2.75 and 3.75 d after infection. Mean CFSE intensity of undivided cells, common variance and the height of each Gaussian component were fitted. The individual means related to the mean of the undivided cells as follows: $\mu_i = (\mu_0 - b)\,2^{-i} + b$, where $\mu_0$ is the mean CFSE intensity of undivided cells, $\mu_i$ is the mean CFSE intensity of cells that have divided i times and b is the mean background fluorescence intensity. Mean division number $\mu_{mean}$ was obtained as follows: $\mu_{mean} = \frac{\sum_{i=0}^{j}\mu_i h_i}{\sum_{i=0}^{j} h_i}$, where $\mu_i$ is the mean CFSE intensity of cells that have divided i times, $h_i$ is the fitted height of the respective Gaussian component and *j* is the maximum number of divisions.

### Reporting summary

Further information on research design is available in the Nature Portfolio Reporting Summary linked to this article.

## Data availability

Sequencing data have been deposited in the GEO under the primary accession code GSE200360. Source data are provided with this paper. All other data supporting this study are available in the main article and Supplementary Information.

## Code availability

The code used in the manuscript for processing and analysis of next-generation sequencing data can be found at https://github.com/gpdealmeida/zehn_nat_imm_2023/, https://hoohm.github.io/dropSeqPipe/ and https://gitlab.lrz.de/ImmunoPhysio/bulkSeqPipe/.

## References


63. Kim, S. K. et al. Generation of mucosal cytotoxic T cells against soluble protein by tissue-specific environmental and costimulatory signals. *Proc. Natl Acad. Sci. USA* **95**, 10814–10819 (1998).
64. Battegay, M. et al. Quantification of lymphocytic choriomeningitis virus with an immunological focus assay in 24- or 96-well plates. *J. Virol. Methods* **33**, 191–198 (1991).
65. Heer, A. K., Harris, N. L., Kopf, M. & Marsland, B. J. $CD4^+$ and $CD8^+$ T cells exhibit differential requirements for CCR7-mediated antigen transport during influenza infection. *J. Immunol.* **181**, 6984–6994 (2008).
66. Alfei, F. et al. TOX reinforces the phenotype and longevity of exhausted T cells in chronic viral infection. *Nature* **571**, 265–269 (2019).
67. Koster, J. & Rahmann, S. Snakemake—a scalable bioinformatics workflow engine. *Bioinformatics* **34**, 3600 (2018).
68. Bolger, A. M., Lohse, M. & Usadel, B. Trimmomatic: a flexible trimmer for Illumina sequence data. *Bioinformatics* **30**, 2114–2120 (2014).
69. Dobin, A. et al. STAR: ultrafast universal RNA-seq aligner. *Bioinformatics* **29**, 15–21 (2013).
70. Anders, S., Pyl, P. T. & Huber, W. HTSeq—a Python framework to work with high-throughput sequencing data. *Bioinformatics* **31**, 166–169 (2015).
71. Ewels, P., Magnusson, M., Lundin, S. & Kaller, M. MultiQC: summarize analysis results for multiple tools and samples in a single report. *Bioinformatics* **32**, 3047–3048 (2016).
72. Love, M. I., Huber, W. & Anders, S. Moderated estimation of fold change and dispersion for RNA-seq data with DESeq2. *Genome Biol.* **15**, 550 (2014).
73. Ritchie, M. E. et al. limma powers differential expression analyses for RNA-sequencing and microarray studies. *Nucleic Acids Res.* **43**, e47 (2015).
74. Wickham, H. *ggplot2: Elegant Graphics for Data Analysis* (Springer, 2016).
75. Kolde, R. pheatmap: Pretty Heatmaps. r package version 1.0.12 . https://CRAN.R-project.org/package=pheatmap (2019).
76. Waltman, L & Jan van Eck, Nees. A smart local moving algorithm for large-scale modularity-based community detection. N.J. Eur. Phys. J. B (2013).
77. Soumillon, M., Cacchiarelli, D., Semrau, S., Oudenaarden, A. & Mikkelsen, T. S. Characterization of directed differentiation by high-throughput single-cell RNA-seq. Preprint at *bioRxiv* https://doi.org/10.1101/003236 (2014).
78. Martin, M. Cutadapt removes adapter sequences from high-throughput sequencing reads. *EMBnet Journal* https://doi.org/10.14806/ej.17.1.200 (2011).
79. Macosko, E. Z. et al. Highly parallel genome-wide expression profiling of individual cells using nanoliter droplets. *Cell* **161**, 1202–1214 (2015).
80. McCarthy, D. J., Campbell, K. R., Lun, A. T. & Wills, Q. F. Scater: pre-processing, quality control, normalization and visualization of single-cell RNA-seq data in R. *Bioinformatics* **33**, 1179–1186 (2017).
81. Satija, R., Farrell, J. A., Gennert, D., Schier, A. F. & Regev, A. Spatial reconstruction of single-cell gene expression data. *Nat. Biotechnol.* **33**, 495–502 (2015).
82. Butler, A., Hoffman, P., Smibert, P., Papalexi, E. & Satija, R. Integrating single-cell transcriptomic data across different conditions, technologies, and species. *Nat. Biotechnol.* **36**, 411–420 (2018).
83. Yu, G., Wang, L. G., Han, Y. & He, Q. Y. clusterProfiler: an R package for comparing biological themes among gene clusters. *Omics* **16**, 284–287 (2012).

84. Liberzon, A. et al. The Molecular Signatures Database (MSigDB) hallmark gene-set collection. *Cell Syst.* **1**, 417–425 (2015).
85. Amezquita, R. A. et al. Orchestrating single-cell analysis with Bioconductor. *Nat. Methods* **17**, 137–145 (2020).
86. Street, K. et al. Slingshot: cell lineage and pseudotime inference for single-cell transcriptomics. *BMC Genomics* **19**, 477 (2018).
87. Yang, X. et al. Fatty acids enhance the maturation of cardiomyocytes derived from human pluripotent stem cells. *Stem Cell Rep.* **13**, 657–668 (2019).
88. Zheng, G. X. et al. Massively parallel digital transcriptional profiling of single cells. *Nat. Commun.* **8**, 14049 (2017).
89. Hafemeister, C. & Satija, R. Normalization and variance stabilization of single-cell RNA-seq data using regularized negative binomial regression. *Genome Biol.* **20**, 296 (2019).
90. Hao, Y. et al. Integrated analysis of multimodal single-cell data. *Cell* **184**, 3573–3587 (2021).
91. Angerer, P. et al. destiny: diffusion maps for large-scale single-cell data in R. *Bioinformatics* **32**, 1241–1243 (2016).
92. Ge, H., Xu, K. & Ghahramani, Z. Turing: a language for flexible probabilistic inference. *Proc. Mach. Learn. Res.* **84**, 1682–1690 (2018).

## Acknowledgements

We thank B. Youngblood and L. Klotz for input, feedback and suggestions; H. Kohlhof and E. Peelen from Immunic Therapeutics, Gräfelfing, Germany for performing the leflunomide pharmacokinetic; M. J. Bevan, formerly University of Washington, for the permission to use a dataset generated by D.Z. in his laboratory, T. Herbinger, B. Dötterböck, W. Schmid, L. Carrie and C. Amette for technical assistance; and S. Schleicher and C. Lechner for animal husbandry. R. Thimme (University of Freiburg) for the provision of a human tetramer staining protocol. Work in the D.Z. laboratory was supported by a European Research Council starting grant (ProtecTC) and subsequently a European Research Council consolidator grant (ToCCaTa), grants from the Swiss National Science Foundation (CRSII3_160708, 310030E-164187, 51PHP0_157319 and PP00P3_144883), the Swiss Vaccine Research Institute (SVRI), grants from the German Research Foundation (DFG, SFB1054 and SFB1371) and a grant from the German Israeli Foundation (GIF no. 1440). A.M.S. is supported by European Union's Horizon 2020 research and innovation program under the Marie Skłodowska-Curie grant agreement no. 754462, by the DFG (419162346 and SFB1371), the Klaus Tschira Foundation and the German Scholars Organization (KT 34). H.A.M. is a Humboldt Postdoctoral Research Fellow sponsored by the Alexander von Humboldt Foundation. T.K. is supported by the DFG (SFB1054-B06 (ID 210592381), TRR128-A07 (ID 213904703), TRR128-A12 (ID 213904703), TRR128-Z02 (ID 213904703), TRR274-A01 (ID 408885537), TRR355-B07 (ID 490846870) and EXC 2145 (SyNergy, ID 390857198)) and by the Hertie Network of Clinical Neuroscience.

## Author contributions

S.G.O., S.S. and D.Z. initiated the study and made the primary observation. S.S., A.M.S. and D.Z. conceptualized and coordinated the full study, analyzed the data and wrote the paper, and A.M.S. and D.Z. acquired funding. S.S., S.G.O. and K.K. contributed to the design of the study. S.S. and K.K. performed the core experiments and analyzed data, while initial experiments were performed by S.G.O. Additional major experiments and data analysis were performed by A.-K.G., A.M.S., D.Z., H.A.M., J.B., L.A., L.V.D., M.v.H., T.C. and Z.E. S.S., A.M.S., C.W. and A.-K.G. generated transcriptome data. K.K., M.W., P.R., T.N., T.H. and G.P.A. performed computational and statistical analyses of the sequencing data. T.N. and T.H. performed mathematical modeling based on experimental data generated by S.S. I.K., M.J.G.T.V. and C.A.M. selected and recruited participants and L.V.D. processed and immunophenotyped the human blood. D.J.P., F.B., A.G., N.B.B., P.K., M.K., V.F., M.I., M.P., T.K. and E.L.P. provided important scientific input.

## Competing interests

The authors declare no competing interests.

## Additional information

**Extended data** is available for this paper at https://doi.org/10.1038/s41590-023-01436-x.

**Supplementary information** The online version contains supplementary material available at https://doi.org/10.1038/s41590-023-01436-x.

**Correspondence and requests for materials** should be addressed to Anna M. Schulz or Dietmar Zehn.

**Peer review information** *Nature Immunology* thanks Katherine Kedzierska and the other, anonymous, reviewer(s) for their contribution to the peer review of this work. Primary Handling Editor: N. Bernard, in collaboration with the *Nature Immunology* team.

https://doi.org/10.1038/s41590-023-01436-x

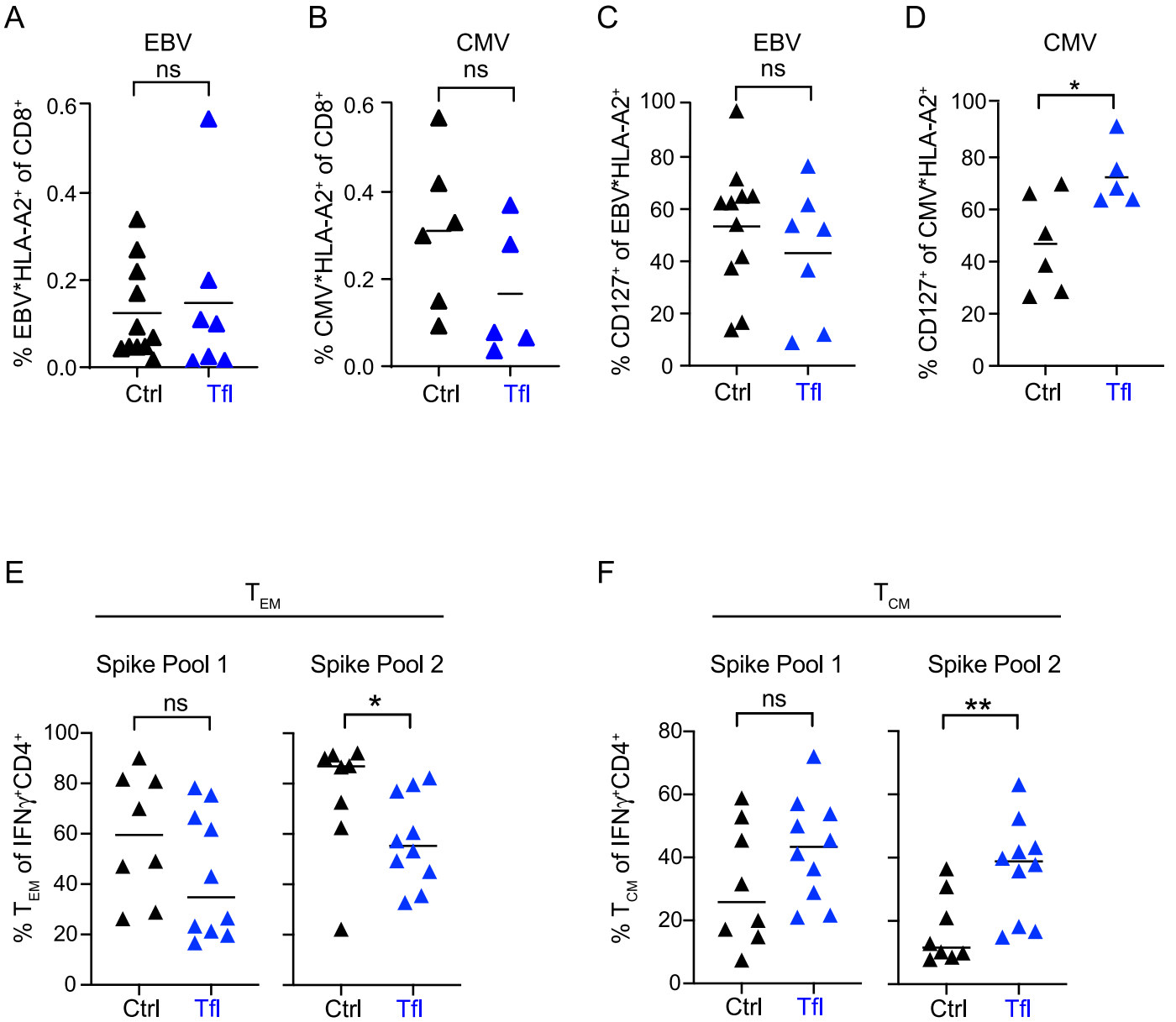


**Extended Data Fig. 1 | Phenotypes of T cells in DHODH inhibitor treated patients. A–D**, peripheral mononuclear cells were obtained from HLA-A2 positive patients with multiple sclerosis that were long-term treated with teriflunomide (Tfl) or without (Ctrl). Donors were stained with HLA-A2 multimers loaded with the EBV peptide GLCTLVAML (**A**, **C**) or CMV NLVPMVATV (**B**, **D**) peptide. Shown are the frequencies of multimer positive cells among total $CD8^+$ T cells (**A**, **B**) and the percentages of multimer positive $CD8^+$ T cells that express CD127 (**C**, **D**). **E** and **F**, blood samples from healthy controls (Ctrl) and Teriflunomide (Tfl) treated patients were obtained 14 days after applying the $2^{nd}$ dose of the Bnt162b2 mRNA vaccine. Isolated PBMC's were stimulated with overlapping peptide pools of the SARS-CoV-2 spike protein. Shown are the frequencies of IFNγ positive $CD4^+$ T cells that bear a $CD45RA^-/CCR7^-$ effector memory ($T_{EM}$) phenotype (**E**) or $CD45RA^-/CCR7^+$ central memory ($T_{CM}$) phenotype (**F**). n = 8 for Ctrl or n = 10 for Tfl treated patients. Symbols represent throughout individual patients and the line the mean of the group. Two-tailed, unpaired t-tests were performed to calculate significance with *$p < 0.05$, **$p < 0.01$, and ns=not significant ($p > 0.05$). Supplementary Fig. 7–9 contain gating information.

https://doi.org/10.1038/s41590-023-01436-x

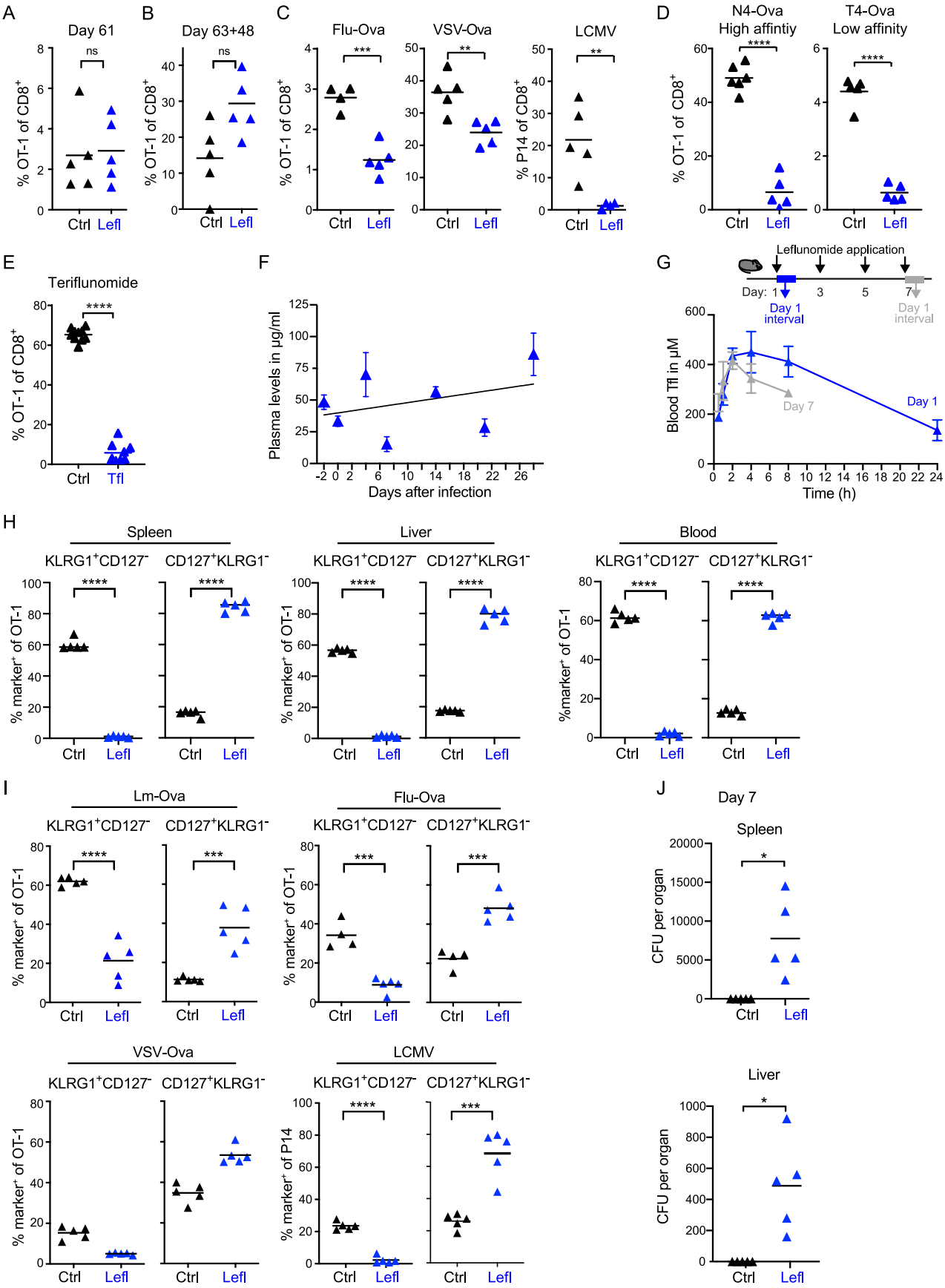


**Extended Data Fig. 2 | See next page for caption.**

https://doi.org/10.1038/s41590-023-01436-x

**Extended Data Fig. 2 | Suppression of pyrimidine synthesis blocks effector T cells in various infections. A-E**, similarly as indicated in Fig. 1, mice received a low dose of CD45.1 congenic OT-1 or P14, Leflunomide (Lefl) or Teriflunomide (Tfl), and either an infection with Lm-Ova, Ovalbumin expressing Influenza (Flu-OVA), Ovalbumin expressing Vesicular stomatitis virus (VSV-OVA), wildtype Lymphocytic choriomeningitis virus (LCMV), and recombinant Listeria monocytogenes expressing Ovalbumin encoding the high affinity ligand (Lm-N4) or a low affinity altered peptide ligand (Lm-T4). **A**, frequency of OT-1 T cells among total blood $CD8^+$ T cells 61 days post Lm-Ova infection. **B**, memory OT-1 T cells were isolated from a different experiment from control and Leflunomide treated mice on day 63 and transferred into naïve hosts. These hosts were then infected with Lm-Ova. Depicted are secondary memory OT-1 at 48 days after the Lm-Ova challenge (note that data are derived from the same experiment shown in Fig. 1f). The further plots show: **C**, the frequencies of OT-1 among total splenic $CD8^+$ T cells on day 7 after the indicated infections, **D**, after high or low affinity stimulation, and **E**, under Teriflunomide instead of Leflunomide treatment in an Lm-Ova infection. **F**, Teriflunomide plasma levels determined over a 28-day period in mice that were treated with Leflunomide as indicated in Fig. 1a. **G**, Pharmacokinetic of Teriflunomide in the blood one day after a single dose injection of Leflunomide (Blood Day 1), or on day 7 after applying the treatment regime shown in the scheme (Blood Day 7). **H**, corresponding to the setup explained in A-E, day 7 OT-1 T cells obtained from different organs from Lm-Ova infected mice were analyzed for KLRG1 and CD127 expression. **I**, similar analysis for day 7 splenic OT-1 or P14 obtained from the indicated infections. **J**, spleens and livers from Lm-Ova infected Leflunomide treated and control mice were analyzed for bacteria load on day 7 post infection. Symbols represent individual mice, the line the mean of a group. A linear regression analysis is shown in **F**. Symbols in **F** and **G** show the mean of a group and error bars represent standard deviation (SD). n = 3 (**F** and **G**), or 5-10 (**A-E** and **H-J**) mice per group. All infection experiments were performed at least two times. Two-tailed, unpaired t-tests were performed to calculate significance with $^*p < 0.05$, $^{**}p < 0.01$, $^{***}p < 0.001$, $^{****}p < 0.0001$, and ns=not significant ($p > 0.05$). Supplementary Fig. 10 contains gating information.

https://doi.org/10.1038/s41590-023-01436-x

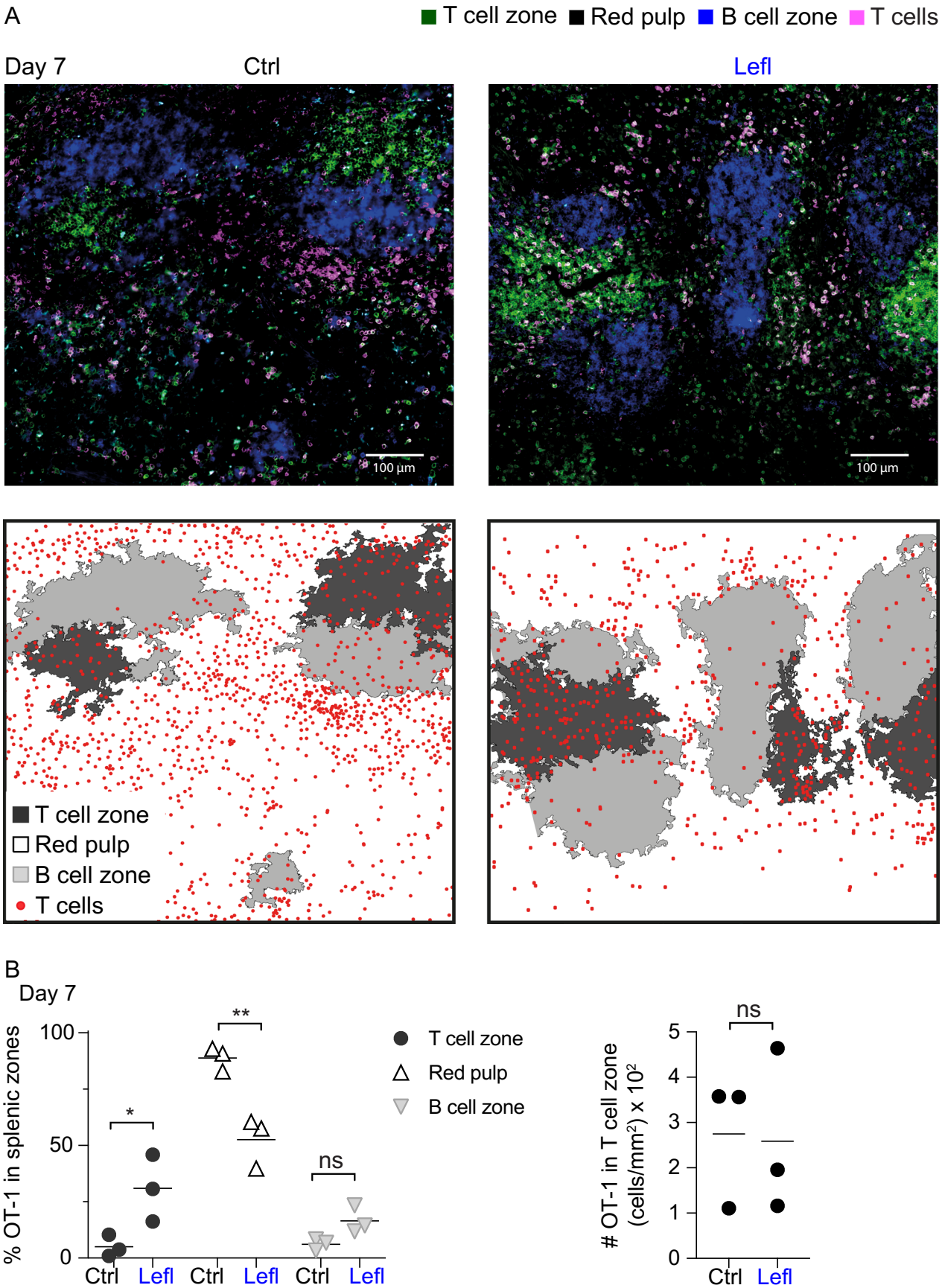


**Extended Data Fig. 3 | See next page for caption.**

https://doi.org/10.1038/s41590-023-01436-x

**Extended Data Fig. 3 | Pyrimidine starvation confines antigen-specific T cells to the splenic T cell zone.** Mice were engrafted with a low number of CD45.1$^+$ congenic OT-1 T cells, infected with Lm-Ova, and treated with (Lefl) and without Leflunomide (Ctrl). Spleens were harvested 7 days post infection. **A**, upper panels show splenic sections stained with B220 (blue), CD3 (green), and CD45.1 (red). Lower panels show vectored images, which display the localization of individual OT-1 in red. **B**, the graphs show the relative distribution of OT-1 in the three anatomical locations and the total OT-1 numbers per mm$^2$ in the indicated anatomical location. Data points represent individual mice, center line shows the mean. Data are representative of n = 3 (Ctrl) and n = 3 (Lefl) mice. Two-tailed, unpaired t-tests were performed to calculate significance with *$p < 0.05$, ** $p < 0.01$, and ns=not significant ($p > 0.05$).

https://doi.org/10.1038/s41590-023-01436-x

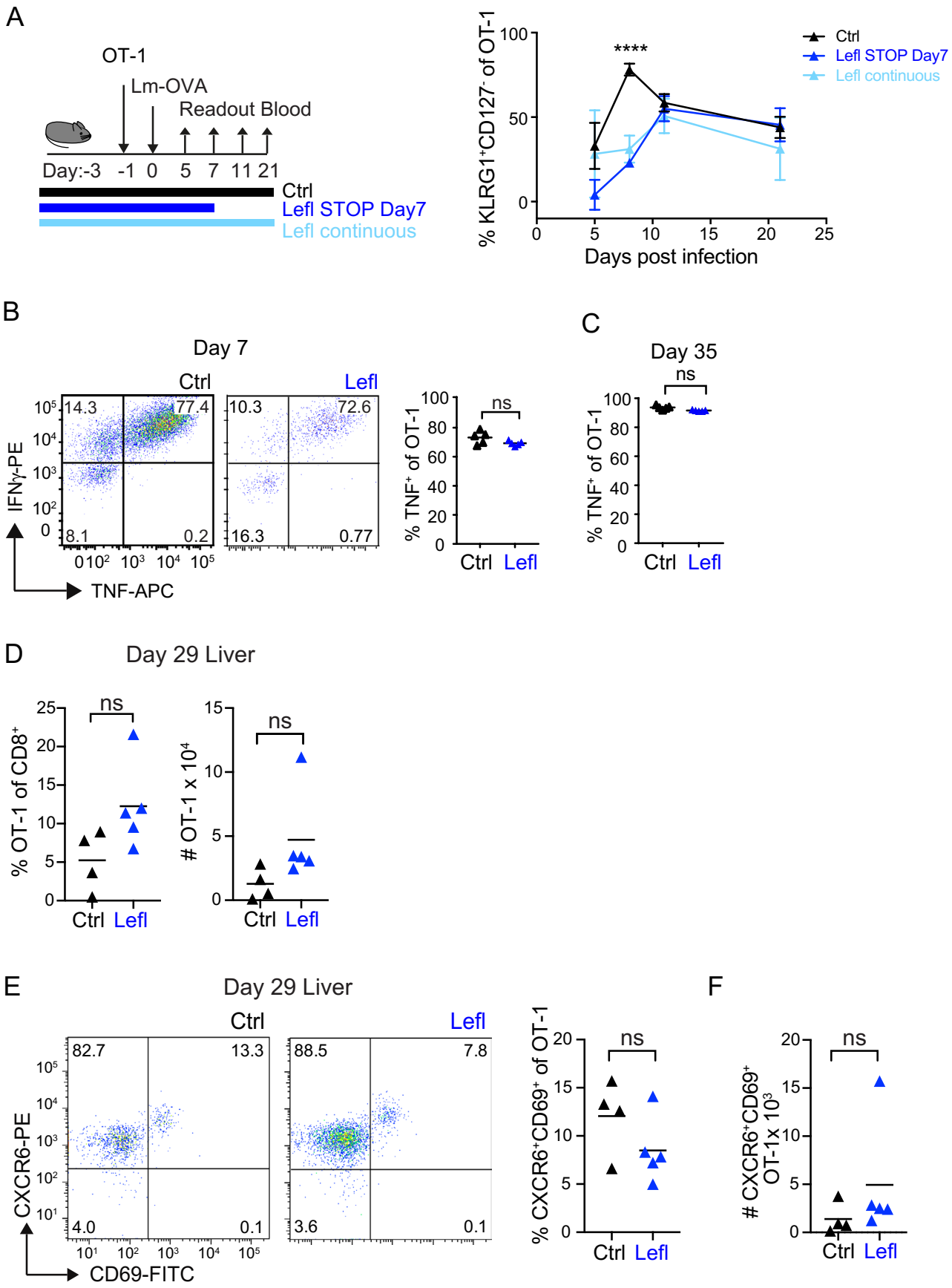


**Extended Data Fig. 4 | See next page for caption.**

https://doi.org/10.1038/s41590-023-01436-x

**Extended Data Fig. 4 | Extended phenotyping of OT-1 T cells activated in the presence of leflunomide. A**, schematic representation of the experimental setup and treatment scheme: Naïve control (Ctrl) or leflunomide (Lefl STOP Day 7 and Lefl continuous) treated host mice received $1 \times 10^4$ naïve OT-1 and were infected with Lm-Ova. Data graph shows the frequency of KLRG1$^+$ CD127$^-$ OT-1 at 5, 8, 11 and 21 days post infection. **B, C**, OT-1 T cells isolated at 7 and 35 days post infection from control (Ctrl) and leflunomide (Lefl) treated Lm-Ova infected mice. Cells were briefly *ex vivo* re-stimulated with Ova-peptide in the presence of brefeldin A and then stained intracellularly for IFNγ and TNF. Representative dot plots are shown. The scatter plots depict all mice per group in the shown representative experiment. **D-F**, Naïve host mice received a low number of naïve OT-1 and the hosts were infected with Lm-Ova. Cells from the liver were recovered at 29 days post infection post liver perfusion. Data graphs showing the frequencies of OT-1 among total CD8$^+$ T cells and total OT-1 numbers in the liver (**D**). Representative flow cytometry dot plots and data graphs showing the frequencies of CXCR6$^+$ CD69$^+$ OT-1 on day 29 post infection (**E**) and the total number of total CXCR6$^+$ CD69$^+$ OT-1 in the liver (**F**). The scatter plots depict all mice per group in the shown representative experiment. Symbols in **A** represent the mean of the group, in **B-F** individual mice and the lines the mean of a group. Error bars in **A** show the standard deviation (SD). n = 5 mice per group in **A-C** and n = 4 (Ctrl) and n = 5 (Lefl) mice in **D-F**. Data are representative of 2 independent experiments. Two-tailed, unpaired t-tests were performed to calculate significance with ***$p < 0.001$, and ns=not significant ($p > 0.05$). Supplementary Fig. 11 contains gating information.

https://doi.org/10.1038/s41590-023-01436-x

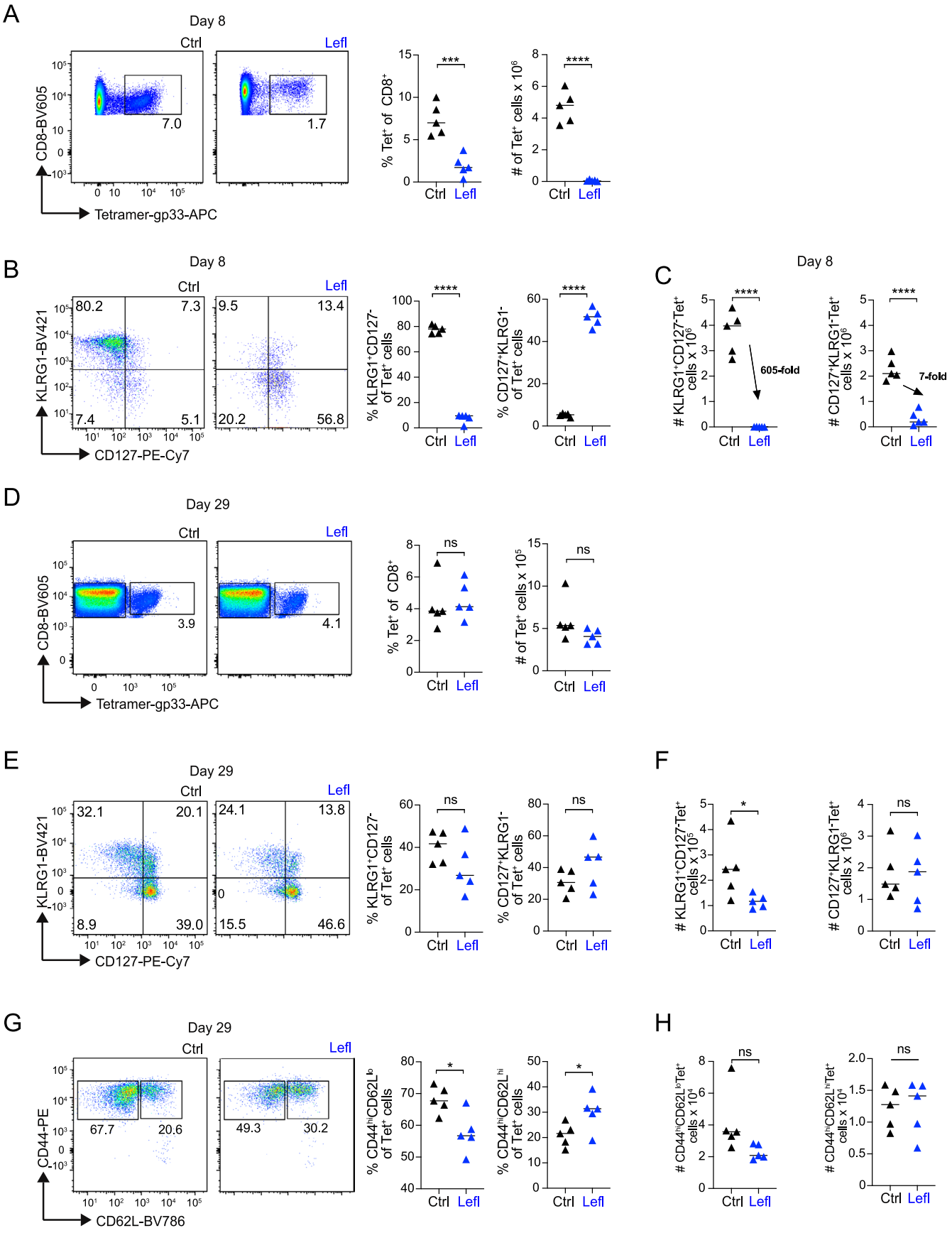


**Extended Data Fig. 5 | See next page for caption.**

https://doi.org/10.1038/s41590-023-01436-x

**Extended Data Fig. 5 | Leflunomide reduces endogenous, pathogen-specific effector T cells.** Naïve host mice were infected with LCMV Armstrong and the endogenous T cell response in the spleen was analyzed using Tetramer-gp33 staining on day 8 and day 29 post infection. **A**, representative flow cytometry dot plots and data graphs showing the frequency, and total numbers, of splenic Tetramer-gp33$^+$ CD8$^+$ T cells on day 8 post infection. **B**, representative flow cytometry dot plots and data graphs showing the frequencies of KLRG1$^+$ CD127$^-$ and CD127$^+$ KLRG1$^-$ T cells within the Tetramer$^+$ population on day 8 post infection. **C**, data graphs showing the total number of KLRG1$^+$ CD127$^-$ and CD127$^+$ KLRG1$^-$T cells within the Tetramer$^+$ population on day 8 post infection. The arrows and values indicate the fold reduction of T cell numbers in Leflunomide treated group as compared to the control treated group. **D**, representative flow cytometry dot plots and data graphs showing the frequency and total numbers of splenic Tetramer$^+$ T cells on day 29 post infection. **E**, Representative flow cytometry dot plots and data graphs showing the frequencies of KLRG1$^+$ CD127$^-$ and CD127$^+$ KLRG1$^-$ T cells within the Tetramer$^+$ population on day 29 post infection. **F**, data graphs show the total number of KLRG1$^+$ CD127$^-$ and CD127$^+$ KLRG1$^-$T cells within the Tetramer$^+$ population on day 29 post infection. **G, H**, representative flow cytometry plots and data graphs showing the frequencies **(G)** and total numbers **(H)** of CD44$^+$ CD62L$^-$ and CD44$^+$ CD62L$^+$ T cells within the Tetramer$^+$ population on day 29 post infection. The scatter plots depict all mice per group, with n = 5. Symbols represent throughout individual mice and the line the mean of a group. Two-tailed, unpaired t-tests were performed to calculate significance with *$p < 0.05$, *** $p < 0.001$, ****$p < 0.0001$, and ns=not significant ($p > 0.05$). Supplementary Fig. 12 contains gating information.

https://doi.org/10.1038/s41590-023-01436-x

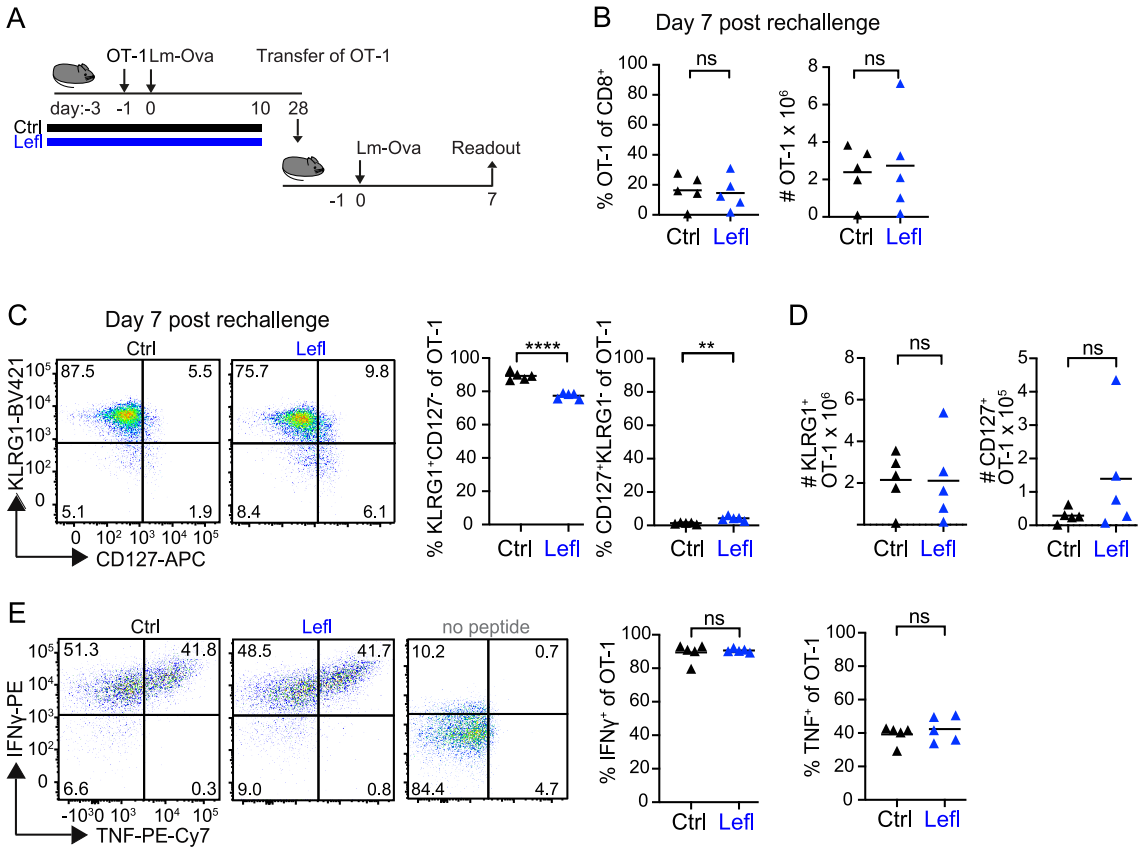


**Extended Data Fig. 6 | T cells from leflunomide treated and untreated mice secrete cytokines similarly in recall responses. A**, schematic representation of the experimental setup of the recall experiment: Primary, naïve control (Ctrl) or leflunomide (Lefl) treated host mice received a low number of naïve OT-1 and were infected with Lm-Ova. After 28 days, memory OT-1 were recovered from the spleen and transferred into untreated, naïve secondary hosts, which were subsequently infected with Lm-Ova. **B**, data graphs show the frequencies of OT-1 among total $CD8^+$ T cells, and total OT-1 numbers, recovered from the spleen of secondary host mice on day 7 post infection. **C, D**, representative flow cytometry dot plots and data graphs showing the frequencies **(C)** and numbers **(D)** of $KLRG1^+$ $CD127^-$ and $CD127^+$ $KLRG1^-$ OT-1 from secondary host mice on day 7 post infection. **E**, representative flow cytometry dot plots and data graphs showing the frequencies of cytokine-producing $IFN\gamma^+$ and $TNF^+$ OT-1 from secondary host mice on day 7 post Lm-Ova infection, after a brief *ex vivo* re-stimulation with or without Ova peptide in the presence of brefeldin A followed by intracellular cytokine staining. The scatter plots depict all mice per group. Symbols represent throughout individual mice, lines the mean of a group. n = 5 mice per group. Data are representative of 2 independent experiments. Two-tailed, unpaired t-tests were performed to calculate significance with $^{**}p < 0.01$ and $^{****}p < 0.0001$, and ns=not significant ($p > 0.05$). Supplementary Fig. 13 contains gating information.

https://doi.org/10.1038/s41590-023-01436-x

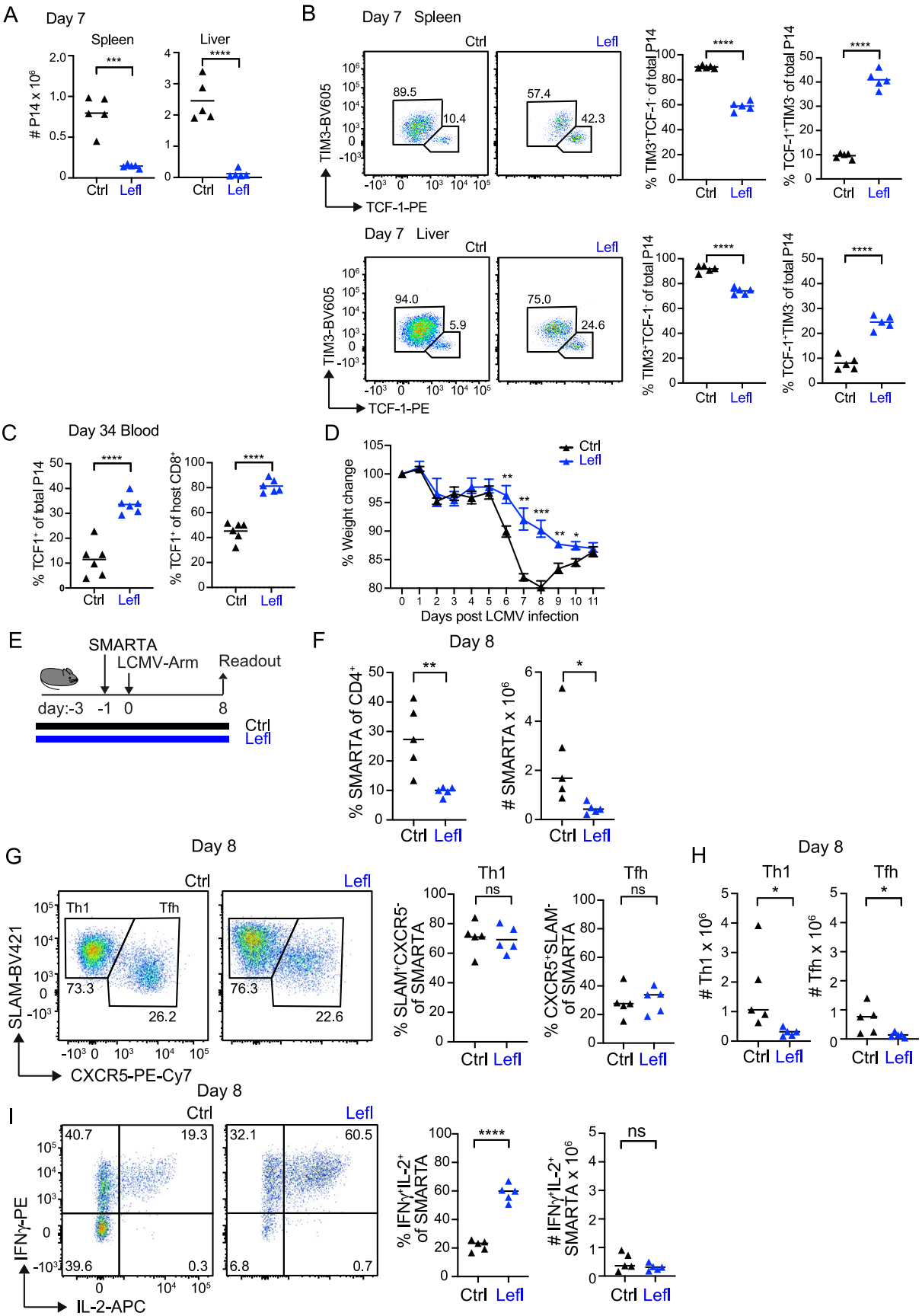


**Extended Data Fig. 7 | See next page for caption.**

https://doi.org/10.1038/s41590-023-01436-x

**Extended Data Fig. 7 | Leflunomide reduces weight in chronic infections and CD4 T cells in acute LCMV infections.** Mice received leflunomide treatments between days -3 and 5 every other day and on day 0 a LCMV docile (**A, B**), or clone 13 (**C, D**) infection. **A**, total numbers of P14 7 days post infection. **B**, representative flow plots show the frequencies of P14 expressing TIM3 or TCF-1 in spleen and liver. Diagrams show the frequencies of $TIM3^+$ $TCF\text{-}1^-$ and $TCF\text{-}1^+$ $TIM3^-$ P14 T cells in spleen (upper panel) and liver (lower panel). **C**, Diagrams show the frequencies of $Tcf1^+$ P14 (left panel) and $TCF\text{-}1^+CD8^+$ host cells (left panel) in the blood of mice that have been treated with or without leflunomide every other day. **D**, body weight curves of up to day 5 treated and untreated LCMV clone 13 infected mice. **E**, schematic illustration of the experimental setup used in **F-I**: Naïve control (Ctrl) or leflunomide (Lefl) treated host mice received $3 \times 10^3$ SMARTA T cells and were infected with $2 \times 10^5$ pfu LCMV Armstrong. Mice were analyzed 8 days post infection. **F**, data graphs show the frequencies of SMARTA T cells among total $CD4^+$ cells and total SMARTA numbers in the spleen. **G**, representative flow cytometry plots and data graphs showing the frequencies and **H**, total numbers of $SLAM^+CXCR5^-$ Th1 and $SLAM^-CXCR5^+$ Tfh cells. **I**, representative flow cytometry dot plots and data graphs showing the frequencies and numbers of cytokine-producing $IFN\gamma^+IL\text{-}2^+$ SMARTA T cells. The scatter plots depict all mice per group. Symbols in **A**-**C** and **F**-**I** represent individual mice and in **D** the mean of a group. Error bars in **D** represent the standard error of the mean of five biological replicates. The line in **A**-**C** and **F**-**I** represents the mean of the group. n = 5 (**A**, **B** and **F**-**I**) and n = 6 (**C**) mice per group. Two-tailed, unpaired t-tests were performed to calculate significance with $*p < 0.05$, $**p < 0.01$, $***p = 0.001$, $****p = 0.0001$, and ns=not significant ($p > 0.05$). Supplementary Fig. 14 contains gating information.

https://doi.org/10.1038/s41590-023-01436-x

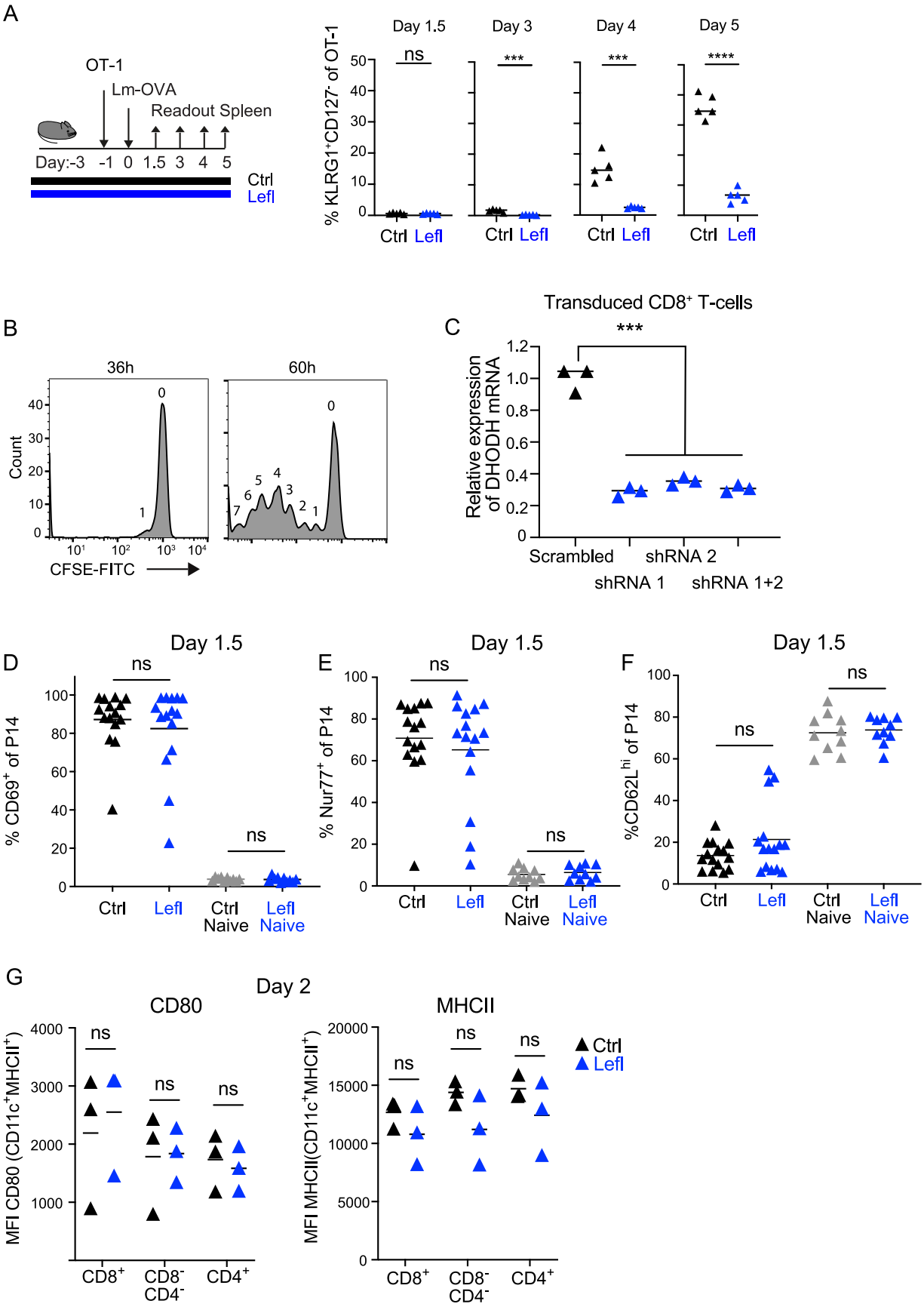


**Extended Data Fig. 8 | See next page for caption.**

https://doi.org/10.1038/s41590-023-01436-x

**Extended Data Fig. 8 | OT-1 T cells expansion kinetics and DC maturation under leflunomide treatment. A**, schematic representation of the experimental setup: Primary, naïve control (Ctrl) or leflunomide (Lefl) treated host mice received $3 \times 10^5$ (Day 1.5), $1 \times 10^5$ (Day 3 and Day 4), or $2 \times 10^4$ (Day 5) naïve OT-1 and were infected with Lm-Ova. Data graphs show the frequency of $KLRG1^+CD127^-$ OT-1 on Day 1.5, 3, 4 and 5 post infection. **B**, in order to assess the time point, when OT-1 start to proliferate in a Listeria infection, naïve host mice received $10^6$ naïve, CFSE labeled OT-1 and the hosts were infected with Lm-Ova. OT-1 were recovered at 36 and 60 h post infection from spleen and analyzed by flow cytometry. Histograms show representative CFSE dilution profiles, where numbers indicate the division. Scatter plots in (**A**) depict all mice per group in the shown representative experiment. **C**, relative expression of DHODH mRNA relative to 18 S mRNA in $CD8^+$ T cells sorted for Ametrine expression 48 hours after transduction with either the retroviral construct for Scrambled, DHODH shRNA 1, 2 or 1 + 2 as determined by qPCR. The scatter plot depicts three technical replicates per group in the shown representative experiment. **D**-**F**, mice were treated without (Ctrl) or with leflunomide (Lefl), infected with LCMV Armstrong and analyzed for TCR signaling in Nur77 transgenic P14 T cells 1.5 days post infection. Data graphs show the percentages of $CD69^+$ (**D**), $Nur77^+$ (**E**) and $CD62L^{hi}$ (**F**) P14. **G**, splenic DCs were analyzed for the activation markers CD80 and MHCII from control (Ctrl) and leflunomide (Lefl) treated mice 2 days post Lm-OVA infection. Data in **A** and B are representative for at least 2 individual experiments with n = 5 mice (**A**) and n = 3 mice (**B**) per group. Symbols in **C** represent technical replicates or individual mice (**D**-**G**), and the line the mean of a group (**D**-**G**). n = 15 mice per group for infected Ctrl and Lefl and n = 10 mice per group for Ctrl naïve and Lefl naïve (**D**-**F**), and n = 3 mice per group (**G**). Two-tailed, unpaired t-tests were performed to calculate significance with ***p = 0.001, ****p = 0.0001, and ns=not significant ($p > 0.05$). Supplementary Fig. 15 contains gating information.

https://doi.org/10.1038/s41590-023-01436-x

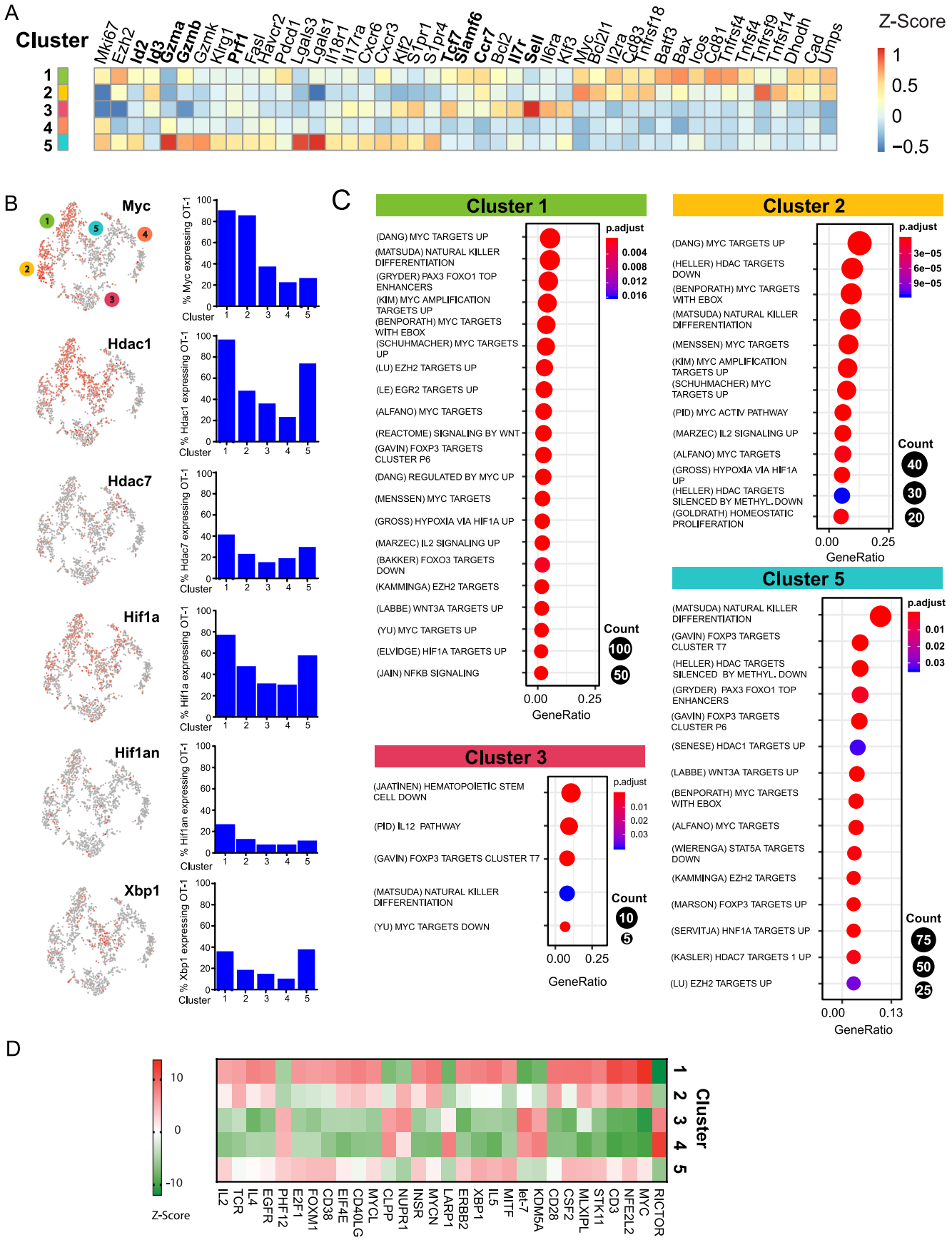


**Extended Data Fig. 9 | See next page for caption.**

https://doi.org/10.1038/s41590-023-01436-x

**Extended Data Fig. 9 | Single-cell transcriptomic data of leflunomide treated and untreated cells.** The analysis relates to Fig. 5. **A**, heatmap depicting the cluster specific expression of selected genes among the clusters. **B**, tSNE plots with overlaid expression of predicted upstream regulators in red. Each dot represents a cell. Bar graphs show the percentage of cells expressing the respective upstream regulators in each predicted cluster. **C**, plots depict an enrichment analysis for gene sets controlled by upstream regulators. p-values were adjusted using Benjamini & Hochberg method. **D**, heatmap shows the cluster resolved activity of the top 30 upstream regulators. Upstream regulators were in both cases predicted by Ingenuity Pathway Analysis (QIAGEN IPA).

https://doi.org/10.1038/s41590-023-01436-x

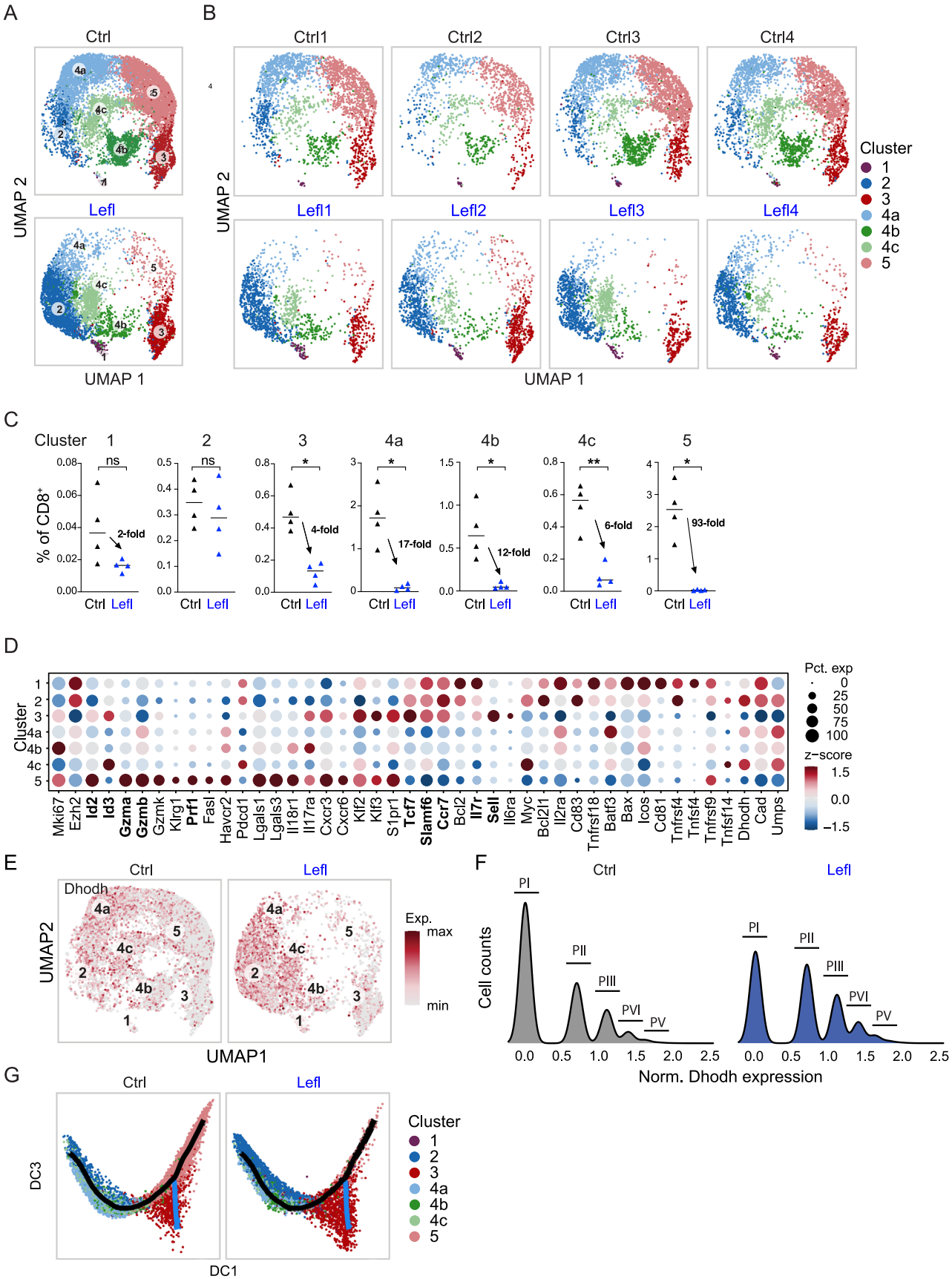


**Extended Data Fig. 10 | See next page for caption.**

https://doi.org/10.1038/s41590-023-01436-x

**Extended Data Fig. 10 | Reproduction of single-cell transcriptomic data after leflunomide treated. A** and **B**, louvain clusters depicted in the reduced space calculated by UMAP for control (Ctrl) and leflunomide (Lefl) treated mice from 4 biological replicates each. Overlays of all 4 replicates (**A**) and individual sample (**B**) data are presented. **C**, frequencies of the respective clusters of OT-1 T cells defined in A within in the total $CD8^+$ population. **D**, frequencies of cells expressing the indicated genes (circle size) and their respective scaled expression levels (color intensity) in each cluster. **E**, *Dhodh* expression levels depicted over the reduced space calculated by UMAP for control (Ctrl) and leflunomide (Lefl) treated mice. **F**, frequency histogram representing the distribution of *Dhodh* expression levels in cells from control (Ctrl) and leflunomide (Lefl) treated mice. **G**, developmental trajectories for effector and memory branches depicted over the diffusion map for each condition. Cells are colored according to the clustering. Each dot in **A**, **B**, **E** and **G** represents a cell. Symbols in **C** represent individual mice, n = 4 mice per group, and the conditions in **C** were compared for each cluster using two-tailed, unpaired t-tests with $^*p < 0.05$, $^{**}p < 0.01$, and ns=not significant ($p > 0.05$).

nature portfolio

Corresponding author(s): Anna Schulz, Dietmar Zehn

Last updated by author(s): Jan 31, 2023

# Reporting Summary

Nature Portfolio wishes to improve the reproducibility of the work that we publish. This form provides structure for consistency and transparency in reporting. For further information on Nature Portfolio policies, see our Editorial Policies and the Editorial Policy Checklist.

## Statistics

For all statistical analyses, confirm that the following items are present in the figure legend, table legend, main text, or Methods section.

| n/a | Confirmed | |
|---|---|---|
| ☐ | ☒ | The exact sample size (*n*) for each experimental group/condition, given as a discrete number and unit of measurement |
| ☐ | ☒ | A statement on whether measurements were taken from distinct samples or whether the same sample was measured repeatedly |
| ☐ | ☒ | The statistical test(s) used AND whether they are one- or two-sided<br>*Only common tests should be described solely by name; describe more complex techniques in the Methods section.* |
| ☒ | ☐ | A description of all covariates tested |
| ☒ | ☐ | A description of any assumptions or corrections, such as tests of normality and adjustment for multiple comparisons |
| ☐ | ☒ | A full description of the statistical parameters including central tendency (e.g. means) or other basic estimates (e.g. regression coefficient) AND variation (e.g. standard deviation) or associated estimates of uncertainty (e.g. confidence intervals) |
| ☐ | ☒ | For null hypothesis testing, the test statistic (e.g. *F*, *t*, *r*) with confidence intervals, effect sizes, degrees of freedom and *P* value noted<br>*Give P values as exact values whenever suitable.* |
| ☒ | ☐ | For Bayesian analysis, information on the choice of priors and Markov chain Monte Carlo settings |
| ☒ | ☐ | For hierarchical and complex designs, identification of the appropriate level for tests and full reporting of outcomes |
| ☒ | ☐ | Estimates of effect sizes (e.g. Cohen's *d*, Pearson's *r*), indicating how they were calculated |

*Our web collection on statistics for biologists contains articles on many of the points above.*

## Software and code

Policy information about availability of computer code

| | |
|---|---|
| Data collection | Detailed descriptions on data handling are provided in the methods section of the manuscript. |
| Data analysis | The following software and packages were used:<br>- FlowJo (TreeStar, BD) Version 10<br>https://www.flowjo.com/solutions/flowjo<br><br>- Prism (GraphPad) versions 7-9<br>https://www.graphpad.com/scientific-software/prism/<br><br>- Cutadapt v1.16<br>Martin, M. Cutadapt removes adapter sequences from high-throughput sequencing reads. EMBnet.journal; Vol 17, No 1: Next Generation Sequencing Data AnalysisDO - 10.14806/ej.17.1.200 (2011).<br><br>- bbmap v38.22<br>https://jgi.doe.gov/data-and-tools/software-tools/bbtools/<br><br>- STAR v2.5.3a annotation release #91 and genome build #38 from Mus musculus (Ensembl) and STAR 2.7.3a<br>Dobin, A., Davis, C.A., Schlesinger, F., Drenkow, J., Zaleski, C., Jha, S., Batut, P., Chaisson, M. & Gingeras, T.R. STAR: ultrafast universal RNA-seq aligner. Bioinformatics 29, 15-21 (2013).<br><br>- scater v1.12.2 |

McCarthy, D.J., Campbell, K.R., Lun, A.T. & Wills, Q.F. Scater: pre-processing, quality control, normalization and visualization of single-cell RNA-seq data in R. Bioinformatics 33, 1179-1186 (2017).

- Seurat v2.3.4 and Seurat v4.0.1
Hao, Y., Hao, S., Andersen-Nissen, E., Mauck, W.M., 3rd, Zheng, S., Butler, A., Lee, M.J., Wilk, A.J., Darby, C., Zager, M., Hoffman, P., Stoeckius, M., Papalexi, E., Mimitou, E.P., Jain, J., Srivastava, A., Stuart, T., Fleming, L.M., Yeung, B., Rogers, A.J., McElrath, J.M., Blish, C.A., Gottardo, R., Smibert, P. & Satija, R. Integrated analysis of multimodal single-cell data. Cell 184, 3573-3587.e3529 (2021).

- Pheatmap
https://github.com/raivokolde/pheatmap

- Molecular Signature Database (MSigDB) V6.2
https://www.gsea-msigdb.org/gsea/msigdb/

- Bioconductor scRNAseq pipeline
https://bioconductor.org/packages/release/data/experiment/html/scRNAseq.html

- 10x Genomics Cell-Ranger v6.0.1, pre-built mouse reference v2020-A (10x Genomics) based on mm10 - GENCODE vM23/Ensembl 98
https://support.10xgenomics.com/single-cell-gene-expression/software/pipelines/latest/installation

- sctransform v0.3.2
Hafemeister, C. & Satija, R. Normalization and variance stabilization of single-cell RNA-seq data using regularized negative binomial regression. Genome Biol 20, 296 (2019).

- destiny v3.4.0
Angerer, P., Haghverdi, L., Büttner, M., Theis, F.J., Marr, C. & Buettner, F. destiny: diffusion maps for large-scale single-cell data in R. Bioinformatics 32, 1241-1243 (2016).

The code used in the manuscript for processing and analysis of NGS data can be found under: https://github.com/gpdealmeida/zehn_nat_imm_2023/, https://hoohm.github.io/dropSeqPipe/), and https://gitlab.lrz.de/ImmunoPhysio/bulkSeqPipe/.

For manuscripts utilizing custom algorithms or software that are central to the research but not yet described in published literature, software must be made available to editors and reviewers. We strongly encourage code deposition in a community repository (e.g. GitHub). See the Nature Portfolio guidelines for submitting code & software for further information.

## Data

Policy information about availability of data

All manuscripts must include a data availability statement. This statement should provide the following information, where applicable:

- Accession codes, unique identifiers, or web links for publicly available datasets
- A description of any restrictions on data availability
- For clinical datasets or third party data, please ensure that the statement adheres to our policy

All gene expression data (next generation sequencing and single cell sequencing) will be made accessible to the general public prior to submission of the final manuscript.

## Human research participants

Policy information about studies involving human research participants and Sex and Gender in Research.

| | |
|---|---|
| Reporting on sex and gender | Patients and healthy volunteers were recruited irrespectively of gender and age and solely based on availability.<br>We will update the information about gender and age. |
| Population characteristics | Study of CMV and EBV T cell responses in Teriflunomide treated MS patients: We recruited MS patients with and without Teriflunomide treatment based on availability and the agreement to participate in the study. Donors were screened for the presence of the HLA-A*0201 allele. For technical reasons (availability of suitable peptide MHC multimers) only HLA-A0201 positive donors could be included into the study.<br><br>Patient information EBV/CMV study:<br>- Control EBV: #1 female 56 years, #2 female 51years, #3 female 28 years, #4 male 34 years, #5 female 29 years, #6 female 38 years, #7 female 44 years, #8 male years 45, #9 male 46years, #10 female 35 years, #11 male 34 years<br>- Teriflunomide EBV: #1 male 35 years, #2 male 21 years, #3 male 27 years, #4 female 67 years, #5 female 51 years, #6 female 52 years, #7 female 34 years<br>- Control CMV: #1 male 38 years, #2 female 29 years, #3 female 38 years, #4 female 44 years, #5 male 46 years, #6 male 34 years<br>- Teriflunomide CMV: #1 male 35 years, #2 male 52 years, #3 female 67 years, #4 female 51 years, #No. 5 female 52 years.<br><br>Study of SARS-CoV2 vaccine specific T cell responses in Leflunomide treated MS patients and healthy volunteers: We randomly recruited MS patients that receive Leflunomide treatment based on availability and the agreement to participate in the study. Similarly, we randomly recruited healthy among the personal of the Technical University of Munich based on availability and the agreement to participate in the study. |

| | |
|---|---|
| | Patient information SARS-CoV2 study:<br>- Healthy controls: #1 male 57 years, #2 male 64 years, #3 female 51 years, #4 male 53 years, #5 male 29 years, #6 male 28 years, #7 female 29 years, #8 male 45 years<br>- Teriflunomide MS patients: #1 female 45 years, #2 female 40 years, #3 male 53 years, # 4female 43 years, #5 female 58 years, # 6 male 49 years, #7 male 41 years, #8 female unknown, #9 male 54 years, #10 male 50 years. |
| Recruitment | Study of CMV and EBV T cell responses in Teriflunomide treated or untreated MS patients were recruited out of patients visiting the Department of Neurology of the Klinikum Rechts der Isar or among the patients of Dr. Kleiter (Behandlungszentrum Kempfenhausen für Multiple Sklerose Kranke, gemeinnützige GmbH, Berg, Germany).<br><br>Study of SARS-CoV2 vaccine specific T cell responses in Leflunomide treated MS patients and healthy volunteers: Donors were recruited out of patients visiting the Neurological practice "Neurologische Gemeinschaftspraxis am Kaiserplatz" of Dr. C. Mayer, Kaiserstraße 14, 60311 Frankfurt, Germany. Healthy control were recruited among personal of the Technical University of Munich that responded to local announcements for participation in our study.<br><br>For both studies, we can exclude a self-selection bias as we included all available participants and because specific outcomes were not foreseeable when the patients or healthy volunteers were recruited. |
| Ethics oversight | The study was approved by the ethics board of the Klinikum Rechts der Isar. Written consent was obtained from all patients that donated blood samples for the study. |

Note that full information on the approval of the study protocol must also be provided in the manuscript.

# Field-specific reporting

Please select the one below that is the best fit for your research. If you are not sure, read the appropriate sections before making your selection.

☒ Life sciences ☐ Behavioural & social sciences ☐ Ecological, evolutionary & environmental sciences

For a reference copy of the document with all sections, see nature.com/documents/nr-reporting-summary-flat.pdf

# Life sciences study design

All studies must disclose on these points even when the disclosure is negative.

| | |
|---|---|
| Sample size | Sample size was in mouse experiments determined based on a statistical report utilizing Mann-Whitney U Test. |
| Data exclusions | No data were excluded from the analysis. |
| Replication | Reproducibility of mouse experiments was ensured by choosing a group size based on a statistical report written by our statistician. Experiments were repeated the times indicated in the figure legends. All experiment shown in the main figures were performed at least two times. All attempts of replication individual results were successful. |
| Randomization | The individual mice were randomly assigned to each group. Covariants like sex and age were kept similar.<br><br>Human study participants were selected on the basis of availability. Randomizations were not performed given that we had only two groups - healthy donors and MS patients. |
| Blinding | Murine studies: Experiments were performed unblinded since only objective data and no subjective (scoring) data were obtained.<br><br>Human studies: Blinding was not possible given the above indicated ways of recruiting the patients. There was also no need for blinding as only objective data and no subjective (scoring) data were obtained. |

# Reporting for specific materials, systems and methods

We require information from authors about some types of materials, experimental systems and methods used in many studies. Here, indicate whether each material, system or method listed is relevant to your study. If you are not sure if a list item applies to your research, read the appropriate section before selecting a response.

## Materials & experimental systems

| n/a | Involved in the study |
|---|---|
| ☐ | ☒ Antibodies |
| ☐ | ☒ Eukaryotic cell lines |
| ☒ | ☐ Palaeontology and archaeology |
| ☐ | ☒ Animals and other organisms |
| ☒ | ☐ Clinical data |
| ☒ | ☐ Dual use research of concern |

## Methods

| n/a | Involved in the study |
|---|---|
| ☒ | ☐ ChIP-seq |
| ☐ | ☒ Flow cytometry |
| ☒ | ☐ MRI-based neuroimaging |

# Antibodies

Antibodies used

We used the following mouse specific antibodies in our studies:
Antigen' 'Label' 'Supplier' 'Clone' 'CatalogNr' 'Dilution
CD127' 'APC' 'Biolegend' 'A7R34' '135012' '1:400
CD127' 'APC' 'ebioscience' 'A7R34' '17-1271:82' '1:400
CD127' 'APC' 'Tonbo biosciences' 'A7R34' '20-1271:U100' '1:400
CD127' 'Brilliant Violet 421' 'Biolegend' 'A7R34' '135023' '1:400
CD127' 'Brilliant Violet 711' 'Biolegend' 'A7R34' '135035' '1:400
CD127' 'efluor 660' 'ebioscience' 'A7R34' '50-1271' '1:400
CD127' 'PE' 'Biolegend' 'SB/199' '121112' '1:200
CD127' 'PE' 'ebioscience' 'SB/199' '12-1273' '1:200
CD127' 'PE' 'ebioscience' 'A7R34' '12-1271:83' '1:400
CD127' 'PE-Cy7' 'Biolegend' 'A7R34' '135013' '1:400
CD127' 'PerCP-eFluor 710' 'ebioscience' 'SB/199' '46-1273-80' '1:200
CD150 (SLAM)' 'APC' 'Invitrogen-ThermoFisher' 'mShad150' '48-1502-82' '1:200
CD150 (SLAM)' 'eFluor 450' 'Invitrogen-ThermoFisher' 'mShad150' '48-1502-82' '1:200
CD27' 'PerCP-eFluor 710' 'ebioscience' 'LG.7F9' '460271' '1:800
CD3' 'Alexa Fluor 488' 'Biolegend' '17A2' '100210' '1:400
CD4' 'APC' 'Biolegend' 'RM4-4' '116014' '1:200
CD4' 'APC' 'Biolegend' 'GK1.5' '100412' '1:200
CD4' 'biotin' 'ebioscience' 'GK1.5' '13-0041:85' '1:800
CD4' 'Brilliant Violet 711' 'Biolegend' 'GK1.5' '100447' '1:200
CD4' 'efluor 450' 'ebioscience' 'GK1.5' '48-0041:82' '1:200
CD4' 'eFluor 450' 'ebioscience' 'GK1.5' '48-0041:80' '1:200
CD4' 'FITC' 'ebioscience' 'RM4-4' '11:0043-85' '1:800
CD4' 'FITC' 'ebioscience' 'GK1.5' '11:0041:82' '1:200
CD4' 'PE' 'ebioscience' 'RM4-4' '12-0043-82' '1:400
CD4' 'PE' 'Thermo Fisher' 'GK1.5' '12-0041:82' '1:200
CD4' 'PE-Cy7' 'Biolegend' 'Gk1.5' '100422' '1:200
CD4' 'PerCP-Cy5.5' 'Biolegend' 'RM4-4' '116012' '1:200
CD44' 'APC' 'Biolegend' 'IM7' '103012' '1:200
CD44' 'APC-Cy7' 'Biolegend' 'IM7' '103028' '1:200
CD44' 'biotin' 'ebioscience' 'IM7' '13-0441:81' '1:200
CD44' 'Brilliant Violet 421' 'Biolegend' 'IM7' '103039' '1:200
CD44' 'PE' 'Biolegend' 'IM7' '103007' '1:200
CD44' 'PE' 'Biolegend' 'IM7' '103008' '1:200
CD44' 'PE-Cy7' 'eBioscience' 'IM7' '25-0441:82' '1:200
CD44' 'PE-Cy7' 'Biolegend' 'IM7' '103030' '1:200
CD44' 'PerCp-Cy5.5' 'ebioscience' 'IM7' '45-0441:80' '1:200
CD45.1' 'Alexa Fluor 488' 'Biolegend' 'A20' '110717' '1:200
CD45.1' 'Alexa Fluor 594' 'Biolegend' 'A20' '110750' '1:200
CD45.1' 'Alexa Fluor 647' 'Biolegend' 'A20' '110720' '1:200
CD45.1' 'Alexa Fluor 700 ' 'Biolegend' 'A20' '110724' '1:200
CD45.1' 'APC' 'Biolegend' 'A20' '110714' '1:200
CD45.1' 'APC-Cy7' 'Biolegend' 'A20' '110715' '1:200
CD45.1' 'APC-eFlour 780' 'ebioscience' 'A20' '47-0453' '1:200
CD45.1' 'biotin' 'Biolegend' 'A20' '110704' '1:200
CD45.1' 'Biotin' 'ebioscience' 'A20' '13-0453-85' '1:200
CD45.1' 'Brilliant Violet 421' 'Biolegend' 'A20' '110731' '1:200
CD45.1' 'Brilliant Violet 605' 'Biolegend' 'A20' '110737' '1:200
CD45.1' 'eFluor 450' 'ebioscience' 'A20' '48-0453-82' '1:200
CD45.1' 'FITC' 'ebioscience' 'A20' '11:0453-85' '1:200
CD45.1' 'Pacific Blue' 'Biolegend' 'A20' '110722' '1:200
CD45.1' 'PE' 'Biolegend' 'A20' '110707' '1:200
CD45.1' 'PE' 'ebioscience' 'A20' '12-0453-83' '1:200
CD45.1' 'PE-Cy7' 'Tonbo biosciences' 'A20' '60-04553-U100' '1:200
CD45.1' 'PE-Cy7' 'ebioscience' 'A20' '25-0453-82' '1:200
CD45.1' 'PE-Dazzle' 'Biolegend' 'A20' '110747' '1:200
CD45.1' 'PerCP-Cy5.5' 'Biolegend' 'A20' '110728' '1:200
CD45.1' 'PerCP-Cy5.5' 'ebioscience' 'A20' '45-0453-82' '1:200

CD45.2’ ‘Alexa Fluor 488’ ‘Biolegend’ ‘104’ ‘109815’ ‘1:400
CD45.2’ ‘Alexa Fluor 594’ ‘Biolegend’ ‘104’ ‘109850’ ‘1:200
CD45.2’ ‘Alexa Fluor 700’ ‘ebioscience’ ‘104’ ‘56-0454’ ‘1:400
CD45.2’ ‘Alexa Fluor 700’ ‘ebioscience’ ‘104’ ‘56-0454-82’ ‘1:200
CD45.2’ ‘APC’ ‘Biolegend’ ‘104’ ‘109814’ ‘1:200
CD45.2’ ‘APC’ ‘Tonbo biosciences’ ‘104’ ‘20-0454-u100’ ‘1:200
CD45.2’ ‘APC’ ‘ebioscience’ ‘104’ ‘17-0454-82’ ‘1:200
CD45.2’ ‘APC-Cy7’ ‘Biolegend’ ‘104’ ‘109823’ ‘1:200
CD45.2’ ‘APC-Fire 750 ’ ‘Biolegend’ ‘104’ ‘109851’ ‘1:200
CD45.2’ ‘Biotin’ ‘Biolegend’ ‘104’ ‘109804’ ‘1:200
CD45.2’ ‘Brilliant Violet 421’ ‘Biolegend’ ‘104’ ‘109831’ ‘1:200
CD45.2’ ‘Brilliant Violet 510’ ‘Biolegend’ ‘104’ ‘109837’ ‘1:200
CD45.2’ ‘Brilliant Violet 711’ ‘Biolegend’ ‘104’ ‘109847’ ‘1:200
CD45.2’ ‘eFluor 450’ ‘ebioscience’ ‘104’ ‘48-0454-82’ ‘1:200
CD45.2’ ‘FITC’ ‘Biolegend’ ‘104’ ‘109806’ ‘1:200
CD45.2’ ‘FITC’ ‘ebioscience’ ‘104’ ‘11:0454-85’ ‘1:200
CD45.2’ ‘Pacific Blue’ ‘Biolegend’ ‘104’ ‘109820’ ‘1:200
CD45.2’ ‘PE’ ‘Biolegend’ ‘104’ ‘109807’ ‘1:200
CD45.2’ ‘PE-Cy7’ ‘Biolegend’ ‘104’ ‘109829’ ‘1:200
CD45.2’ ‘PE-Cy7’ ‘ebioscience’ ‘104’ ‘25-0454-82’ ‘1:200
CD45.2’ ‘PE-Dazzle’ ‘Biolegend’ ‘104’ ‘109845’ ‘1:200
CD45.2’ ‘PerCP-Cy5.5’ ‘Biolegend’ ‘104’ ‘109828’ ‘1:200
CD45.2’ ‘PerCP-Cy5.5’ ‘ebioscience’ ‘104’ ‘45-0454-82’ ‘1:200
CD45.2’ ‘VioletFluor 450’ ‘Tonbo biosciences’ ‘104’ ‘75-0454-U100’ ‘1:200
CD45.2 ’ ‘FITC’ ‘Tonbo biosciences’ ‘104’ ‘35-0454-U500’ ’ 1:300
CD45.2 ’ ‘PE’ ‘ebioscience’ ‘104’ ‘12-0454-82’ ‘1:200
CD45R (B220)’ ‘Alexa Fluor 647’ ‘Biolegend’ ‘RA3-6B2’ ‘103226’ ‘1:200
CD45R (B220)’ ‘biotin’ ‘ebioscience’ ‘RA3-6B2’ ‘13-0452-85’ ‘1:800
CD45R (B220)’ ‘eFluor 450’ ‘ebioscience’ ‘RA3-6B2’ ‘48-0452’ ‘1:200
CD45R (B220)’ ‘efluor 660’ ‘ebioscience’ ‘RA3-6B2’ ‘50-0452’ ‘1:200
CD45R (B220)’ ‘FITC’ ‘ebioscience’ ‘RA3-6B2’ ‘11:0452-85’ ‘1:800
CD45R (B220)’ ‘Pacific blue’ ‘Biolegend’ ‘RA3-6B2’ ‘103230’ ‘1:200
CD45R (B220)’ ‘PerCP-Cy5.5’ ‘Biolegend’ ‘RA3-6B2’ ‘103221’ ‘1:400
CD45R (B220)’ ‘VioletFluor 450’ ‘Tonbo biosciences’ ‘RA3-6B2’ ‘75-0452-U100’ ‘1:400
CD45R/B220’ ‘Brilliant Violet 421’ ‘Biolegend’ ‘RA3-6B2’ ‘103251’ ‘1:200
CD62L’ ‘Brilliant Violet 785’ ‘Biolegend’ ‘MEL-14’ ‘104440’ ‘1:200
CD62L’ ‘Fitc’ ‘Biolegend’ ‘MEL-14’ ‘104405’ ‘1:200
CD62L’ ‘FITC’ ‘Tonbo biosciences’ ‘MEL-14’ ‘35-0621:U500’ ‘1:200
CD62L’ ‘PE’ ‘ebioscience’ ‘MEL-14’ ‘12-0621:83’ ‘1:200
CD62L’ ‘PE’ ‘Biolegend’ ‘MEL-14’ ‘104407’ ‘1:200
CD62L’ ‘PE-Cy7’ ‘ebioscience’ ‘MEL-14’ ‘25-0621:82’ ‘1:800
CD62L’ ‘PE-eFluor 610’ ‘Invitrogen-ThermoFisher’ ‘DREG56’ ‘61:0629-41’ ‘1:200
CD69’ ‘Alexa Fluor 488’ ‘Biolegend’ ‘H1.2F3’ ‘104516’ ‘1:200
CD69’ ‘Alexa Fluor 647’ ‘Biolegend’ ‘H1.2F3’ ‘104518’ ‘1:200
CD69’ ‘Alexa Fluor 700’ ‘Biolegend’ ‘H1.2F3’ ‘104539’ ‘1:200
CD69’ ‘Biotin’ ‘Thermo Fisher’ ‘H1.2F3’ ‘13-0691:81’ ‘1:200
CD69’ ‘Brilliant Violet 421’ ‘Biolegend’ ‘H1.2F3’ ‘104527’ ‘1:200
CD69’ ‘Brilliant Violet 605’ ‘Biolegend’ ‘H1.2F3’ ‘104529’ ‘1:200
CD69’ ‘Brilliant Violet 711’ ‘Biolegend’ ‘H1.2F3’ ‘104537’ ‘1:200
CD69’ ‘FITC’ ‘ebioscience’ ‘H1.2F3’ ‘11:0691:81’ ‘1:200
CD69’ ‘PE’ ‘ebioscience’ ‘H1.2F3’ ‘12-0691:83’ ‘1:200
CD69’ ‘PE’ ‘ebioscience’ ‘H1.2F3’ ‘12-0691:82’ ‘1:200
CD69’ ‘PerCP-Cy5.5’ ‘Biolegend’ ‘H1.2F3’ ‘104521’ ‘1:200
CD8’ ‘Alexa Fluor 488’ ‘Biolegend’ ‘53-6.7’ ‘100726’ ‘1:200
CD8’ ‘Alexa Fluor 647’ ‘Biolegend’ ‘53-6.7’ ‘100727’ ‘1:200
CD8’ ‘Alexa Fluor 700’ ‘ebioscience’ ‘53-6.7’ ‘56-0081:82’ ‘1:200
CD8’ ‘APC’ ‘Biolegend’ ‘53-6.7’ ‘100711’ ‘1:200
CD8’ ‘APC’ ‘Biolegend’ ‘53-6.7’ ‘100712’ ‘1:200
CD8’ ‘APC-Cy7’ ‘Biolegend’ ‘53-6.7’ ‘100713’ ‘1:200
CD8’ ‘APC-eFlour 780’ ‘ebioscience’ ‘53-6.7’ ‘470081’ ‘1:200
CD8’ ‘APC-Fire 750 ’ ‘Biolegend’ ‘53-6.7’ ‘100765’ ‘1:200
CD8’ ‘biotin’ ‘ebioscience’ ‘53-6.7’ ‘13-0081:82’ ‘1:200
CD8’ ‘Brilliant Violet 410’ ‘Biolegend’ ‘53-6.7’ ‘100737’ ‘1:200
CD8’ ‘Brilliant Violet 510’ ‘Biolegend’ ‘53-6.7’ ‘100751 ’ ‘1:200
CD8’ ‘Brilliant Violet 605’ ‘Biolegend’ ‘53-6.7’ ‘100743’ ‘1:200
CD8’ ‘Brilliant Violet 711’ ‘Biolegend’ ‘53-6.7’ ‘100747’ ‘1:200
CD8’ ‘Brilliant Violet 711’ ‘Biolegend’ ‘53-6.7’ ‘100748’ ‘1:200
CD8’ ‘eVolve 655’ ‘eBioscience’ ‘53-6.7’ ‘15530827’ ‘1:200
CD8’ ‘FITC’ ‘ebioscience’ ‘53-6.7’ ‘110081’ ‘1:800
CD8’ ‘FITC’ ‘Biolegend’ ‘53-6.7’ ‘100706’ ‘1:200
CD8’ ‘Pacific Blue’ ‘Biolegend’ ‘53-6.7’ ‘100725’ ‘1:200
CD8’ ‘PE’ ‘ebioscience’ ‘53-6.7’ ‘12008182’ ‘1:800
CD8’ ‘PE’ ‘ebioscience’ ‘53-6.7’ ‘12-0081:82’ ‘1:200
CD8’ ‘PerCP-Cy5.5’ ‘Tonbo biosciences’ ‘53-6.7’ ‘65-0081:U100’ ‘1:400
CD8’ ‘PerCP-Cy5.5’ ‘ebioscience’ ‘53-6.7’ ‘45-0081:82’ ‘1:200
CD8’ ‘PerCP-Cy5.5’ ‘Biolegend’ ‘53-6.7’ ‘100734’ ‘1:200

CXCR5' 'APC' 'BD Pharmingen' '2G8' '560615' '1:200
CXCR5' 'Biotin' 'ebioscience' 'SPRCL5' '13-7185-82' '1:200
CXCR5' 'PE' 'ebioscience' 'SPRCL5' '12-7185-80' '1:200
CXCR5' 'PerCP-eFluor 710' 'ebioscience' 'SPRCL5' '46-7185-80' '1:200
CXCR6' 'Alexa Fluor 647' 'Biolegend' 'SA051D1' '151114' '1:200
CXCR6' 'Alexa Fluor 647' 'Biolegend' 'SA051D1' '151115' '1:200
CXCR6' 'APC' 'R&D' '221002' 'FAB2145A-025' '1:200
CXCR6' 'Brilliant Violet 421' 'Biolegend' 'SA051D1' '151109' '1:200
CXCR6' 'Brilliant Violet 711' 'Biolegend' 'SA051D1' '151111' '1:200
CXCR6' 'PE' 'Biolegend' 'SA051D1' '151104' '1:200
EOMES' 'PerCP-eFluor 710' 'ebioscience' 'Dan11mag' '46-4875-80' '1:200
GranzymeB' 'APC' 'Invitrogen-ThermoFisher' 'GB12' 'MHGB05' '1:150
GranzymeB' 'PE' 'ebioscience' '16G6' '12-8822-80' '1:400
GranzymeB' 'PE' 'eBioscience' 'NGZB' '12-8898-80' '1:200
IFNg' 'FITC' 'ebioscience' 'XMG1.2' '11:7311:41' '1:200
IFNg' 'FITC' 'Biolegend' 'XMG1.2' '505806' '1:200
IFNg' 'PE' 'ebioscience' 'XMG1.2' '12-7311:82' '1:200
IFNg' 'PE-Cy7' 'Thermo Fisher' 'XMG1.2' '25-7311:41' '1:200
IL-2' 'APC' 'ebioscience' 'JES6-5H4' '17-7021:81' '1:200
IL-2' 'Brilliant Violet 421' 'Biolegend' 'JES6-5H4 ' '503825' '1:200
IL-2' 'PE' 'ebioscience' 'JES6-5H4' '12-7021:81' '1:200
IL-2' 'PerCP-Cy5.5' 'ebioscience' 'JES6-5H4' '45-7021:82' '1:200
KLRG1' 'APC' 'ebioscience' '2F1' '17-5893-82' '1:200
KLRG1' 'biotin' 'ebioscience' '2F1' '13-5893-82' '1:200
KLRG1' 'biotin' 'Biolegend' '2F1' '138405' '1:200
Klrg1' 'Brilliant Violet 421' 'Biolegend' '2F1/KLRG1' '138413' '1:200
KLRG1' 'eFluor 450' 'ebioscience' '2F1' '48-5893' '1:200
KLRG1' 'FITC' 'Tonbo biosciences' '2F1' '35-5893-U100' '1:400
KLRG1' 'FITC' 'eBioscience' '2F1' '11:5893' '1:200
KLRG1' 'PE-Cy7' 'ebioscience' '2F1' '25-5893' '1:400
Tbet' 'Brilliant Violet 711' 'Biolegend' '4B10' '644819' '1:200
Tbet' 'PE-Cy7' 'Invitrogen-ThermoFisher' '4B10' '25-5825-80' '1:200
TCF1' 'Alexa Fluor 647' 'Cell Signaling' 'C63D9' '6709S' '1:200
TCF1' 'PE' 'BD Pharmingen' 'S33966' '564217' '1:200
TCF1' 'Rabbit mAb' 'Cell Signaling' 'C63D9' '2203' '1:200
Tim-3' 'Brilliant Violet 605' 'Biolegend' 'RMT3-23' '119721' '1:200
Tim-3' 'eFluor 450' 'Invitrogen-ThermoFisher' '8B.2C12' '48-5871:80' '1:200
Tim-3' 'PE' 'Biolegend' 'RMT3-23' '119703' '1:200
Tim-3' 'PerCP-Cy5.5' 'Biolegend' 'RMT3-23' '119717' '1:200
TNF' 'APC' 'Biolegend' 'MP6-XT22' '506308' '1:200
TNF' 'APC' 'Biolegend' 'MP6-XT22' '506307' '1:200
TNF' 'pe' 'BD Pharmingen' 'MP6-XT22' '554419' '1:200
TNF' 'PE-Cy7' 'ebioscience' 'MP6-XT22' '25-7321' '1:200
TNF' 'PE-Cy7' 'ebioscience' 'MP6-XT22' '25-7321:82' '1:200
TNF' 'PerCP-eFluor 710' 'Thermo Fisher' 'MP6-XT22' '46-7321:80' '1:200
TNF' 'PerCP-eFluor 710' 'ebioscience' 'MP6-XT22' '46-7321:82' '1:200

We used the following human specific antibodies in our studies:
Antigen' 'Label' 'Supplier' 'Clone' 'CatalogNr' 'Dilution
CD8' 'OKT-8' 'BioXCell' 'Pacific blue (self conjugated)' 'BE0004-2' '1:640
CD4' 'RPA-T4' 'BioXCell' 'Alexa Fluor 633 (self conjugated)' 'BE0288' '1:640
CD3' 'UCHT1' 'BioXCell' 'Alexa Fluor 700 (self conjugated)' 'BE0231' '1:640
CD45RA' 'HI100' 'BioLegend' 'Brilliant Violet 711' '304137' '1:20
CCR7' 'G043H7' 'BioLegend' 'PE-Dazzle' '353236' '1:20
TNF' 'Mac11' 'Biolegend' 'FITC' '502906' '1:20
IFNg' 'B27' 'BioXCell' 'Alex Fluor 555 (self conjugated)' 'BE0245' '1:640

Validation

For antibody specificities, we refer to the information provided by the supplying companies.

## Eukaryotic cell lines

Policy information about cell lines and Sex and Gender in Research

Cell line source(s)

BHK-21 cells, originally provided by M. J. Bevan, University of Washington
Vero cells, originally provided by M. J. Bevan, University of Washington
Phoenix E cells, originally provided by M. J. Bevan, University of Washington

Authentication

Since we used only cell-lines that we have been using in the lab for several years, we did not specifically authenticated them. However, we made sure that all used cell-lines showed the expected results and were in good condition prior to using them.

| | |
|---|---|
| Mycoplasma contamination | Mycoplasma tests are routinely performed and found to be negative. |
| Commonly misidentified lines (See ICLAC register) | To the best of our knowledge, no commonly misidentified cell lines were used in the study. |

## Animals and other research organisms

Policy information about studies involving animals; ARRIVE guidelines recommended for reporting animal research, and Sex and Gender in Research

| | |
|---|---|
| Laboratory animals | C57BL/6 mice were obtained from Charles River and C57BL/6.SJL from Jackson Laboratory and both lines were maintained by intercrossing. Nur77 and OT-1 TCR transgenic mice (both Jackson Laboratory); and P14 TCR and SMARTA transgenic mice obtained from A. Oxenius (ETHZ, Switzerland) are on a C57BL/6 background. These lines were maintained crossing them with C57BL/6 and C57BL/6.SJL mice.<br>Mice were bred and maintained in SPF facilities and infected in conventional or SPF animal facilities. Maximum 5 mice per cage were housed with unlimited access to food (Ssnif V1124-300) and water.<br>Experiments were performed with at least 6 weeks old male and female mice, in compliance with the institutional and governmental regulations and were approved by the veterinarian authorities of the Swiss Canton Vaud and the "Regierung von Oberbayern" in Germany.<br>Experimental groups were non-blinded and animals were randomly assigned to experimental groups. |
| Wild animals | No wild animals were used. |
| Reporting on sex | The findings we report apply to both sexes. |
| Field-collected samples | No field collection samples were used. |
| Ethics oversight | Experiments were approved by the veterinarian authorities of the Swiss Canton Vaud and the "Regierung von Oberbayern" in Germany. |

Note that full information on the approval of the study protocol must also be provided in the manuscript.

## Flow Cytometry

### Plots

Confirm that:

☒ The axis labels state the marker and fluorochrome used (e.g. CD4-FITC).

☒ The axis scales are clearly visible. Include numbers along axes only for bottom left plot of group (a 'group' is an analysis of identical markers).

☒ All plots are contour plots with outliers or pseudocolor plots.

☒ A numerical value for number of cells or percentage (with statistics) is provided.

### Methodology

| | |
|---|---|
| Sample preparation | Single cell suspensions from spleen and liver were obtained by mashing spleens through 100 µM nylon cell strainers. Red blood cell lysis was performed with hypotonic ACK buffer. Single cells suspensions from infected mice were directly used as described in the essays described below. Single cells suspension from the Liver were, after a washing step, further separated by re-suspending them in 35% physiological Percoll solution in DMEM, and then added on top of a 65% Percoll solution in PBS. Naïve OT-1 or P14 T-cells were enriched by negative selection using a CD8+ T-cell isolation kit II (Miltenyi Biotech) and naïve SMARTA T-cells with the CD4+ T-cell isolation kit (Miltenyi Biotech).<br><br>Single cell suspensions were stained using the following mouse antibodies (mAb): CD8 (clone 53-6.7), CD4 (clone RM4-4 or GK1.5), CD45.1 (clone A20), CD45.2 (clone 104), CD127 (clone A7R34 or eBioSB/199), KLRG1 (clone 2F1), CD27 (clone LG.7F9), CD62L (clone MEL-14), CD69 (clone H1.2F3), CD44 (clone IM7), CD185 (CXCR5, clone SPRCL5), CD186 (CXCR6, clone SA051D1), CD366 (TIM3, clone RMT3-23), CD150 (SLAM, clone TC15-12F12.2). After staining, cells were washed twice and fixed for 15 min in PBS, 1% formaldehyde, 2% glucose, 0.03% Azide. For intracellular staining, cells were re-stimulated in vitro with 5 mM SIINFEKL or KAVYNFATC peptide for the last 5 h. 7 µg/ml Brefeldin A was added 30 min after starting the culture. Cells were fixed and permeabilized using the Cytofix/Cytoperm Kit (BD) and stained with monoclonal antibodies against IFN-γ (clone XMG1.2), TNF (clone MP6-XT22), IL-2 (clone JES6-5H4) and Granzyme B (without peptide stimulation; clone GB12). Intracellular staining for TCF-1 (clone S33966), Eomes (clone Dan11mag), and T-bet (clone eBio4B10) antibodies was performed with the Foxp3/transcription factor staining kit (eBioscience). Flow cytometry measurements of cells were acquired on a CytoFLEX (Beckmann Coulter), LSR-Fortessa or LSR-II instrument (both BD). For flow cytometry-based sorting, live cells were stained in PBS, 2% FCS and sorted using a FACSAriaFusion instrument (BD). Antibodies were obtained from eBioscience, Tonbo Biosciences, bioXcell, Invitrogen, bioLegend, and BD Biosciences. All flow cytometry data were analyzed using FlowJo (TreeStar, BD) and population analysis of CFSE data was performed using the FlowJo's Proliferation Modeling Platform according to the manufacturer's instructions. |
| Instrument | BD FACS Fortessa, Beckman Coulter CytoFLEX |

| | |
|---|---|
| Software | Flow Jo Version 9 and 10, BD FACSDiva Software |
| Cell population abundance | Post sort purity was >95% |
| Gating strategy | We used standard gating strategies: Live / Dead discrimination based on FSC and SSC signals, gating on the typical lymphocyte population based on FSC SSC signals, doublet exclusion based on FSC-H and FSC-A comparison, back-gating tests to ensure that minor sub-populations were not excluded by the gating strategy |

☒ Tick this box to confirm that a figure exemplifying the gating strategy is provided in the Supplementary Information.